

Optimal Battery Energy Storage System Sizing in EV Fast Charging Applications

A Multi-objective Framework for Demand Charge Management at Fast Charging Stations Using Genetic Algorithms

G.A. Koolman



Optimal Battery Energy Storage System Sizing in EV Fast Charging Applications

A Multi-objective Framework for Demand Charge Management at Fast Charging Stations using Genetic Algorithms

by

G.A. Koolman

to obtain the degree of Master of Science
in Electrical Power Engineering

at the Delft University of Technology,
to be defended publicly on Wednesday December 16, 2020 at 9:30 AM.

| | | |
|-------------------|-----------------------------|------------------------|
| Student number: | 4270975 | |
| Thesis committee: | Prof. dr. ir. P. Bauer, | DCE&S, TU Delft, Chair |
| | Dr. ir. G.R. Chandra Mouli, | DCE&S, TU Delft |
| | Dr. ir. M. Cvetkovic, | IEPG, TU Delft |
| | ir. S. Er, | Royal HaskoningDHV |

The public version of this thesis is available at <http://repository.tudelft.nl/>
In this version some sensitive data are excluded.

Cover image credit goes to EVBox

Abstract

The need for proper fast charging infrastructures is one of the key challenges for the wide adoption of electrical vehicles (EV). The high pulsating demand of fast charging stations (FCS) together with high demand tariffs can cause monthly DSO demand charges to account for a significant fraction of a station's electric bill. Therefore, weakening the business case for stations located in these high tariff regions.

To tackle this issue, demand charge management (DCM) can be applied to suppress peak power demands at FCSs using battery energy storage systems (BESS). This enables the reduction of cost while retaining the station's fast charging capabilities. However, the implementation of such systems remains a large investment and the proper BESS sizing in fast charging applications is not well studied.

This thesis proposes a multi-objective approach for optimal BESS sizing at FCSs considering demand charges and station performance. A BESS assisted FCS model is formulated to analyse the performance of a station's design based on power flow, charging delays and the expected BESS lifetime. Furthermore, based on a worst-case demand scenario, a multi-objective optimization framework is formulated using the genetic algorithm NSGA-II to obtain the optimal BESS and grid-tie sizing for an existing FCS. Lastly, with demand data measured at four FCSs in the Netherlands, a set of numerical case studies has been conducted in the Mosaik and Pymoo environments to assess the feasibility and the effectiveness of the proposed formulation. These case studies provide new insights on the demand charge reduction and optimal sizing regarding different station characteristics, BESS prices, and demand tariffs. These insights show how the FCS utilization rate and installed capacity can effect the optimal BESS sizing and how different demand tariffs or BESS cost can result in different optimal power to energy (P/E) ratios, and thus affecting the performance of a BESS.

Keywords: battery energy storage systems, demand charge management, electrical vehicles, fast charging stations, genetic algorithms, multi-objective optimizations, nsga-II

Acknowledgements

This thesis represents my results and findings during my MSc. graduation project at Royal HaskoningDHV. I hope that this project further strengthens the relationship between the TU Delft and the company, and may this lead to many more opportunities in the future for further collaboration. Despite the rather unprecedented year, I can still look back to a time filled with learning experiences and self development moments that will have an immense impact on the rest of my career. From an idea that initiated during a casual lunch break, went and develop from a simple thesis proposal to a full-fledged project, where I genuinely enjoyed working countless of hours on without ever getting tired of the topic. All with one goal in mind, to make a meaningful contribution to the scientific community. I hope this thesis accomplishes this goal and in the process help contribute in accelerating our transition to a fully electric transportation system.

First of all I would like to thank my company supervisors Sukru Er and Herbert Polman. Their professional guidance and constant feedback has certainly contributed to the quality of this thesis. Also, I would like to extend my gratitude to Laurens Nordkamp for giving me the opportunity in the first place and for allowing me to explore my own thesis topic at Royal HaskoningDHV.

I would like to also thank my university supervisor Prof. Pavol Bauer, for granting me the chance to pursue my thesis at a company and to help guiding me through the procedures. Additionally, I would like to also thank the rest of my thesis committee Gautham Chandra Mouli and Milos Cvetkovic, for giving me inspiration in the beginning that helped formulate the thesis proposal and for taking the time to read and asses this thesis for my defence.

Furthermore, I would like to thank Roland for sharing with me his valuable industry insights and Marco Stecca for being a fantastic sparring partner during this process. I truly believe that his guidance were key in helping me maintain a high level of academic quality in this thesis.

Lastly, I would like to thank all of my friends, housemates and colleagues that supported me through my studies in Delft, Crossfit Coolhaven for keeping me fit during these past years and an immense gratitude to my parents for always loving me unconditionally, believing in me and for always giving me the freedom to explore my interests. Without them non of this would of been possible. *Masha danki pa tur cos!*

*G.A. Koolman
Rotterdam, December 2020*

*"We tend to overestimate what
we can do in a day, and underestimate
what we can do in a year"*

BILL GATES

Contents

| | |
|---|------|
| Abstract | iii |
| Acknowledgements | v |
| List of Figures | ix |
| List of Tables | xi |
| Abbreviations | xiii |
| Nomenclature | xv |
| 1 Introduction | 1 |
| 1.1 Energy Transition | 1 |
| 1.2 Electric Vehicle Trends | 1 |
| 1.3 Fast Charging Trends and Challenges | 3 |
| 1.4 Battery Energy Storage Trends | 4 |
| 1.5 Thesis Motivation | 5 |
| 1.5.1 Problem statement. | 5 |
| 1.5.2 Previous work survey. | 6 |
| 1.5.3 Research questions and objectives | 7 |
| 1.5.4 Thesis Outline | 8 |
| 2 Literature Review | 9 |
| 2.1 EV Fast Charging | 9 |
| 2.1.1 FCS configurations. | 9 |
| 2.1.2 State of the art technology and standards | 10 |
| 2.1.3 Load demand | 11 |
| 2.1.4 Impact to the distribution grid | 12 |
| 2.2 Demand Charge Management | 14 |
| 2.2.1 Demand charges. | 14 |
| 2.3 Grid-connected Energy Storage Systems | 16 |
| 2.3.1 Lithium-ion based batteries | 18 |
| 2.3.2 Ageing and lifetime | 18 |
| 2.3.3 Grid-connected Applications | 19 |
| 2.3.4 Sizing | 19 |
| 2.3.5 Modeling. | 20 |
| 2.4 Multi-objective optimizations. | 23 |
| 2.4.1 Multi-objective problems | 23 |
| 2.4.2 Genetic algorithms. | 24 |
| 2.4.3 NSGA-II | 25 |
| 3 Fast Charging Station Model Design | 27 |
| 3.1 Fast Charging Station Model | 27 |
| 3.2 Model Diagram | 28 |
| 3.3 Station Demand. | 29 |
| 3.4 Energy Management System | 29 |
| 3.5 BESS Model | 30 |
| 3.5.1 Operation and controls | 31 |
| 3.5.2 Power capability | 32 |
| 3.5.3 Inverter efficiency | 33 |
| 3.5.4 Model Verification | 33 |

| | | |
|-------|--|----|
| 3.6 | Lifetime Model | 35 |
| 3.7 | Quality of Service | 37 |
| 4 | Multi-Objective Design Problem Formulation | 39 |
| 4.1 | FCS Design Problem | 39 |
| 4.2 | Objective Functions. | 40 |
| 4.3 | Design Constraints | 40 |
| 4.4 | Optimal Sizing Framework | 41 |
| 4.4.1 | Optimization Model | 41 |
| 4.4.2 | Sizing Procedure | 41 |
| 5 | Optimization and Simulation Results | 43 |
| 5.1 | Stations and Case Studies description. | 43 |
| 5.2 | Case 0: DCM without BESS | 46 |
| 5.3 | Case 1: BESS assisted DCM for different station types in Switzerland | 46 |
| 5.4 | Case 2: BESS assisted DCM in different demand tariff regions (low, mid, high) | 48 |
| 5.5 | Case 3: BESS assisted DCM with expected BESS price drop in 2030 | 50 |
| 5.6 | Case 4: BESS assisted DCM with BESS power capability of 2C. | 51 |
| 5.7 | Impact of DCM on BESS Lifetime | 52 |
| 5.8 | Impact on performance. | 53 |
| 5.9 | Key Results | 55 |
| 6 | Conclusion | 57 |
| 6.1 | Answers to research questions | 57 |
| 6.1.1 | How to formulate a multi-objective optimization framework for optimal BESS and grid-tie sizing in order to minimize demand charges and charging delays at FCS? | 57 |
| 6.1.2 | How do FCS demand influences the optimal design? | 58 |
| 6.1.3 | How do demand tariffs and BESS costs influence the optimal design parameters? | 58 |
| 6.1.4 | What impact do the sizing framework have on the BESS lifetime? | 58 |
| 6.2 | Main Contributions | 58 |
| 6.3 | Further research | 58 |
| A | Rain flow Cycle-counting Algorithm | 61 |
| B | Mosaik | 63 |
| C | Pymoo | 65 |
| D | BESS Model Verification | 67 |
| D.1 | BESS constraints | 67 |
| D.2 | BESS efficiencies | 68 |
| E | Result Tables | 69 |
| F | Conference Paper Draft | 73 |
| | Bibliography | 85 |

List of Figures

| | | |
|------|--|----|
| 1.1 | Global EV sales between 2016 and 2019 in million units [3] | 2 |
| 1.2 | The expected growth of fast charging points in the Netherlands [10] | 3 |
| 1.3 | Global cumulative energy storage installations projections by BNEF [17] | 4 |
| 1.4 | Breakdown the energy storage deployed internationally by technology type, excluding pumped hydro storage [18]. | 5 |
| 2.1 | Electrical configuration for FCSs [60] | 10 |
| 2.2 | An overview of the standardized EV sockets capable of DC charging [61] [62] | 10 |
| 2.3 | Charging speed curves at 175kW chargers for different EV models [65] | 11 |
| 2.4 | Distribution of fast charging sessions throughout the day (24 hours) at Fastned stations [66] | 12 |
| 2.5 | A weekday (left) and weekend (right) FCS demand profile generated from petrol station data [37]. | 12 |
| 2.6 | Impact of large FCS on distribution transformer loading (left), and system bus voltage (right) [26]. | 13 |
| 2.7 | Maximum demand charge rates by utility service territory in the US [14] | 14 |
| 2.8 | Various Energy storage technologies [73] | 16 |
| 2.9 | Simplified schematic of a BESS, power electronics coupling and grid integration [19]. | 17 |
| 2.10 | A generic battery modeling framework for economical assessments [77]. | 20 |
| 2.11 | A flow-chart on how BESS lifetime estimation is performed using Rainflow cycle counting algorithm [50]. | 22 |
| 2.12 | (a) Cycle-life curve, (b) Calendar-life curve, Both valid for 25 °C and 20% EoL criterion [53] | 22 |
| 2.13 | Flowchart for the MOO preference-based method [80]. | 24 |
| 2.14 | Flowchart for the MOO ideal based method [80]. | 24 |
| 2.15 | An abstraction of the procedure in genetic algorithms | 25 |
| 2.16 | The NSGA-II procedure [84]. | 26 |
| 2.17 | The crowding distance calculation [84]. | 26 |
| 3.1 | A system diagram of a BESS assisted AC connected FCS | 27 |
| 3.2 | System diagram of the complete FCS model. | 28 |
| 3.3 | Example of a FCS demand for a week in January. | 29 |
| 3.4 | Control Flowchart for the EMS model | 30 |
| 3.5 | Control flowchart for the BESS model | 31 |
| 3.6 | Power capability curve obtained with the BESS power constraints | 32 |
| 3.7 | (a) Power flows between the BESS and inverter, (b) Piece-wise inverter efficiency curve model | 33 |
| 3.8 | Top: IEC 62660-1 DST power set-points. Bottom: BESS model simulation results in SOC | 34 |
| 3.9 | Example of a cycle count obtained from the modified rain-flow cycle counting algorithm | 35 |
| 3.10 | Diagram of the BESS lifetime model | 36 |
| 3.11 | Charging delay concept | 37 |
| 3.12 | The number of charging EVs during mismatch periods for a station with 450kW installed capacity and - stalls | 38 |
| 3.13 | Quality of Service implementation flowchart | 38 |
| 4.1 | A schematic overview of the proposed design optimization framework | 42 |
| 5.1 | Worst case demand profile for all stations | 44 |
| 5.2 | Results for Case 0: DCM without BESS | 46 |
| 5.3 | Results for Case 1: BESS assisted DCM in Switzerland - A | 47 |
| 5.4 | Results for Case 1: BESS assisted DCM in Switzerland - B | 47 |
| 5.5 | BESS power rating [kW] vs BESS energy rating [kWh] (P/E ratio) in Switzerland | 48 |
| 5.6 | Results for Case 2: BESS assisted DCM in different regions - A | 49 |
| 5.7 | Results for Case 2: BESS assisted DCM in different regions - B | 49 |

| | | |
|------|---|----|
| 5.8 | BESS P/E ratio in regions with different demand tariffs for all stations. | 50 |
| 5.9 | Results for Case 3: BESS assisted DCM for Switzerland in 2030 | 50 |
| 5.10 | PE ratio in countries for Switzerland in 2030 for all stations | 51 |
| 5.11 | Results for Case 3: BESS assisted DCM for the Netherlands in 2030 | 51 |
| 5.12 | Results for Case 4: BESS assisted DCM for the Netherlands with 2C power capability | 52 |
| 5.13 | Expected BESS lifetime in Switzerland for all stations | 52 |
| 5.14 | Station: D - $E_b=0$, $P_b=0$, $P_G=225$ - - Annual DCM Cost = €38,880 (-41.4%) | 53 |
| 5.15 | Performance of a 2 minute delay optimal FCS design with demand D in Switzerland using E_b^{\max} = 135, $P_b^{\max}=100$, $P_G^{\max}=130$, $C_{kW}=€14.4/kW$, and $L_{\text{exp}}: 11$ Years - Annual DCM Cost = €30,750 (-53.7%) | 53 |
| 5.16 | Performance of a 2 minute delay optimal FCS design with demand A in Switzerland using $E_b^{\max}=140$, $P_b^{\max}=110$, $P_G^{\max}=85$, $C_{kW}=14/kW$, $L_{\text{exp}}: 14$ Years - Annual DCM Cost = €21,492 (-56.8%) | 54 |
| 5.17 | Performance of a 2 minute delay optimal FCS design with demand D in NYC using $E_b^{\max}=600$, $P_b^{\max}=155$, $P_G^{\max}=75$ $C_{kW}=14/kW$ - $L_{\text{exp}}: 14$ years - Annual DCM Cost = €64,573 (-66.9%) | 54 |
| 5.18 | Comparison of the performed BESS cycles at a 2 minute delay FCS located in Switzerland and one in NYC | 55 |
| A.1 | An overview on how the the rain-flow algorithm works [50] | 62 |
| B.1 | An overview of Mosaik's architecture [94] | 64 |
| C.1 | An overview of Pymoo's architecture [96] | 65 |
| C.2 | An overview of some existing multi-objective frameworks in Python [96] | 66 |
| D.1 | Power set-points for the BESS power constraints | 67 |
| D.2 | Power constraints verification results | 68 |
| D.3 | power set-points for the BESS efficiency verification | 68 |
| D.4 | Initial efficiency verification results | 68 |

List of Tables

| | | |
|------|---|----|
| 1.1 | The expected EV share for different vehicle modalities in the Netherlands [5]. | 2 |
| 2.1 | IEC 61851-1 Charging Modes [58] | 9 |
| 2.2 | Performance comparison of lithium-ion chemistries found in stationary applications [19] | 18 |
| 2.3 | Various BESS tasks classified into application families | 19 |
| 3.1 | Input and output parameters for the FCS models. | 28 |
| 3.2 | Verification IEC 62660-1 performance test summary | 34 |
| 5.1 | FCS station details in worst-case usage period (some data are excluded in this version) | 43 |
| 5.2 | BESS project costs for LFP chemistry and associated power converter. | 45 |
| 5.3 | DSO monthly demand tariffs per region | 45 |
| 5.4 | List of the study cases for the optimizaiton | 45 |
| 5.5 | The annual demand charges without DCM per station in considered regions | 46 |
| E.1 | Case 0 results DCM without BESS - DCM Cost [%] | 69 |
| E.2 | Case 1 results - BESS assisted DCM in Swiss - Station A | 69 |
| E.3 | Case 1 results - BESS assisted DCM in Swiss - Station B | 69 |
| E.4 | Case 1 results - BESS assisted DCM in Swiss - Station C | 70 |
| E.5 | Case 1 results - BESS assisted DCM in Swiss - Station D | 70 |
| E.6 | Case 2 results - DCM without BESS | 70 |
| E.7 | Case 2 results - BESS assisted DCM in NL | 70 |
| E.8 | Case 2 results - BESS assisted DCM in NYC | 71 |
| E.9 | Case 3 results - BESS assisted DCM in Swiss - Station D - 2030 | 71 |
| E.10 | Case 3 results - BESS assisted DCM in NL - Station F - 2030 | 71 |
| E.11 | Case 4 results - BESS assisted DCM in NL - Station F - 2C | 71 |

Abbreviations

- BESS** Battery Energy Storage Systems. iii, 4
- BMS** Battery Management System. 17
- CAES** Compressed Air Energy Storage. 16
- DCM** Demand Charge Management. iii, 5
- DOD** Depth of Discharge. 18
- DSO** Distribution System Operators. 3
- DST** Dynamic Stress Test. 33
- EA** Evolutionary Algorithms. 24
- EMS** Energy Management System. 17
- EoL** End of Life. 6, 19, 35
- EV** Electrical Vehicles. iii, 1
- FCR** Frequency Containment Reserve. 6, 59
- FCS** Fast Charging Station. iii, 3
- GA** Genetic Algorithm. 7, 24
- KPI** Key Performance Indicators. 19, 39
- LFP** Lithium Iron Phosphate. 4, 50
- LIB** Lithium-ion Batteries. 18
- MILP** Mixed-integer Linear Programming. 6
- MOO** Multi-objective Optimization. 5
- MOP** Multi-objective Problem. 23
- NSGA-II** Non-Sorting Genetic Algorithm - II. iii, 5
- NYC** New York City. x, 14, 54
- P/E** Power to Energy ratio. iii, 45, 58
- PHS** Pumped Hydro Storage. 16
- PSO** Particle Swarming Optimization. 23
- QoS** Quality of Service. 28, 42
- RES** Renewable Energy Sources. 6
- SOC** State of Charge. 6
- TMS** Thermal Management System. 17

Nomenclature

- B_{mode} BESS dispatch signal. 29–31
- C^{bess} BESS energy capacity cost. 45
- C^{conv} BESS power capability cost. 45
- C^{dem} Monthly DSO demand tariff in €/kW. 40
- D_{cal} Calendar degradation. 36
- D_{cycle} Cycle degradation. 35
- $E_{b,t-1}$ BESS energy content at time $t - 1$. 31
- E_b^{max} BESS energy capacity. x, 31, 39, 41, 53, 54
- LC Total BESS lifetime consumed. 36
- L_{exp} Expected BESS lifetime in years. 36, 41
- $N_{EV,t}$ Represents the number of EVs charging at the FCS during a power mismatch period. 37
- N_{max} The maximum number of cycles at a given DOD and SOC range defined by the cycle-life model. 35
- N_c The consumed cycles by the BESS at a given DOD and average SOC range. 35
- P_G^{max} Maximum grid-tie capacity. x, 29, 30, 39, 41, 53, 54
- P_b^{max} BESS power rating. x, 31, 39, 41, 53, 54
- $P_{EV,t}$ EV demand power at time t . 29, 30, 37
- $P_{G,t}$ Grid-tie power at time t . 29, 30
- $P_{b,ch,t}$ BESS charge power at time t . 31
- $P_{b,dis,t}$ BESS discharge power at time t . 31
- $P_{ems,ch,t}$ EMS charge power signal at time t . 29–31
- $P_{ems,dis,t}$ EMS discharge power signal at time t . 29, 31
- $P_{fcs,t}$ The power capability of the FCS at time t (this includes both the grid-tie and BESS discharge power).
37
- P_{vect} A vector containing the EV demand history during a power mismatch period. 38
- $S_{b,ch}$ BESS upper SOC limits for maximum power delivery. 32
- $S_{b,dis}$ BESS lower SOC limits for maximum power delivery. 32
- $SOC_{b,t}$ BESS SOC at time t . 29, 31
- T_{max} Maximum charging delay in minutes. 41
- $T_{max}(SOC)$ The maximum calendar lifetime at a given SOC level. 36
- T_c The time consumed at a given SOC range. 36
- T_{freq} The percentage increase in station utilization caused by the total amount of extra charging time. 41

-
- T_{util} The total amount of time a station is being occupied for charging. 39
- Δt_d Instantaneous time delay due to power mismatch at time t . 37, 38
- β_{cap} BESS capacity fade over-sizing cost factor. 40
- β_{pow} BESS power fade over-sizing cost factor. 40
- $\eta_{inv}(P)$ BESS inverter efficiency. 33
- n_{pop} Population size. 41

1

Introduction

1.1. Energy Transition

An increasing concern for the scientific community is centered around tackling the global climate change problem. The main contribution to climate change is the rising global CO₂ emissions resulting from fossil fuel consumption. The transportation sector accounts for approximately 25% of these global energy-related emissions. Of these emissions, around 70% is due to the use of combustion vehicles [1]. These appalling figures have promoted people to become more aware of protecting the environment and enabled governments around the globe to set emission goals and introduce regulatory changes that encourage the reduction of CO₂ emissions. The Netherlands is a great example of this, where the Dutch government imposed a climate agreement that states a goal of 49% carbon emission reduction by 2030 [2].

One of the major disruptions to the transportation sector, set to tackle our carbon emission problem, is the wide adoption of electrical vehicles (EV). Replacing the use of combustion-based vehicles with EV reduces fossil fuel consumption, hence reducing CO₂ emissions and further increases energy security. With the intention being, that electrification of our current transportation would use electricity produced by renewable energy sources as fuel and lessen our overall carbon footprint.

1.2. Electric Vehicle Trends

For the last five years electric mobility has been expanding at a rapid pace. After a rapid growth (62% annually) between 2016 and 2018, EV sales globally amounted to 2.08 million vehicles in 2018. Despite the slow down in 2019 (which is attributed to the shrink of the overall light vehicle market), EV sales still managed to lead a significant market share growth that year and hit 2.3 million vehicles [3]. With China remaining the largest market, followed by Europe and the US. This growth can be observed in the market share charts given in Figure 1.1. With this current pace Mckinsey predicts approximately 10 to 11 million EVs in the US alone by 2030 [4].

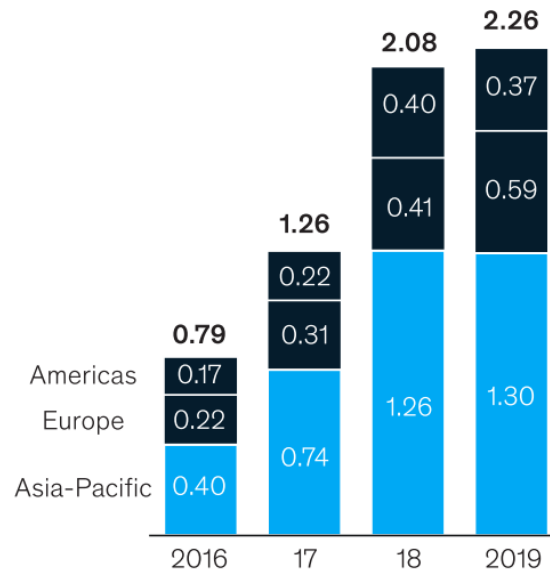


Figure 1.1: Global EV sales between 2016 and 2019 in million units [3]

The 3 main driving factors of this strong growth are:

- Policies and incentives
- Battery Technology
- Charging infrastructures

Due to geo-strategic reasons, as well as public awareness and desire for sustainability, governments on an international level are introducing stricter CO₂ regulations on the combustion engine car industry. These policies and incentives are either imposed on the manufacturers or consumers. A great example of this is found in the EU, where recently introduced regulation fines car manufacturers for not complying with the set CO₂ target of 95 grams per km by 2021. Similarly, the California Zero Emission Vehicle program in the US introduces new requirements for manufacturers to increase their selling share of EVs to be permitted to continue selling combustion engine vehicles. Both of these regulations are meant to pressure manufacturers to make the move to EV [3].

On the consumer side, great examples of incentives can be found in Germany, where in 2020 the federal government increased the EV price subsidies by 50% and extended them until 2025. Consumer incentives can also be non-monetary, an increasing number of municipalities are exempting EVs from their restriction on vehicles entering the city center. In China for example, on top of the current tier 1 cities, 10 to 20 additional cities are to be included to their congestion reduction plan by 2025 [3].

The Dutch government took a step further and implemented a complete ban on emission producing passenger cars by 2030 [2]. This legalisation is expected to cause a surge in the number of EVs in the Netherlands. Using these trends, Elaadnl projects the following growth figures shown in Table 1.1. This outlook is a mid-scenario projection for the Dutch EV situation in 2035 [5].

Table 1.1: The expected EV share for different vehicle modalities in the Netherlands [5].

| Vehicle Type | Current EV share | ElaadNL Outlook 2035 (Mid scenario) | | |
|-----------------------|------------------|-------------------------------------|-----------|-----------------------------------|
| | | Future EV share | EV Amount | Electricity demand (TWh) per year |
| Passenger vehicles | 2.2% | 35% | 3,000,000 | 7.8 |
| Public Busses | 17.8% | 95% | 4,700 | 0.6 |
| Delivery vehicles | 1.7 % | 61% | 618,600 | 3.7 |
| City logistics trucks | 0.5% | 83% | 25,000 | 1.2 |
| Freight trucks | 0% | 42% | 48,500 | 4.9 |

Although advances in battery technology and charging infrastructures have aided in the recent growth of EV sales. They continue to be the cause of challenges for wide adoption of EVs. The batteries of EVs are still not comparable to gas tanks of combustion vehicles today. Concerns related to charging speeds and driving range continue to be wide spread among consumers. This fear is known as 'range anxiety' or 'charging anxiety' [6]. A study performed on consumers even suggest, that 83% of consumers who would not consider an EV, cited battery life and charging anxiety as the reason [7]. This makes having a proper fast charging infrastructure essential for the wide adoption of EVs.

1.3. Fast Charging Trends and Challenges

Currently, most fast charging stations (FCS) have a single or multi-stall configuration and offer charging speeds ranging from 50 to 175kW per stall, with some hosts already extending this power up to 350kW [8]. Worldwide, ambitious plans are in place for expanding the current fast charging infrastructures. In Europe, five of the largest car manufacturers are collaborating under the name Ionity to build a fast-charger network of 400 stations by 2020 [9]. In the US, one manufacturer is investing USD 2 billion in fast-charging stations along freeways in 39 US states and public chargers in 17 metropolitan areas. In Asia, the Chinese State Grid Corporation is constructing 120,000 charging stations in central and eastern China by 2020 [3].

Apart from the EV manufacturers, the success of fast charging hosts is becoming more prevalent. Fastned for example in the Netherlands went from a small startup to a well established fast charging host in western Europe owning and operating already 118 stations in the Netherlands, Belgium, Germany and UK. Ultimately, Fastned strives to expand their network to 1000 stations in Europe [8]. Additionally, also the oil and gas industry are making the move to EV by investing into their own EV charging initiatives such as, New Motion (Shell), Ecotricity (BP) and Pitpoint (Total) [10].

Currently, fast charging is mostly only seen as a facilitator of long-distance driving for electric vehicles. For this reason, the deployment of FCS generally occurs next to freeways. However, as EV ownership increases in urban areas, city planners and officials are contemplating whether inner-city FCS can be the alternative for the growing congestion of slow public chargers [11]. Additionally, other transportation methods such as busses, taxis and trucks are also becoming electric. Such modalities will also require fast charging infrastructures to accommodate their intense usage patterns [12]. In the Netherlands alone, Elaadnl projects between 2400 to 7900 fast charging points by 2025. Even with the lowest projections this equals a doubling of the current scenario [10]. These projections are given in Figure 1.2.

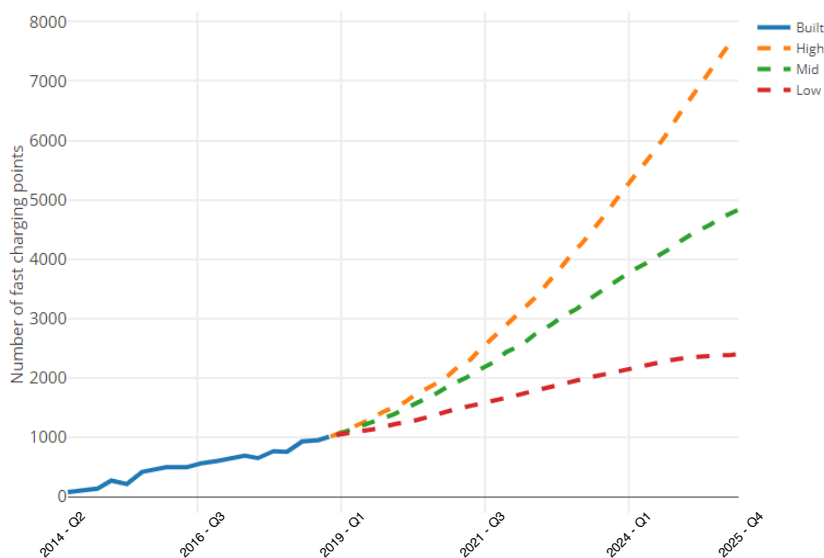


Figure 1.2: The expected growth of fast charging points in the Netherlands [10]

The same study also analysed the challenges FCS hosts will face due to these projections. According to their study, location issues and the high dependency on distribution system operator (DSO) tariffs are the two major concerns. Station location is an issue because not all petrol station or points of interests for FCSs can

provide the desired grid capacity. GVB a bus operator in the Netherlands is currently facing these issues while transitioning to an electric bus fleet. Due to the requirement of multiple fast charging points in the inner-city routes of Amsterdam, costly grid-enforcement's are being performed to supply this demand [13].

The operational costs for FCSs are highly dependent on the DSO demand tariffs [10]. Demand charges is a fee based on the highest measured peak power (in kW) during a monthly billing period. The demand tariff is the price per kW the DSO uses to determine the monthly demand charges. In the Netherlands these demand tariffs range between EUR 2 to 3/kW and are quite low compared to other countries. However, outside of the Netherlands demand tariffs vary significantly between DSOs, in the US half of all DSOs have a demand tariff of \$15/kW and higher, where some states like New York have a demand tariff of more than \$50/kW [14]. In Europe, Switzerland also has high demand tariffs ranging from 4 to 14.4 €/kW [15].

Because demand charges account for a significant portion of a FCSs electric bill, the economic impact of high demand charges can quickly weaken the business case for a FCS. For some FCS this can be up to 90% of its electric bill [4]. Under such circumstances there is a clear incentive for FCS to limit their peak power usage [14].

By implementing peak-shaving with battery energy storage systems (BESS) assisted power balance, both the DSOs and FCSs can tackle these capacity and high demand charge issues. Examples of such pilot projects can already be found in the field. Alfen a dutch BESS integrator together with Shell, are currently running such pilot projects where a 350kWh battery is being incorporated for peak shaving at one of Shell's ultra fast EV charging station [16].

1.4. Battery Energy Storage Trends

In addition to the rapid growth of EV, the transition to more wind and solar in our power system also had significant impact on energy storage trends. The amount of installed energy storage capacity around the world is expected to see an exponential increase by 2040. BNEF predicts this to go from the current 9GW/172GWh to around 1095GW/2850 GWh as shown in Figure 1.3, with China and the US having the larger share of these installations.

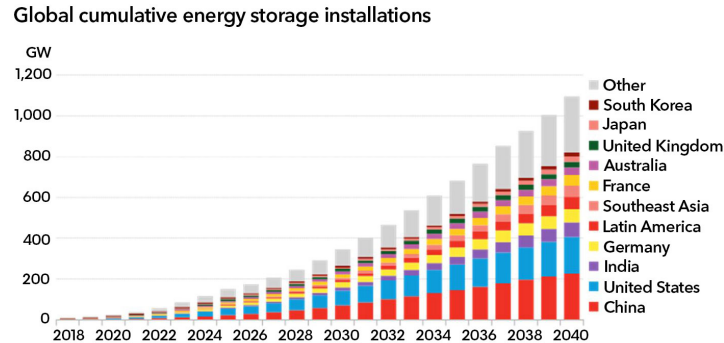


Figure 1.3: Global cumulative energy storage installations projections by BNEF [17]

Having dominated the consumer electronics market and now being the dominating technology for the EV market, lithium-ion based energy storage continues to have the largest share of 48% in the currently deployed energy storage around the globe as shown in Figure 1.4 [18]. Due to this large share, the technology experienced a 85% reduction in costs between 2010-2018 and is predicted to further halve in cost by 2030 [17]. This sharp decline in cost will aid the future energy storage growth and will add huge scale to the battery manufacturing sector.

Because of Lithium-ion's outstanding performance in efficiency, fast response, low self discharge and long lifetime, the technology has also become an attractive contender for the short and medium time stationary applications [19]. Of the different families of Li-ion technology available on the market, lithium iron phosphate (LFP) based batteries are seen as the key player for grid-connected applications. Praised for its long lifetime and low self-discharge, the cost of LFP based BESS projects are also expected to drop from €490/kWh to around €190/kWh by 2030 [20]. A significant decrease, making the business case for behind-the-meter

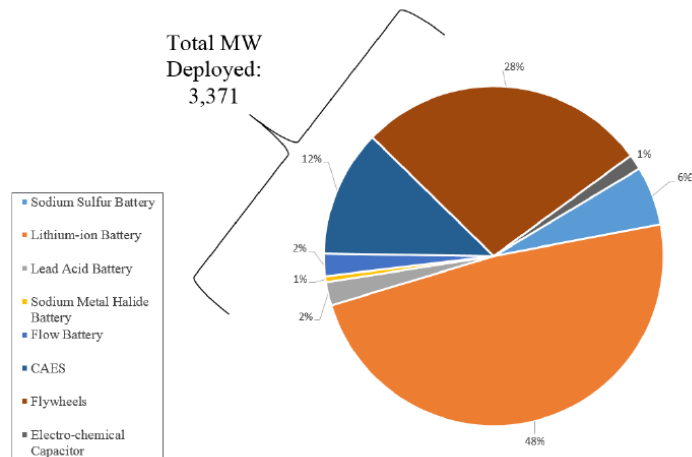


Figure 1.4: Breakdown the energy storage deployed internationally by technology type, excluding pumped hydro storage [18].

applications such as peak-shaving at FCS even more attractive.

1.5. Thesis Motivation

1.5.1. Problem statement

To achieve wide adoption of EVs and reduce the so-called 'range anxiety' among EV owners, major changes would have to come to our current EV fast charging infrastructure. To assist long-range EV travel this entails the mass deployment of FCSs along freeways and other points of interest. Additionally, urban cities would have to facilitate public fast charging points intended for other EV modalities or inhabitants in dense living areas where access to domestic charging is limited. With charging speeds from a single stall already ranging from 50 to 375 kW. FCSs with a number of charging points are electrical loads that create large demand spikes in the electricity grid during peak usage. For DSOs, this might result in grid-congestion on the distribution grid and lead to costly grid infrastructure reinforcements. Likewise, for FCS hosts this can lead to costly grid-connection upgrades and high demand charges.

Both issues can be deferred or mitigated by suppressing these high peak demands using peak shaving techniques. Simplest solution is to resort to power balancing techniques to perform demand charge management (DCM). However, this simply decreases the charging speeds during peak moments, increases charging duration and might result into long queuing. Making this solution undesired for most FCS owners and users. Most literature suggests BESS assisted DCM as a solution for reducing demand charges. The BESS can serve as a buffer between the grid-tie and the EV demand. This would limit the peak power being supplied from the grid-tie while retaining some fast charging capabilities being supplied by the BESS. However, BESS projects remain a large investment and the FCS's charging has to have some reliability. Therefore, making it difficult to find the optimal sizing of such system. Furthermore, the technical feasibility and business case for such systems are influenced by multiple factors such as the station utilization, technology prices and DSO tariffs. Additionally, the irregular nature of FCS demand might accelerate BESS degradation due to complicated cycling profiles. For this reason, multiple key performance indexes of a BESS assisted FCS should be analysed before determining an optimal design. Recent studies suggests these to be primarily operational costs and waiting times. Using these objectives a trade-off can be found between the grid-tie reduction and BESS sizing in order to reduce demand charges while retaining acceptable charging speeds.

Therefore, a multi-objective optimization (MOO) framework can be constructed to find a Pareto-front with the optimal BESS and grid-tie sizing based on reducing DCM costs and charging delays. DCM costs comprises of the demand charges and BESS related costs. Charging delays are extra charging time users experience when both the BESS and grid-tie capacity supply the FCS demand, therefore resorting to reduced charging speeds. In this thesis a multi-objective approach for optimal BESS sizing is proposed to perform DCM at FCSs. Moreover, this framework uses the genetic algorithm NSGA-II to perform the design opti-

mization. Both the FCS model and design optimization are implemented in the python based simulation framework Mosaik and MOO framework Pymoo, respectively.

1.5.2. Previous work survey

This section gives a survey of the existing research conducted on BESS assisted FCSs. Moreover, research on related topics such as, grid impact due to EV charging, FCS demand, BESS sizing optimizations and BESS degradation are also given. With this survey a research gap is identified in the current literature that gives form to the thesis objectives.

A large portion of the current literature on how to mitigate the impact of EV on the distribution grids are focused on coordinated charging techniques and on integration of renewable energy sources (RES) with energy storage for slow charging applications in the distribution grid [21–24]. However, most of these studies do not directly translate to FCS applications due to the load demand differences and the contradiction in objectives the two possess.

The general impact of EV charging on the distribution grid is reviewed in study [25]. With the impact of FCS specifically on the distribution grid being studied in paper [26]. This study performed an analysis of a FCS located in a rural area in the US and concluded that FCSs causes higher transformer loading percentages, distorted demand curves, voltage flickering above permitted limits, and voltage drop below the allowable limit of 0,95 pu. To determine a FCS demand curve, the papers [26–28] carried out a Monte Carlo simulation using arrival distributions of EV battery capacities and state of charge (SOC) in combination with traffic densities to generate a load profile for a FCS. Unlike the other approaches based on the Monte Carlo procedure, paper [29] determines the expected power requirements of a FCS with an analytical probabilistic procedure. Here the battery size and SOC of the EVs are assumed as input independent random variables. It should be noted that to the author's knowledge there is no literature that included a FCS demand profile obtained from actual power measurements.

Due to these impacts on the distribution grid, papers [26, 27, 30] suggests the deployment of energy storage as a necessary action to be able to keep FCSs in the distribution grid in the future. The papers [6, 15, 28, 31–37] study the integration of energy storage in EV fast charging applications. In [34], an optimization on the energy and power rating is studied for energy storage applications at FCSs, however, this study was limited to a flywheel and super capacitor energy storage. Papers [31, 35, 37] all present a mixed-integer linear programming (MILP) formulation of these systems and performs a single objective optimization based on operational costs. In [31] and [32] the feasibility of adding frequency containment reserve (FCR) as second function for the BESS is investigated. Both papers concluded that FCR does not impact performance on the FCS and paper [31] obtained a 10% increase in revenues due to the additional grid services. However, it should be mentioned that the cost analysis is performed on one case that is sized specifically for FCR inclusion. Furthermore, this study also contained an analysis of the BESS degradation using a thermal model and concluded that a FCS does not have significant impact on the degradation. It should be noted, that the amount of cycles and cycle depth were not taken into consideration in the degradation model and the EoL criterion was set to 30%. In [15] and [6] a FCS sizing methods based on waiting times at the station is proposed. Remarkable is that both study suggests these waiting times to not exceed 5 to 6 minutes. In both study the waiting times are dependent on the stochastic EV arrival times, number of charging points available and size of the BESS implemented. Both papers performed a simple cost analysis on the sizing calculated and confirmed it's economical feasibility. In [38] a more extensive study was performed on the mitigation of EV congestion at FCSs by the amount of charging units installed based on waiting time and cost-benefit. In this paper the FCS service is modeled in terms of queuing and uses charging records in Japan to determine the future waiting times.

Currently to the author's knowledge the literature does not include studies performing a multi-objective optimization for BESS assisted FCSs. However, there are some literature studying MOOs for EV charging station planning and extensive literature on MOOs being applied to sizing for micro-grid and distribution grid applications. In [39] a multi-stage search strategy was implemented to realise a distribution network expansion planning incorporating the impact of EV charging stations. In [40] and [41] both authors used genetic algorithms for solving a multi-objective planning of EV charging station location challenges. Outside of EV charging, [42] proposed the use of genetic algorithms to solve energy unit commitment challenges. In the

studies performed in [43–49] all authors employed genetic algorithms (GA) to solve multi-objective energy storage related challenges for the distribution grid or micro-grid applications. Where operational costs, RES production, BESS lifetime and location were taken into consideration.

The general literature on battery degradation is also quite extensive, the following literature's investigates the degradation of BESS considering complex cycling profiles. In [50] the cycle-life degradation of Li-ion batteries due to solar photo-voltaic variability is studied. In [51], [52] and [53] the degradation of sodium-sulfur and Li-ion batteries respectively, are analysed for frequency regulation applications. In [54] the same assessment is performed for short term wind power applications. These literature all used a cycle counting method to determine the degradation and models based on accelerated battery ageing tests. A thermal based and throughput based model is presented in [55] and [56], respectively, however both models are based on battery operating conditions in automotive applications.

1.5.3. Research questions and objectives

From the literature it is clear that BESS is a feasible solution for reducing the peak power demands and demand charges at FCS. Currently, the literature contains mostly research on sizing optimizations based on one objective, either costs or waiting times. Whereas research into multi-objective optimizations investigating how both objectives impact the BESS sizing and limited grid-tie ratings is lacking. These aspects are important to FCS owners due to the large investments of BESS projects and the limited trade-off on waiting times (quality of service) at FCSs. Furthermore, the literature lacks studies on the effect that battery degradation might have due to the complex cycling for FCS applications. Lastly, all literature implemented a stochastic method based on petrol station data for estimating the FCS load profile. This gives a good example for a scenario where the activities at FCSs resembles petrol station activities. However, as suggested in [11] and [57], even in a fully adopted EV scenario this would never be the case since EV possesses multiple charging (tanking) options compared to conventional combustion vehicles (which only possesses one). This implies that the future scenario for FCSs are likely not to resemble current petrol station activities. With this thesis project energy measurement data are acquired from a set FCSs located in the Netherlands, from these data demand profiles are generated to perform the design optimizations and assess the feasibility of the proposed framework. In short the goal of this thesis is to develop a MOO framework using genetic algorithms for optimal BESS and grid-tie sizing at FCSs in order to reduce demand charges and charging delays.

To accomplish this goal the following research objectives serve as a guideline for the thesis.

Methodology

- A literature review is performed on EV fast charging, demand charge management, BESS and multi-objective optimizations.
- An analytical model was developed in Mosaik to assess the performance of a BESS assisted FCS based on power flow, charging delays and BESS lifetime.
- A genetic multi-objective optimization framework is formulated to optimize the design of the system with the objective of minimizing demand charges and charging delays. This optimization model is implemented in Pymoo and is scripted in python to communicate between the FCS model.
- The optimization results are compared against DCM without BESS for different study cases and the FCS performance assessed for a set of optimal solutions. All result plots are generated using Matplotlib in python.

Research Questions

- How to formulate a multi-objective optimization framework for optimal BESS and grid-tie sizing in order to minimize demand charges and charging delays at FCS?
 - How is the BESS modeled in the system?
 - How are the charging delays modeled in the system?
 - What objective functions are required for the proposed optimization strategy?

- How do FCS demand influences the optimal design?
- How do demand tariffs and BESS costs influence the optimal design parameters?
- What impact do the sizing framework have on the BESS lifetime?

1.5.4. Thesis Outline

Chapter 1: Introduction

This chapter gives a brief introduction to the current trends and developments of the main research domains of this thesis: electrical vehicles, fast charging and battery energy storage systems. Furthermore, the thesis description is given, a survey is performed on the related literature, the research gap is analysed, and research questions for this thesis defined.

Chapter 2: Literature Review

This chapter gives an extensive literature review on knowledge required to perform this research. This reviews EV fast charging state of the art, demand charge management, grid connected BESS and multi-objective optimizations.

Chapter 3: Fast Charging Station Model

This chapter gives a detailed description of the design choices for the proposed FCS model. This model comprises of 5 modules, EV demand, EMS, BESS, Lifetime model and quality of service model, and is implemented in a python based simulation framework Mosaik.

Chapter 4: Design Optimization Problem Formulation

This chapter presents the formulation for the design optimization problem. The objective functions and design constraints are given. Using the FCS model, a heuristic approach based on NSGA-II is proposed to solve this multi-objective design problem.

Chapter 5: Optimization & Simulation Results

In this chapter the proposed sizing framework is assessed using a set of numerical case studies. These case studies are presented, the optimization results are shown and analysed, and the performance of a set of optimal solution is studied.

Chapter 6: Conclusion and Recommendations

This chapter gives answers to the research questions, summarizes the main contributions of this thesis and gives recommendations on further research in this domain.

2

Literature Review

This chapter gives a review of the state of the art on the related topics. First, the most recent and forthcoming fast charging technologies and standards are discussed, as well as the most recent research on the demand and the challenges these face to the grid. Secondly, DSO related topics are discussed centered around the most recent developments in demand charges and DCM. Then, a number of grid-connected energy storage technologies are compared, applications, sizing considerations, and modeling concerns elaborated. Lastly, the focus is shifted to multi-objective optimizations, where genetic algorithms are explained and compared.

2.1. EV Fast Charging

In general EV charging stations are comprised of the following components, a charging cord, charging stand, plug attachment, power outlet, vehicle connector and protection system. There are two ways an EV can charge at these stations, either with an on-board or off-board charger.

On-board chargers are power electronics located inside these vehicles that permits owners to charge their vehicle everywhere where a standard AC connection is available. Nonetheless, these on-board chargers are limited by their power ratings due to the weight, space and cost constraints associated with EVs. Charging infrastructures that includes off-board chargers seek to extend these limitations by placing the power electronics outside the vehicle.

The IEC 61851-1 standard describes 3 modes for AC charging and one mode for DC charging. These modes are categorized by their connection types and charging speeds. Mode 1 chargers are standard one phase AC connections with charging powers up to 3.7 kW and are mostly used in domestic situations. Mode 2 are medium power AC connections between 3.7 kW and 22 kW and can be mostly found in semi-public locations. Mode 3 are high power AC connections larger than 22kW and are mostly only available in public locations. Lastly, mode 4 are high power DC connections larger than 22 kW and are located only in public locations such as FCSs [58]. An overview of these modes are presented in Table 2.1.

2.1.1. FCS configurations

Typically, FCSs are either installed as a single-stall unit or multi-stall stations. Each stall includes an off-board charger with a rating between 50 to 350 kW. Due to these high power ratings multi-stall stations can easily reach a total power rating of above 1MW per station. Examples of these high-power multi-stalls configurations are seen at Tesla supercharger stations [59] or Fastned stations in Europe[8].

Currently, there are two types of local distribution configurations for state of the art stations, the AC-connected

Table 2.1: IEC 61851-1 Charging Modes [58]

| IEC 61851-1 Charging Modes | | |
|----------------------------|----|-------------|
| Mode 1 | AC | < 3.7 kW |
| Mode 2 | AC | 3.7 - 22 kW |
| Mode 3 | AC | > 22 kW |
| Mode 4 | DC | > 22 kW |

and the DC-connected configurations. Both has its advantages and disadvantages, however due to the maturity of AC distribution technology paired with well established standards, the AC-connected variant is more widely implemented [60]. The AC-connected systems comprises of a step-down transformer and a three phase AC bus feeding multiple charging stalls. Each stall having it's own two stage AC/DC and DC/DC converters. Additionally, a RES or BESS can also be connected to the AC feeder via the same procedure, increasing the number of total converters required. However, employing AC-connected configurations increases system complexity and cost, while at the same time also decreasing the systems efficiency. In contrast to AC-connected systems, DC-connected configurations include one central front-end AC/DC converter followed by a LV rectifier stage or solid state transformer (SST) (that provides the rectification), a voltage step-down and isolation [60]. This combination introduces a DC bus where each stall, RES and BESS can be interfaced using only a DC/DC converter. This reduces the number of converters in the system and increases efficiency. Furthermore, replacing bulky line-frequency transformers with smaller high frequency SSTs reduces the component sizes significantly. This introduces better utilization of station site and further increases power efficiency. Despite it's advantages, DC-connected systems possesses unique challenges in DC metering, protection and it's lack of established standards [60]. A diagram of both configurations is presented in Figure 2.1.

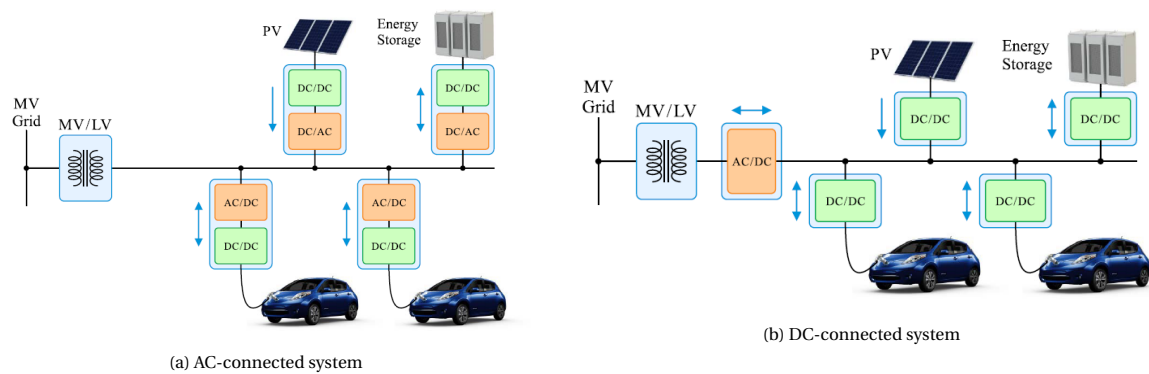


Figure 2.1: Electrical configuration for FCSs [60]

2.1.2. State of the art technology and standards

The IEC-62196 standard defines four different EV plug configurations developed by various governing bodies related to EV fast charging. These standards are, GB/T (120 kW), CHAdeMo (400kW), CCS Type 1 (120kW) and CCS type 2 (175 kW) [61]. In addition to these four standards, Tesla also possesses its own proprietary charging standard with charging capabilities up to 135kW. However, most Tesla EVs in Europe comes included with the CCS type 2 charger to provide 175kW charging [62]. Figure 2.2 gives an overview of these five charging standards, a diagram of their respective socket and electrical ratings. From this it can be seen that the CHAdeMo standard enables the highest power rating of 350kW.

| Standard | CHAdeMo IEEE 2030.1.1 IEC 62196-3 (Configuration AA) | GB/T GB/T 20234.3 IEC 62196-3 (Configuration BB) | CCS Type 1 SAE J1772 IEC 62196-3 (Configuration EE) | CCS Type 2 IEC 62196-3 (Configuration FF) | Tesla |
|-----------------|---|---|---|---|---|
| Coupler Inlet |  |  |  |  |  |
| Maximum Voltage | 1000 V | 1000 V | 600 V | 1000 V | 410 V |
| Maximum Current | 400 A | 250 A | 200 A | 200 A | 330 A |
| Available Power | 400 kW | 120 kW | 150 kW | 175 kW | 135 kW |

Figure 2.2: An overview of the standardized EV sockets capable of DC charging [61] [62]

The limitations on obtaining higher charging speeds are primarily due to physical limitations on cables weight and thermal stresses [63]. Ongoing research are investigating methods on overcoming these constraints, the most promising candidates are cable liquid cooling and wireless charging. Wireless charging or contact-less charging uses inductive power transfer (IPT) technology to transfer energy

between loosely coupled charging-pads. Although still in the research phase, this technology is becoming increasingly more accepted and can make great contributions to autonomous charging or help lift physical cable limitations. [63].

Another EV development accelerating research on higher charging speeds are electric trucks. Due to this demanding modality, en-route FCSs capable of charging above 1MW are needed to make regional transportation and long distance travel for electric trucks feasible [5]. Charin is a collaboration concern between multiple parties within the EV industry and is currently developing this charging standard of 1MW for EVs. The standard is called high power charging for commercial vehicles (HPCCV) and is expected to be delivered by 2021 [64].

2.1.3. Load demand

In addition to the number of stalls, FCS demands on a session scale are highly dependent on the distribution of EV arrival times, SOC and model type. Various vehicle models possess different charging power capabilities, time of arrival influences the daily distribution of charging sessions and the SOC of EVs at arrival impacts the power and duration of each individual session [15]. Figure 2.3 displays how the charging speed capabilities varies for different EV manufacturers at 175kW chargers. Moreover, it is visible how the vehicle SOC significantly impacts the charging speeds. As the SOC increases during charging the speed decreases, with a safety limit included around 80%, indicating the end of the charging session. This limit is imposed to avoid overcharging and accelerated battery degradation of the EV [65].

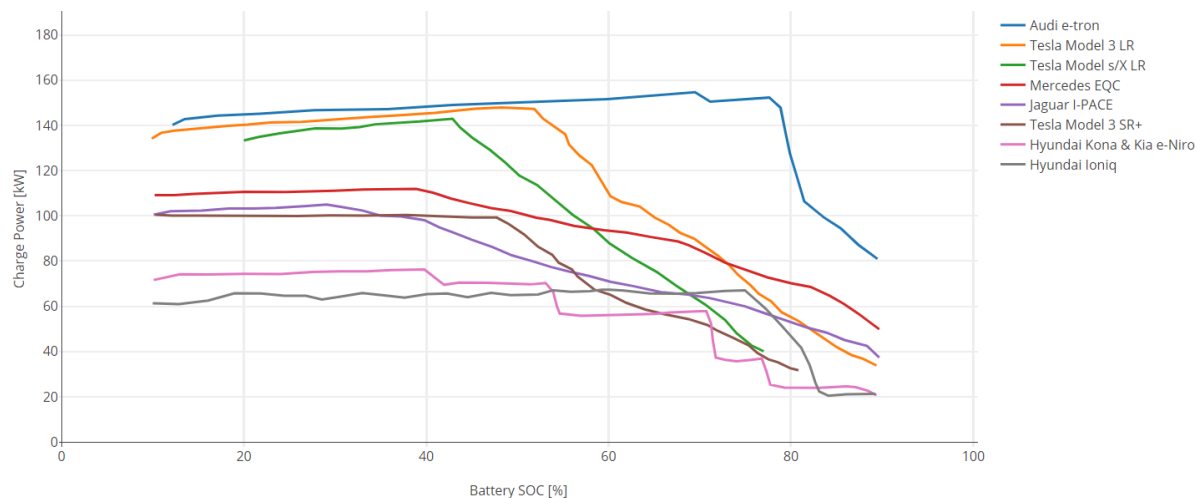


Figure 2.3: Charging speed curves at 175kW chargers for different EV models [65]

In contrast to domestic charging, the FCS demand on a daily scale differs significantly. A greater portion of FCS activities are mainly concentrated around the center of the day and at the end of the working hours on weekdays [66]. This is contrary to domestic slow charging that occurs overnight when owners are at home. Figure 2.4 displays an example of the daily charge session distribution at a Fastned FCS, which gives us an idea of the shape of daily demand profiles.

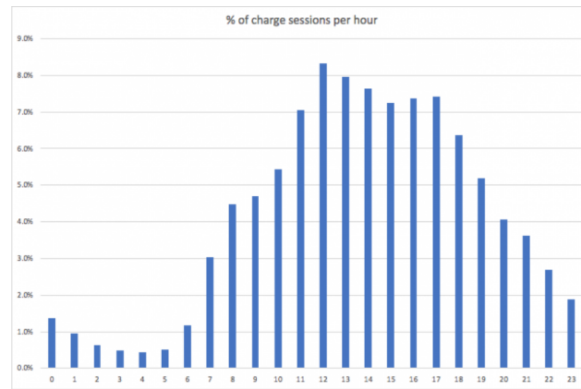


Figure 2.4: Distribution of fast charging sessions throughout the day (24 hours) at Fastned stations [66]

Due to the lack of actual FCS demand data various studies in literature resort to stochastic methods such as Monte Carlo simulations to generate a FCS demand profile from petrol station data [67]. These methods generate good approximations of the power demand in a scenario where FCS activities would resemble petrol station activities. Figure 2.5 shows an example of a daily demand profile generated for weekdays and weekends. Nevertheless, various studies comparing the use patterns at FCS versus petrol stations opposes this scenario [57]. Despite the longer charging (tanking) duration of EVs, the activities at FCSs will most certainly not resemble petrol stations in the future. This due to the additional charging options EVs possess (such as home and workplace charging) compared to conventional combustion vehicles (with only one) [11].

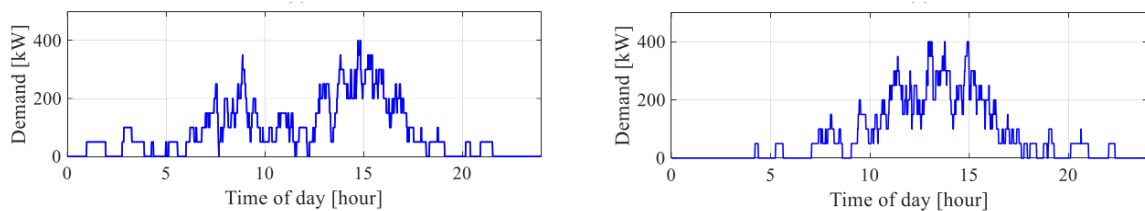


Figure 2.5: A weekday (left) and weekend (right) FCS demand profile generated from petrol station data [37].

On a yearly basis, factors such as seasonal differences in usage and temperature primarily influences the demand. During vacation periods for example, freeways are more occupied due to traveling and likewise, during the wintertime people tend to travel more by car instead of using other transportation methods. Furthermore, extreme temperatures also impact charging speeds and storage capacities [8]. Further introducing complexities to predicting a proper FCS's demand profile. Regardless of this, the period with the highest charging activities at FCSs is around Christmas (December and January) [68]. This is due to a combination of cold weather and increase in holiday travels.

For other fast charging applications, the load demand can be completely different. These demands will likely correlate with the usage patterns of the station's intended EV modality [11]. Electric busses for example, to their traveling schedules and taxis to the distance between various points of interest within a city such as airports, city center, tourist attractions etc.

2.1.4. Impact to the distribution grid

Compared to slow domestic charging, FCS loads has less detrimental effects on the distribution grid. This is due to the fact that FCSs or fast charging points are mostly connected on a robust section of the MV distribution grid [8]. However, in weaker (rural areas) or highly congested areas of the grid, the high pulsating demand of large FCS loads can still pose negative effects to the grid. This high pulsating effect can cause distorted and increased peak demand of the distribution transformer loading. Moreover, in addition to voltage drops, voltage flickering can be introduced to the system, affecting sensitive loads further down the grid [26]. Figure 2.6 shows an example of these effects on the distribution grid being caused by a 3MW FCS located in a rural area inside the US. It shows an increase of 9% in peak transformer loading and an additional voltage

drop of 2%, exceeding the allowable limit set by the national electrical code in the US (0.95 pu).

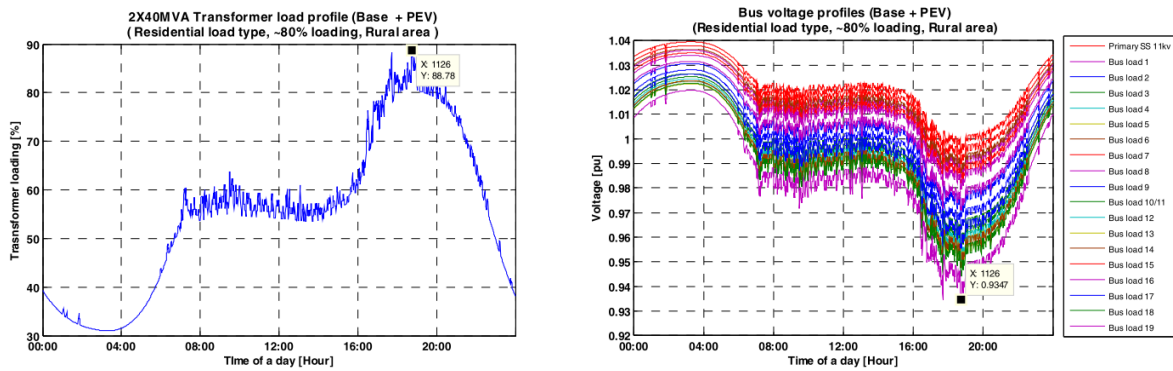


Figure 2.6: Impact of large FCS on distribution transformer loading (left), and system bus voltage (right) [26].

Furthermore, FCS also introduces challenges to the grid-planning of DSO's. In areas farther from a business district, including rural areas, finding sufficient transformer capacity for FCSs is a frequent issue [69]. Likewise, even in dense urban areas a connection to the MV grid is not always directly available [5]. Both can result in costly network upgrades for the DSOs and FCS owners.

2.2. Demand Charge Management

The main objectives of a distribution system operators (DSO) is to deliver reliable and low cost grid operation to it's customers. To achieve these objectives the following value drivers can be defined:

- Grid component investments
- Capacity utilization factor
- Component lifetime
- Operation cost (incl. resistive losses)
- Instrumentation and automation efforts

In most cases capacity on the grid is sufficient, this is attributed due to fact that in practice the grid capacity is usually oversized with safety margins taken into design. However, with the rapid growth of EV and RES, capacity might not stay sufficient anymore and congestion can occur in the distribution grid. Grid congestion refers to a situation where the demand active power transfer exceed the transfer capability of the grid (design parameters). This transfer capability is limited by the following constraints, voltage limits, thermal limits of cables and transformers, MVar bands or protection settings [70]. With the FCS impact analysed in section 2.1.4, these constraints are also relevant for FCS applications.

Congestion mitigation is generally associated with two strategy types, type 1 is the increase transfer capacity, type 2 is the use of coordinated throughput deferral or curtailment strategies [70]. Type 1, can be implemented by simply upgrading the distribution infrastructure with a larger capacity and type 2 with coordinated EV charging, active power curtailment, peak shaving, congestion markets etc. Due to the large investments associated with type 1 strategies, type 2 is usually first investigated.

2.2.1. Demand charges

DSO tariffs have significant impact on operational costs of FCSs. The electricity pricing of a DSO consists of 2 main variables, the consumption charges and demand charges. The consumption charges is a kWh fee for the amount of energy transported by the grid-connection over the monthly billing cycle. The demand charges is the fee for the maximum peak power measured (in kW) within a monthly billing cycle. These demand charges can account for more than 90% of a monthly electric bill of a FCS [4]. Depending on the geographical location and utility jurisdictions, commercial customers are subject to different demand charges by their DSO. For example, in the US half of the utilities have a demand tariff above \$15/kW. These rates ranges from \$2/kW all the way up to \$90/kW. States where EVs are more common (such as New York and California) tend to have high demand charges, in the extreme case of New York City (NYC) demand tariffs can be up to \$50/kW [14]. Figure 2.7 depicts the differences of demand charge rates by utility service territories in the US.

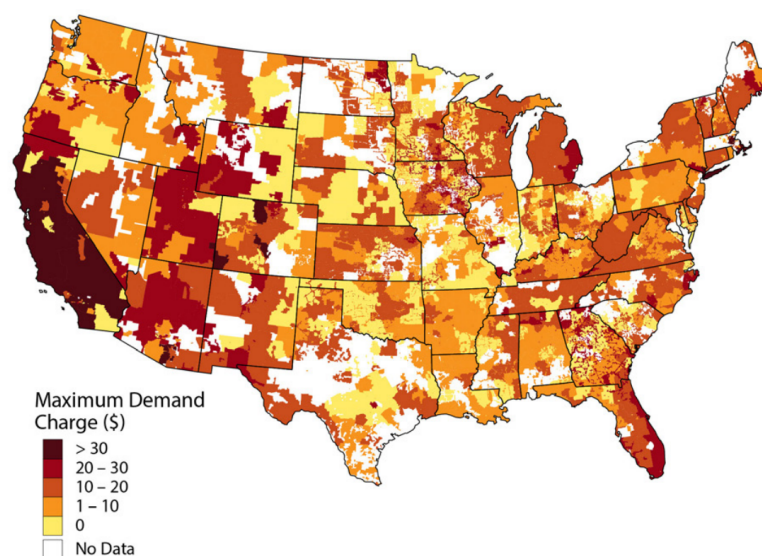


Figure 2.7: Maximum demand charge rates by utility service territory in the US [14]

Similarly to the US, the demand tariffs in Europe also differs per region. With countries such as the Netherlands having rather a low demand tariff of around €3/kW, while Switzerland can have demand tariffs of up to €14.4/kW. To avert the resulting high demand charges in these regions, DCM can be performed in order to decrease the peak demand.

DCM is a frequently used method at commercial and industrial facilities to reduce monthly demand charges [71]. This can occur in different ways, the simplest method is to simply perform demand side management. Demand side management entails the rescheduling of consumption or curtailment of demand. However, this is not desirable in commercial applications since customers comfort is interrupted [72]. Another method is to perform BESS assisted peak-shaving. In this behind the meter application the BESS serves as a buffer between the grid and load, shifting the demand during peak times to un-peak times [73]. Even with the large investment costs of BESS, the study in [74] suggested a break-even demand tariff of around \$9/kW for most BESS supported peak-shaving projects in North-America before 2016. Moreover, based on the cost reduction of Li-ion batteries, this could fall to \$4 to \$5 per kW by 2020.

For FCSs DCM can be performed to either reduce the demand charges at a under-utilized station or to extend the capacities at highly-utilized stations. Consequently, DCM also reduces the impact FCSs can have on the distribution grid.

2.3. Grid-connected Energy Storage Systems

This section gives a literature review on grid-connected energy storage systems. The focus is laid on the lithium-ion technology where the performance and degradation modeling are reviewed along with various sizing methods.

In general grid connected energy storage systems are energy storage's coupled to the grid with the purpose of providing ancillary services such as peak-shaving, voltage control, frequency response, controlled islanding, day ahead optimization etc. [75]. The energy storage component of these systems can be categorized into 3 storage classes, electrical, electrochemical and mechanical. Figure 2.8 gives an overview of these storage classes with their corresponding subgroup of technologies.

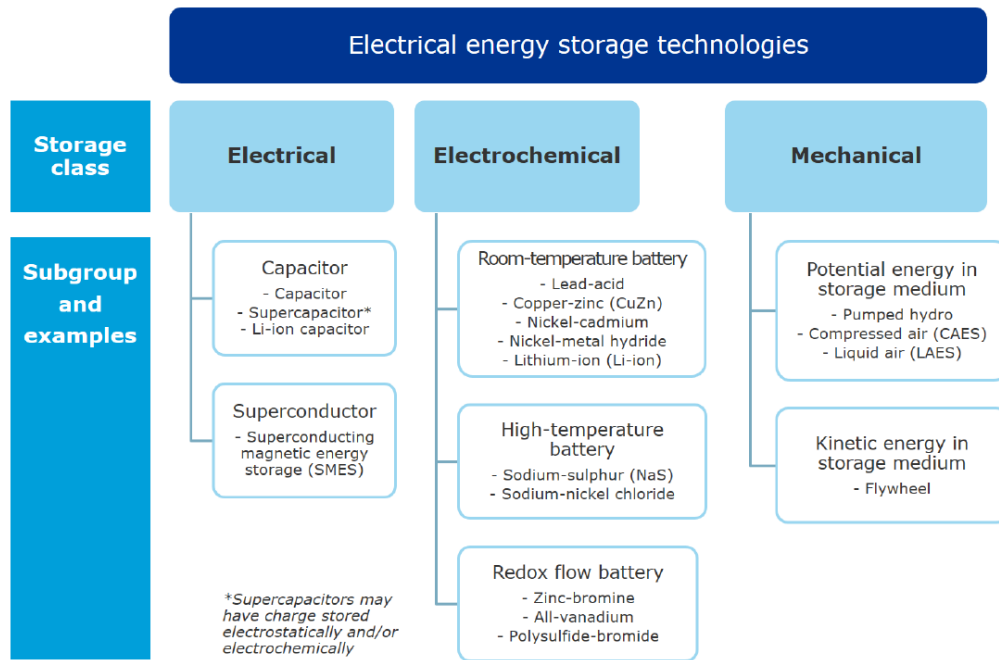


Figure 2.8: Various Energy storage technologies [73]

Mechanical

The 3 most common mechanical storage types are flywheels, pumped hydro storage (PHS) and compressed air energy storage (CAES).

Flywheels store energy by speeding up a low friction rotor. This way the energy is stored into motion. Flywheels are normally used for short period discharges and are good for power quality improvement. However, they have low life expectancy [73].

PHS has the highest number of installed capacity around the world. This type of energy storage stores energy by pumping water from a lower basin to an upper basin. When the energy is required, the water is released and flows back down through turbines producing electricity. Although PHS can store large amounts of energy, the costs tend to be high and large spaces and specific geographical locations are required for PHS projects [73].

CAES technology uses an electrical motor to store energy in the form of compressed air inside a volume. However, this technology requires a large amount of space for high energy amounts. Similarly, liquid air energy storage (LAES) stores energy by liquefying air into tanks and releases this stored energy by expanding the liquefied air in a turbine. In contrast to CAES, LAES does not have geographical constraints [73].

Electrical

Electrical energy storage types utilize either electric or magnetic fields for storing energy. Capacitors store energy in the form of electric fields between two oppositely charged plates and superconductors store en-

ergy in the form of a magnetic field around a superconducting coil. Both has fast responding characteristics and are good for power quality and suppression of intermittency of RES. However, they have low energy densities and are prone to fire explosions [73].

Electrochemical

Electrochemical type storage stores energy by converting electricity into a chemical form and the reverse process when the stored energy is discharged. Electrically charging occurs when an externally applied voltage is higher than the open circuit voltage of the battery. The most common technologies available are lead acid, nickel cadmium (NiCd), sodium sulphur (NaS), lithium-ion (Li-ion) and many more. Due to this class's fast response time, fast discharge time, high power capability, high efficiency, cost and scalability, they are considered the most versatile technology for grid applications [75].

A recent development in the electrochemical class, are Redox flow batteries. These batteries uses two electrolytes as energy carriers. The two electrolytes are divided by an ion-selective membrane separator, which allows selected ions to pass and complete the chemical reaction during charging and discharging. This process allows for the decoupling of the energy capacity and power capability of flow batteries. The capacity correlates with the volumes of active materials, while the power capability determined by the membrane surface area. [75]

A grid connected BESS utilizes a electrochemical energy storage technology. In addition to the energy storage component, a grid-connected BESS includes a system coupling and grid integration section as depicted in Figure 2.9. Battery & storage systems are defined as the parallel connection of several packs (or racks) and these packs contain cells which are grouped into modules. These modules are then connected in a particular series/parallel configuration depending on the systems electrical specifications. Included in this, a thermal management system (TMS), energy management system (EMS) and depending on the grid type a DC/AC power converter. The TMS regulates the modules temperature within the safety margins and the EMS performs energy management for the battery system based on a dispatch program. Both of these components receives an aggregated module level information from the battery management system (BMS). In addition to module state information, the BMS are essential to avoid energy unbalances between modules and provide protection against hazardous and inefficient operating conditions such as under or over-voltages [75]. In most cases the battery & storage system block receives it's power from a DC/AC converter that support bi-directional power flow between the bus bar and the battery. Depending on the voltage rating and current type of the bus bar, a DC/DC stage is present. Together these components are usually grouped inside a container housing, equipped with fire safety protection systems and cooling systems [73]. Furthermore, a system coupling is present in the form of a step-down/up transformer between the grid and power converter to integrate other loads and RES connected to the grid. For micro-grid applications these grid integration components are mostly located before the system coupling.

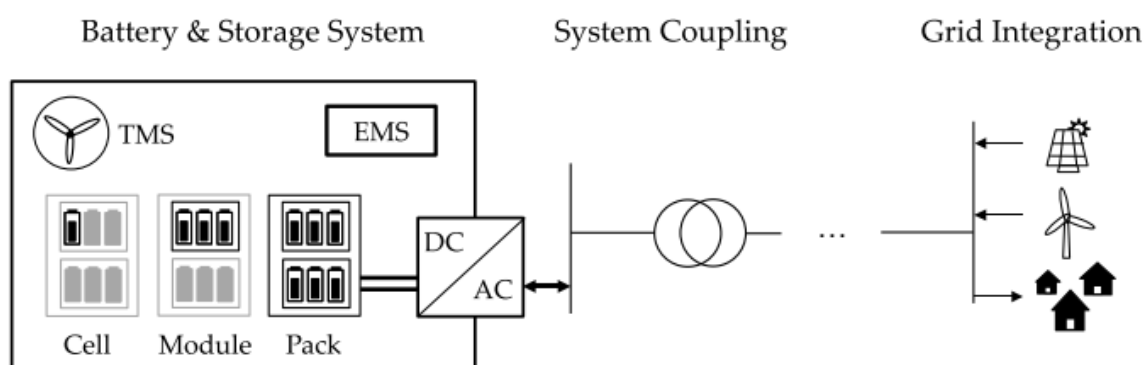


Figure 2.9: Simplified schematic of a BESS, power electronics coupling and grid integration [19].

2.3.1. Lithium-ion based batteries

Analysing the core energy storing technology is essential to understanding the performance and degradation characteristics of the complete energy storage system. Lithium-ion batteries (LIB) are rechargeable batteries where the electrodes are composed of lithium intercalation materials, in which the lithium ions are intercalated between layers of the electrode material, e.g cobalt oxide or graphite. This yield to a reversible process [75]. The family of LIB chemistries are broad and each of them has it's own characteristics and limitations. For grid applications of LIB there are 3 dominant chemistry's frequently considered, NMC, NCA, LFP and LTO chemistries.

Lithium Nickel Manganese Cobalt oxide batteries also referred as NMC batteries provides a good trade off between lifetime, safety and energy density when compared to the other chemistry's. Due to this, NMC batteries are among the most used chemistries in automotive and portable applications which also drive down it's cost. The automotive NMC batteries are expected to be used in grid applications as second life batteries coming from the automotive industry.

The nickel cobalt aluminum oxide (NCA) chemistry offers a high volumetric energy density at the cost of cycle life performance and safety. However, due to it's high energy density this chemistry is also attractive for automotive applications attributing to a competitive cost compared to NMC [75].

The lithium iron phosphate (LFP) chemistry is highly suitable for grid services. This due to it's long lifetime, relatively low cost, high safety and high power capabilities. Moreover, the low voltage swing of LFP batteries allows for cheaper and efficient power electronics converter design. The drawbacks of LFP batteries are their reduced energy density compared to NMC and NCA. This is also explain why this chemistry is less frequently found in automotive applications [52].

The lithium titanate oxide (LTO) chemistry is seen as good candidate for future grid applications. The material further outperforms LFP in high lifetime and safety. However, due to it's recent entrance in the battery market, the chemistry remains costly compared to the other types. Table 2.2 shows an overview of the characteristics comparison between these chemistries.

Table 2.2: Performance comparison of lithium-ion chemistries found in stationary applications [19]

| Characteristic | NMC | NCA | LFP | LTO |
|----------------|-----|-----|-----|-----|
| Cost | ++ | + | - | -- |
| Safety | - | -- | + | ++ |
| Lifetime | - | - | + | ++ |
| Energy Density | + | ++ | - | -- |

2.3.2. Ageing and lifetime

The ageing of batteries lead to capacity decrease and power fading. Regardless of the chemistry, the ageing mechanism of lithium-ion batteries are complex, highly dependent on the operating conditions and originates from multiple processes. In general these complex process are divided into two ageing mechanisms, the calendar-life degradation and cycle-life degradation.

The calendar-life degradation occurs when the battery storage is idle and is mainly driven by side reactions resulting from thermodynamic instabilities of the applied storage chemistry [19]. Moreover, the rate of this degradation is dependent by the idle time, SOC and ambient temperature. This degradation accelerates when the SOC and temperature values are high [52].

The cycle-life degradation are kinetically induced effects such as volume or concentration variations resulting from usage of the battery storage. This can be either characterised in the form of energy throughput or more commonly in the total number and depth of discharge (DOD) of cycles being performed by the battery. In general, the cycle-lifetime is not constant, but increases as the DOD decreases. The total amount of cycles a BESS can perform might be several times higher for a DOD of 10% than for 80%. This aspect is important for applications with high amount of micro-cycles, making multiple micro-cycles that are super positioned over a main cycle to degrade the battery much less than one main cycle [75]. Moreover, the rate of degradation is dependent on operating conditions such as average SOC-level and the ambient temperature during each cycle [52]. Where once more, high average SOC-levels and high temperatures accelerates this degradation. It should be also noted, that some literature might mention high C-rates as a possible culprit for accelerated cycle degradation, however studies has shown, these accelerated degradation to be indirectly caused by high

ohmic heating, and therefore caused by temperature rise [56].

By summing up these two degradation factors together one can determine the expected lifetime of the BESS during design. Because the capacity fade occurs significantly faster than the power capability fade, the lifetime of a BESS is defined as the time it takes for its capacity fade to reach the end of life (EoL) criteria [76]. This EoL criteria can be different for each application. However, the most commonly used EoL is 80% taken from reliability standard IEC62660-1 for li-ion batteries in EV applications. For this reason when a BESS being dimensioned, it is essential to determine the lifetime of the BESS for the specific application [73].

2.3.3. Grid-connected Applications

In the modern grids, BESS can interact with the grid and load in various ways to perform its intended task. These tasks can be categorized into several grid-connected application families, the ancillary services, the behind-the-meter, the energy trade and the grid-support families [19].

Ancillary services uses grid-connected BESS to retain the balance between the power generation and load at all times. This is mostly applied in frequency regulation, black start and droop control. Furthermore, these applications usually possess regulatory constraints (such as market profit schemes or frequency regulations) that should be well analysed in order to achieve profitable BESS operation.

Behind-the-meter applications are frequently found at commercial and industrial users and are mostly centered around either reducing the electrical bill or comply to a particular DSO regulation. Examples of such applications are, PV-BESS systems, peak-shaving and ramping control.

The energy trade applications are mostly performed by enterprises and aims at buying/selling of electricity according to market fluctuations. Lastly, the grid-support family entails applications that serves to defer or completely avoid costly grid reinforcement measures. Herein falls, voltage support, EV-grid integration and balance management [19]. An overview of these application families is given in Table 2.3.

Table 2.3: Various BESS tasks classified into application families

| Application Family | Application | Stakeholder |
|--------------------|----------------------|------------------|
| Ancillary Service | Frequency Regulation | Enterprise |
| | Black-start | Electric Utility |
| | Droop control | All feeders |
| Behind-the-meter | PV-BESS | Private sector |
| | Peak-shaving | Industry |
| | Ramping control | RES feeders |
| Energy Trade | Arbitrage | Enterprise |
| Grid Support | Voltage Support | DSO/Enterprise |
| | EV-Grid integration | DSO/Enterprise |
| | Balance Management | DSO |

2.3.4. Sizing

To design and size a grid-connected BESS to perform a desired task, a study done in [75] lists the following key performance indicators (KPIs) as the most important ones to consider:

- Cost per total energy throughput [€/kWh]
- Cost per power capability [€/kW]
- Energy capacity [KWh]
- Power capability [kW]
- Discharge time [min]
- Charge time [min]
- Energy efficiency [%]
- Lifetime (in the specified application) [year]

Noticeably, volume, weight and thermal characteristics are omitted from this list. This because in most grid-connected applications these omitted characteristics do not pose challenges to the design. Space is often not an issue and ambient temperature conditions are typically regulated at around 25 °C with the TMS.

The typical sizing method for a BESS occurs with the help of a so-called duty cycle analysis [75]. Firstly, the use cases need to be identified and corresponding power profiles either obtained from experimental data or formed based on estimations. One use-case or several use-cases are then selected to represent the average usage or worst case usage over an average day, week or month. This average will be the baseline for the performance evaluation and lifetime prediction. From this analysis the following important components are determined:

- **Energy requirement**

From the energy profile the largest energy content should act as a baseline for the minimum requirements for the energy capacity

- **Power requirement**

From the power profile continuous and peak (dis)charge power can be extracted as well as other measures related to the electrical ratings of the storage and interfaced power electronics.

- **Expected degradation**

For a simple duty cycle analysis only the number of cycles for a certain period is extracted. However, the idle time and temperature can also be determined to get a better estimate of the lifetime.

These values are then used as a starting point for the iterative process of evaluating different commercially available solutions in terms of performance, lifetime and cost. For applications with simple duty-cycles this method can be done by hand calculations. However, for complex duty-cycles model based-dimensioning tools are required. Model based-dimensioning and validation of BESS utilizes BESS models to simulate the duty cycle to obtain the performance, lifetime and cost [75]. This method is often used by battery manufacturers and battery system integrators to validate their battery designs.

2.3.5. Modeling

Depending on the required level of detail a BESS can be modeled in different ways. In general a battery model consists of 3 sub parts, the battery management model, the battery performance model and the battery lifetime model as shown in Figure 2.10.

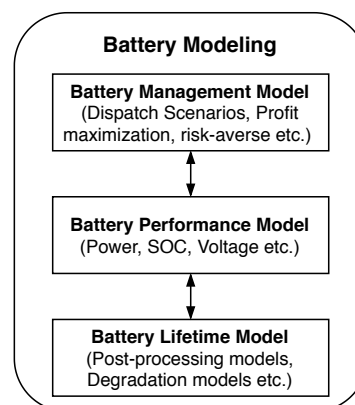


Figure 2.10: A generic battery modeling framework for economical assessments [77].

The battery management model aims to generate the dispatch signals than can manipulate the battery performance based on the desired task. This block usually includes the EMS, which follows a dispatch algorithm that charges or discharges the BESS at the desired moments.

The performance model describes the technical performance and the physical limitations of the battery system. This can be measured by the state variables like SOC, (dis)charge power, voltages etc. Depending on

the complexity level and objective there is a variety of ways to model the performance of a battery. Models often used to determine physical aspects and properties of batteries are, the electrochemical models or electrical model. These models mimic the batteries behavior by simulating the chemical processes that occur inside the battery or uses electrical circuits, respectively. In terms of long-term economic analysis of battery systems, analytical models which describes the battery at a higher level of abstraction are good enough. In such cases only several variables like SOC, charging/discharging power, efficiency and energy capacity are required in the performance model [77].

The battery lifetime model predicts the capacity decrease and power capability fade for a certain duty cycle. This way either the expected lifetime or state of health (SOH) of a battery can be simulated. Lifetime modeling is of high importance for a reliable BESS sizing and cost estimation. Moreover, modeling the performance degradation during it's lifetime can aid in the selection of the optimal EMS scheme. There are two approaches to lifetime modelling, the post-processing and online approach.

The online approach combines the performance model with a lifetime model by updating the performance parameters as the ageing processes progresses in time. Typically post-processing models are very accurate, however, they require complex performance model types such as electrochemical or electrical models that increases computational time [76].

The post-processing approach provides only information about the remaining lifetime after a certain period without updating the performance model. This approach is based on the concept of incremental loss of lifetime caused by the operating conditions and can also be divided into two sub-groups, the throughput counting models and cycle counting models. The throughput counting models simply counts the amount of charge (Ah) or energy (Wh) that passed through the battery and compare this to the maximum throughput value the battery can handle before reaching the EOL criterion. The cycle counting models are more commonly used and are based on the assumption that the magnitude and number the cycles determines the fraction of consumed lifetime. Henceforth, the total battery degradation is modeled as a sum of degradation from all cycles [78]. The higher the magnitude and the number of cycles the faster the battery reaches the EOL criterion. This way cycle counting models obtain higher accuracy than throughput models. Nevertheless, both post-processing models significantly reduces the complexity and computational time required when compared to the online approach [76].

A commonly used cycle counting model for applications with complex cycles is the Rain-flow cycle counting method. The algorithm is a generic cycle counting technique that can extract the cycle and range information from an irregular time series data. Originally used in mechanical engineering for the estimation of material failure by counting fatigue cycles [79]. A slightly modified algorithm can be implemented to extract the frequency and DOD of cycles that a BESS has gone through within a given SOC profile [50]. One important assumption that the algorithm adopts from the Palmgren-miner rule, is that the sequence of cycles does not influence the lifetime of the battery. For example, a high DOD cycle followed by a low DOD cycle has the same impact on the lifetime as a low DOD cycle followed by a high DOD cycle [53]. Utilizing the rain-flow cycle algorithm together with a cycle-life curve, the expected lifetime of a BESS can be estimated using the flow-chart in Figure 2.11. This cycle-life curve can be either obtained from models available in literature such as [53] or obtained from empirical cycle-life curves or calendar-life curves available from battery manufacturers. Figure 2.12 shows an example of a cycle-life curve and calendar-life curve generated from the LFP lifetime model proposed in [53]. A more detailed explanation of the rain-flow cycle counting algorithm procedure is included in appendix A.

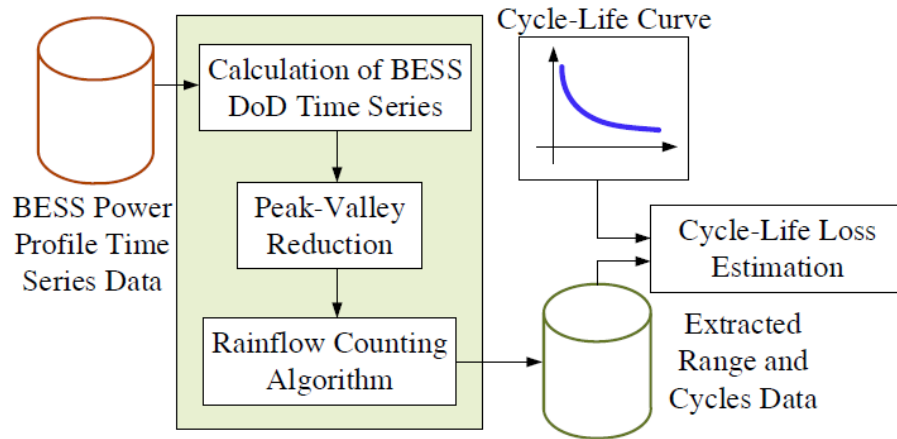


Figure 2.11: A flow-chart on how BESS lifetime estimation is performed using Rainflow cycle counting algorithm [50].

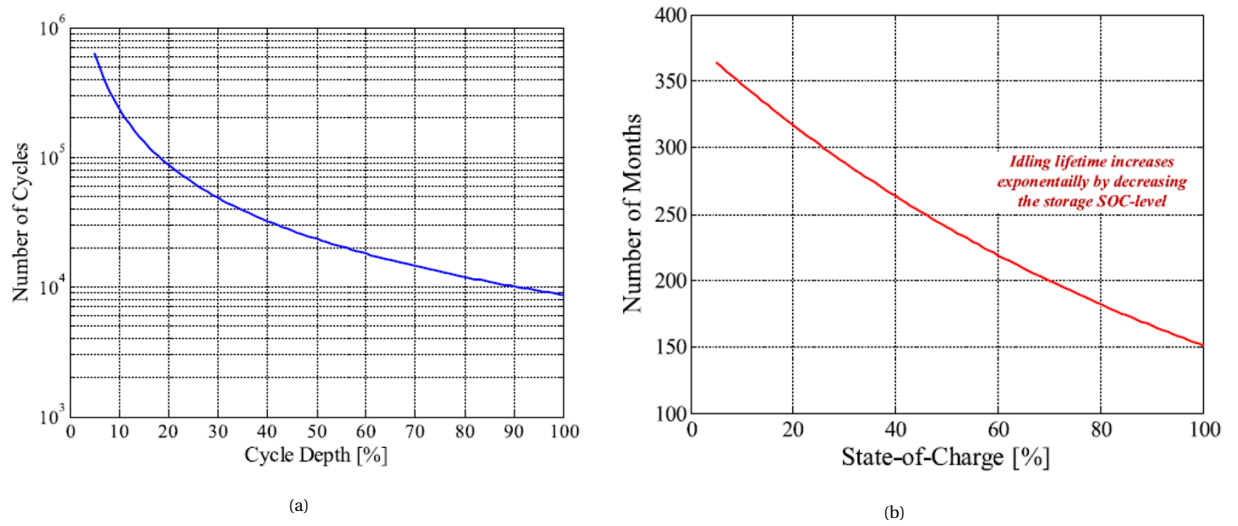


Figure 2.12: (a) Cycle-life curve, (b) Calendar-life curve, Both valid for 25 °C and 20% EoL criterion [53]

2.4. Multi-objective optimizations

This section contains a literature review on multi-objective optimizations. The definition to multi-objective problems is presented and the different solving methods reviewed. Due to the scope of this thesis, the focus is further laid on genetic algorithms, with the attention specifically to the NSGA-II algorithm.

2.4.1. Multi-objective problems

In general terms, the optimization process seeks to minimize or maximize the value of a function by finding the values of the variables from a given domain. The goal is to find values of the variables which are optimal with respect to one or more objectives while respecting all the constraints.

Multi-objective problems (MOPs) are optimization problems that involves more than one competing or conflicting objective functions subject to equality and inequality constraints. Most real-world problem searches and optimization problems involves multi-objectives. The problem formulation in it's simplest form is given by equation (2.1).

$$\begin{aligned}
 & \underset{x}{\text{minimize}} && f_1(x), f_2(x), \dots, f_M(x) \\
 & \text{subject to} && g_j(x) \leq 0, \quad j = 1, 2, \dots, J, \\
 & && h_k(x) = 0, \quad k = 1, 2, \dots, K, \\
 & && x_i^L \leq x_i \leq x_i^U, \quad i = 1, 2, \dots, N
 \end{aligned} \tag{2.1}$$

This formulation represents a MOP with M objectives, N variables, J inequality constraints and K equality constrains. Additionally, the lower and upper boundaries (x_i^L and x_i^U) for each variable x_i are also defined.

There are two types of methods available to solve MOPs, the preference based procedure and the ideal procedure. The preference based procedure can be implemented using both the conventional weighted formula approach (user-defined parameters) or the lexicographic approach (ranks in order of priority) [80]. Both approach formulates the MOP into a single objective problem, giving the possibility of solving these problems using the more classical single objective optimizers such as linear programming, dynamic programming or non-linear programming. However, high-level decision information is required prior to the optimization in order to determine the weighing factor of each objective. In most real life MOPs these high level information are not usually known beforehand.

The preference based procedure can be explained in the 3 steps depicted in Figure 2.13:

- Step 1: Using high level information a weighing factor vector w is determined for every objective function.
- Step 2: The preference vector w is then used to formulate the MOP into a single objective problem.
- Step 3: This single objective problem can then be optimized using a single objective optimizer to find the optimal solution.

The ideal method is implemented using the Pareto approach. Named after the 19th century engineer, economist and sociologist Vilfredo Pareto, this approach searches for as many feasible solutions as possible and returns with a ranking procedure a set of non-dominated solutions to the user. Non-dominated solutions contains a set optimal solutions where there are no one solution better than the other [81]. However this method requires the use of the more unorthodox metaheuristic optimizers such as evolutionary algorithms, particle swarming optimization (PSO), simulated annealing, and ant colony optimizations [82]. These optimizers solve MOPs by efficiently exploring the search space with the goal of finding near-optimal solutions using less computational effort. Hence, they do not guarantee that a global optimum can found, but rather give a good approximation of this.

Figure 2.14 gives a depiction of the two steps procedure for the ideal method:

- Step 1: Calculate multiple trade-off optimal solutions with a wide range of values for the objective functions using a MOO algorithms. These wide range of optimal solutions is a Pareto front.
- Step 2: Once the Pareto front is obtained, choose one of the solutions using high-level information.

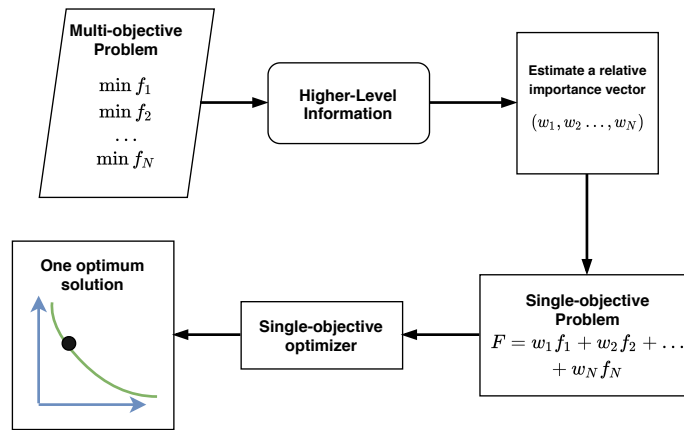


Figure 2.13: Flowchart for the MOO preference-based method [80].

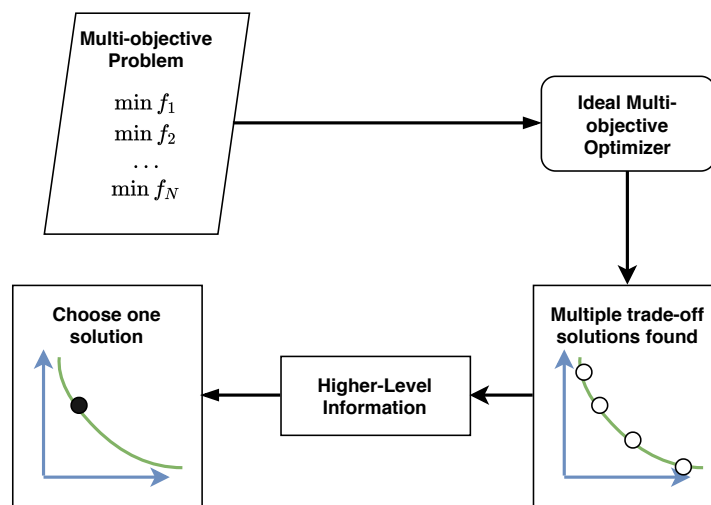


Figure 2.14: Flowchart for the MOO ideal based method [80].

2.4.2. Genetic algorithms

Evolutionary algorithms (EAs) are a set of algorithms that can solve multi-objective problems by applying nature's evolutionary principles to search for a set of Pareto solutions. What makes EAs unique, is its ability to find multiple optimal solutions in one single run [80]. These algorithms all start by initializing a set of solutions (defined as a population) and proceeds by performing an iterative loop. In each iteration the EAs, firstly, evaluate the current population of solutions and selects a new population based on a certain selection criteria. Secondly, it determines whether a set of optimum solutions are found based on an ending criterion. Lastly, if this ending criterion is not met, the existing population are then combined to generate a new set of solutions and the process is repeated.

Genetic Algorithms (GAs) are a subset of EAs that construct it's population using genetic like operators such as selection, crossover and mutation [80]. In general the process of a GA can be described in 5 steps:

- **Encoding:** In this step the points in the parameters space get transformed into bit stream representations called chromosomes.
- **Fitness evaluation:** The fitness of each members are evaluated according to the objective functions.
- **Selection:** Depending on the fitness evaluation of the solutions the proper solutions are selected for the next generation.
- **Crossover:** This step is unique to genetic algorithms, since it exploits the potential of a gene pool by swapping two bits of the parent solution to generate two new offspring solutions using methods such

as simulated binary crossover [83].

- **Mutation:** This step mimics mutation on a chromosome by flipping a bit with a probability equal to a given mutation probability. This rate of mutation is often very low, just like in nature.

The last four steps are repeated until either the Pareto front has been reached or the termination criterion is met. Figure 2.15 displays an abstraction of this iterative process.

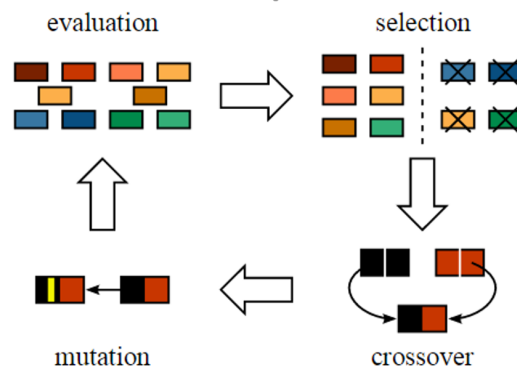


Figure 2.15: An abstraction of the procedure in genetic algorithms

Commonly used GAs are:

- **Non-dominated sorting GA (NSGA):** Uses a fitness assignment scheme which prefers non-dominated solutions and by using sharing strategy diversity among solutions of each non-dominated front. This method progresses to the pareto optimal region front-wise.
- **Vector-evaluated genetic algorithm (VEGA):** Permits crossover between any two solutions in the entire population. This because a crossover between any two good solutions each corresponding to different objective may produce offspring with good compromised solutions. Mutation is applied on each individual a usual.
- **Niched Pareto GA (NPGA):** Uses a binary tournament selection procedure and may be found to be computationally efficient in solving problems having many objectives.

When comparing GAs to other stochastic optimization techniques such as particle swarm, ant colony and annealing etc., GAs often posses better accuracy in it's solutions, while the other techniques often only give a good approximation [80]. However, this makes GAs more computational intensive than the other techniques, and thus depending on the computational speed requirement of an application the correct approach can be selected. For design optimizations, obtaining accurate optimal solutions is more crucial than speed, hence the popularity of GAs for these applications.

2.4.3. NSGA-II

Proposed by Deb et al. in [84], the elitist non-dominated sorting GA or NSGA-II is an improvement algorithm to the early version of NSGA. In addition to diversity preserving and emphasis on non-dominated solutions, NSGA-II ensures elitism by comparing the parent and offspring populations collectively. The algorithm works as follows. Initially, using random sampling, a random parent population P_0 of size N is generated and the first generation is initiated. At any generation t , an offspring population Q_t is generated from the parent population P_t employing the typical genetic operators. Afterwards, P_t and Q_t are combined into population R_t of size $2N$ and sorted based on the rank of the non-dominating fronts (F_1, F_2, \dots). From these sorted fronts the new parent population P_{t+1} of size N is filled one at the time with highest rank fronts first and so on. All fronts that cannot be accommodated will be rejected. However, in the situation when the last allowed front consists of more points than the remaining slots available, as shown in Figure 2.16.

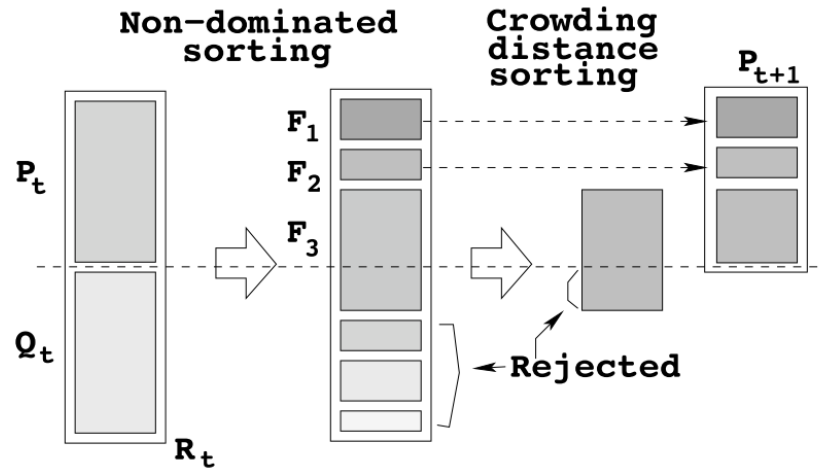


Figure 2.16: The NSGA-II procedure [84].

The points within that front are then sorted based on diversity and the highest are included. The diversity ranking or crowded-sorting is achieved based on the crowding distance d_i of any solution i . Here, d_i is simply the perimeter of the cuboid formed by using the nearest neighbors in the objective space as the vertices depicted in Figure 2.17. This algorithm can be implemented using the python based MOO environment Pymoo which is further reviewed in detail in appendix C.

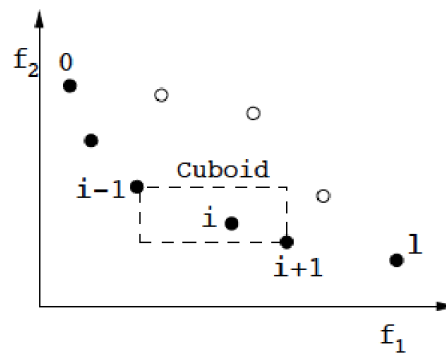


Figure 2.17: The crowding distance calculation [84].

3

Fast Charging Station Model Design

This chapter presents the proposed BESS assisted FCS model that can simulate the performance of a FCS. This model includes several modules: EV demand, EMS, BESS, lifetime, and QoS. For each module the input and output signals are addressed, the function of the module given, and the design choices explained.

3.1. Fast Charging Station Model

In general the FCS model simulates the power flows inside a BESS assisted FCS. The configuration being modeled is the AC configuration FCS shown in Figure 3.1. This FCS includes a N number of DC fast charging stalls, a BESS and a MV/LV transformer that couples the station to the MV grid. The AC configuration is selected due to its maturity and standard of application at most FCS [60]. Furthermore, the task intended for the BESS is to perform peak-shaving on the demand in order to restrict the grid-tie power to a set limit, and thus reducing the stations demand charges.

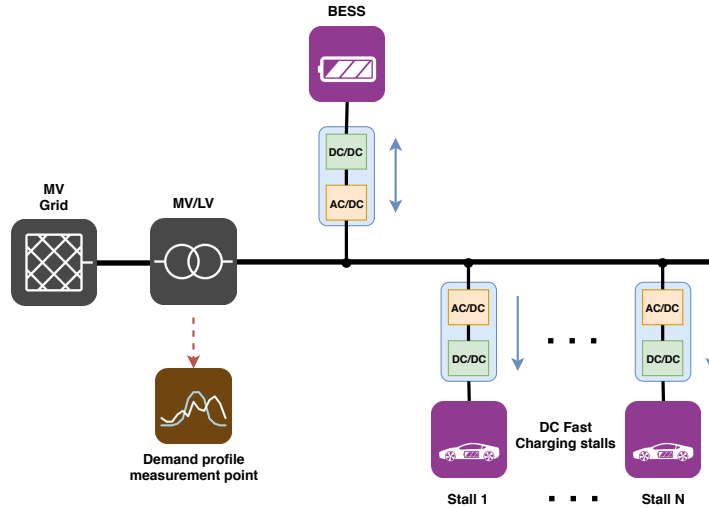


Figure 3.1: A system diagram of a BESS assisted AC connected FCS

From this system the following electrical components are modeled, the grid-tie demand, the FCS demand profile, the EMS and stationary BESS. Moreover, the model includes the performance parameters BESS lifetime and charging delays. The BESS lifetime helps to assess the costs associated to the BESS and the charging delays give an assessment of the quality of service being provided by the FCS design.

Furthermore, an important assumption made regarding the charging delays, is that when both the restricted grid-tie and BESS reaches their designed power limits, it is assumed that a simple power balancing technique is being employed by the charging stalls. This results in equally divided charging delays among active stalls.

The main goal of this model is to assess the performance of a BESS assisted FCS design based on 3 design parameters and a FCS demand profile. The input and output parameters associated with the model are given in Table 3.1.

Table 3.1: Input and output parameters for the FCS models.

| Input | Unit |
|-------------------------|---------|
| BESS Capacity | kWh |
| BESS Power Rating | kW |
| Maximum Grid-tie Power | kW |
| FCS Demand (1 min res.) | kW |
| Output | Unit |
| BESS SoC | % |
| Power Flow | kW |
| Charging Delays | minutes |
| BESS Lifetime | years |

Since charging sessions at FCSs can range from 10-30 minutes and the maximum permissible charging delays are between 0-6 minutes, a model resolution (simulation step t) of 1 minute is selected. This will ensure the capture of the session scale characteristics in the FCS demand profile and give a close approximation of the charging delays. It should be noted however, that due to the post-processing nature of the BESS lifetime model, this parameter is calculated at the end of each simulation. All other parameters are calculated each simulation step t .

3.2. Model Diagram

Figure 3.2 depicts every module within the FCS model including their corresponding inter-connection and data exchange. The blue lines represents the physical power flows, the red dotted lines the signal exchange between each modules and the green lines the performance related results. During the simulation only the red signals are exchanged between modules and the blue and green lines are represented as output results from these modules. In total the model consist of 5 modules, the EV demand, EMS, BESS, lifetime and QoS. Furthermore, the complete model is implemented inside the python based Mosaik simulation environment, which is reviewed in detail in appendix B.

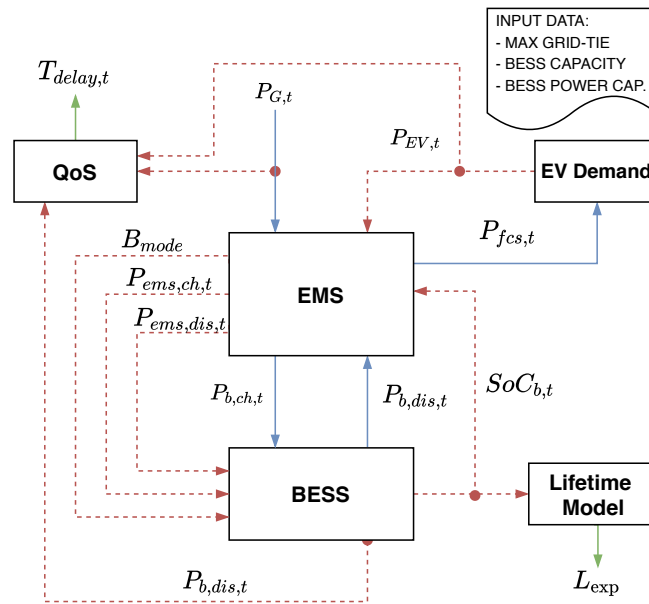


Figure 3.2: System diagram of the complete FCS model.

3.3. Station Demand

The module "EV demand" models the total power demand of all EVs charging at the FCS. For each simulation interval t , this module generates the EV power demand $P_{EV,t}$ in kW for a defined station. For this a pre-defined minute scale power demand profile of a FCS is required for the initialization. As previously mentioned in section 2.1.3, these profiles can either be estimated from stochastic models or obtained from measurement data. This module is implemented in Mosaik using a csv wrapper that include the discrete values of the demand profile. Moreover, physically this module receives the available FCS charging power $P_{FCS,t}$ which later is explained together with the QoS module.

This project uses energy measurements in kWh (1 minute samples) from January obtained at four FCSs in the Netherlands. Using these measurements a demand profile can be generated. The power demand profile in kW is obtained by simply differentiating the kWh measurements over the sampled time. Using actual demand data has it's advantages of giving a more realistic view of the current power demands at FCSs. Furthermore, it will make session level power variations and differences in station utilization rates visible in the simulation. However, because the complex effects of the EV growth on the demand profile falls outside the scope of this project. The measurements obtained from January are assumed to be worst case demand for each data set. Figure 3.3 shows an example of a FCS demand for a week in January at a station with 450 kW of installed charging capacity. It should be also mentioned that in order to comply with data sharing agreements, the date-time and station names included in this thesis are made fictitious on purpose.

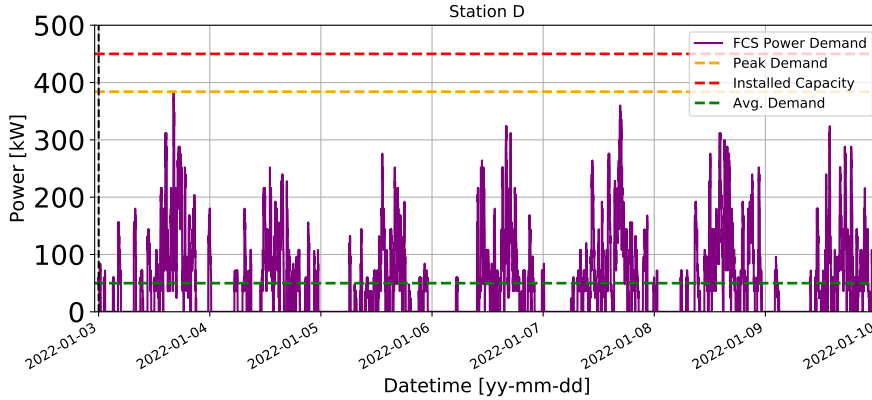


Figure 3.3: Example of a FCS demand for a week in January.

3.4. Energy Management System

As explained in section 2.3, the EMS performs power controls for the battery system according to a dispatch program. In this model the EMS is regarded as the central unit of the system. This model performs the correct power flow controls for the FCS in order to dispatch the BESS correctly for peak-shaving purposes, and thus avoid exceeding the designed grid-tie values.

The objectives of the EMS module are the following:

- Limit the grid-tie power to an assigned value.
- Determine the required charge and discharge power from the BESS.
- Apply typical SOC constraints to the BESS in order to avoid accelerated degradation.
- Determine the system's power capability to supply the stalls.

Initialization parameters: maximum grid-tie capacity (P_G^{max}) [kW]

Inputs: EV power demand ($P_{EV,t}$) [kW], BESS SoC ($SoC_{b,t}$) [%]

Outputs: EMS discharge power signal ($P_{ems,dis,t}$) [kW], EMS charge power signal ($P_{ems,ch,t}$) [kW] and BESS mode signal (B_{mode}), grid-tie power ($P_{G,t}$) [kW]

These objectives are achieved by performing the following control flow chart shown in Figure 3.4 for every simulation step t . The control can be described in two general paths, a charging path and discharging path.

Charging of the BESS occurs when the demand of the station (denoted as $P_{EV,t}$) is smaller than the maximum grid-tie capacity (denoted as P_G^{max}). When this is the case, first the BESS SOC are checked, if this is within the upper constraints, the EMS signals the BESS to charge with the remaining power available ($P_{ems,ch,t}$) from the grid-tie. However, if the BESS is full (above 90%), the grid-tie $P_{G,t}$ will continue to follow the demand and the BESS will go into idle mode. The power values for the EMS charge signal during BESS charging are defined by (3.1).

$$P_{ems,ch,t} = P_G^{max} - P_{ev,t} \quad (3.1)$$

For the discharging path, when the FCS demand is larger than the grid-tie capacity, the lower SOC constraints are checked, if within limits the EMS commands the BESS to discharge the remainder of the power above the grid-tie capacity. However, this occurs within the BESS ratings which are constrained in the BESS module. Likewise, if the BESS is empty (below 5%), the BESS will enter idle mode. When in idle mode in the discharge situation the demand cannot be met and the FCS will resort to power balancing decreasing its charging speeds, thus resulting into charging delays. Additionally, at end of each path the dispatch signal B_{mode} is defined according to the followed path. This signal ensures that the BESS cannot discharge and charge at the same time. Equation (3.2) describes the EMS power signal during discharge and (3.3) the upper and lower SOC constraints. Furthermore, (3.4) describes the the power values for the grid-tie during both conditions.

$$P_{ems,dis,t} = P_{ev,t} - P_G^{max} \quad (3.2)$$

$$5\% \leq SoC_{b,t} \leq 90\% \quad (3.3)$$

$$P_{G,t} = \begin{cases} P_{EV,t} + P_{b,ch,t}, & P_{EV,t} < P_G^{max} \\ P_G^{max}, & P_{EV,t} \geq P_G^{max} \end{cases} \quad (3.4)$$

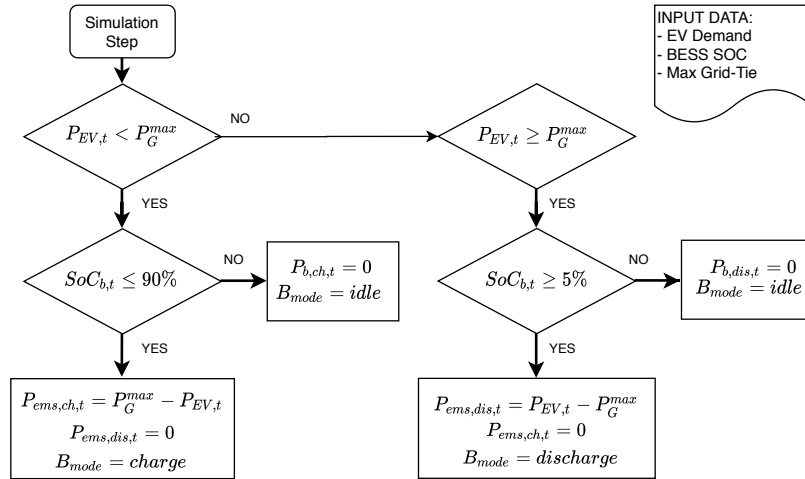


Figure 3.4: Control Flowchart for the EMS model

3.5. BESS Model

Because only energy content and power flows are being analysed by our model, the analytical BESS modeling approach suffices. These models are simple and describes the BESS at a higher level of abstraction [77]. In analytical models the SOC, charging/discharging power, efficiency and energy capacity are required to model

it's performance.

The objectives of the BESS module are the following:

- Dispatch the BESS in the correct mode according to the EMS signals.
- Model the inverter efficiency curve.
- Model the physical power and energy constraints.
- Model the charge and discharge of energy.

Initialization parameters: BESS capacity (E_b^{\max}) [kWh] and BESS power rating (P_b^{\max}) [kW]

Inputs: EMS discharge power signal ($P_{ems,dis,t}$) [kW], EMS charge power signal ($P_{ems,ch,t}$) [kW] and BESS mode (B_{mode})

Outputs: SOC ($SoC_{b,t}$) [%], BESS discharge power ($P_{b,dis,t}$) [kW] and BESS discharge power ($P_{b,ch,t}$) [kW]

3.5.1. Operation and controls

For each simulation step t the control flowchart in Figure 3.5 is executed. According to the battery mode signal received from the EMS, the battery either goes into charge, discharge or idle mode. In both charge and discharge mode, the power constraints are applied to the power signal, the inverter efficiency determined and energy added or removed from the previous BESS energy content ($E_{b,t-1}$). To convert the power into energy (kW to kWh) the power is multiplied by the factor 1/60. Furthermore, in idle mode the BESS does not charge nor discharge any energy. (3.5) describes this charging, discharging and idling procedure, and (3.6) the energy constraint applied to the BESS. This constraint ensures that the BESS cannot be charged or discharged outside of the physical boundaries. Lastly, at the end of each step the SOC is determined by (3.7).

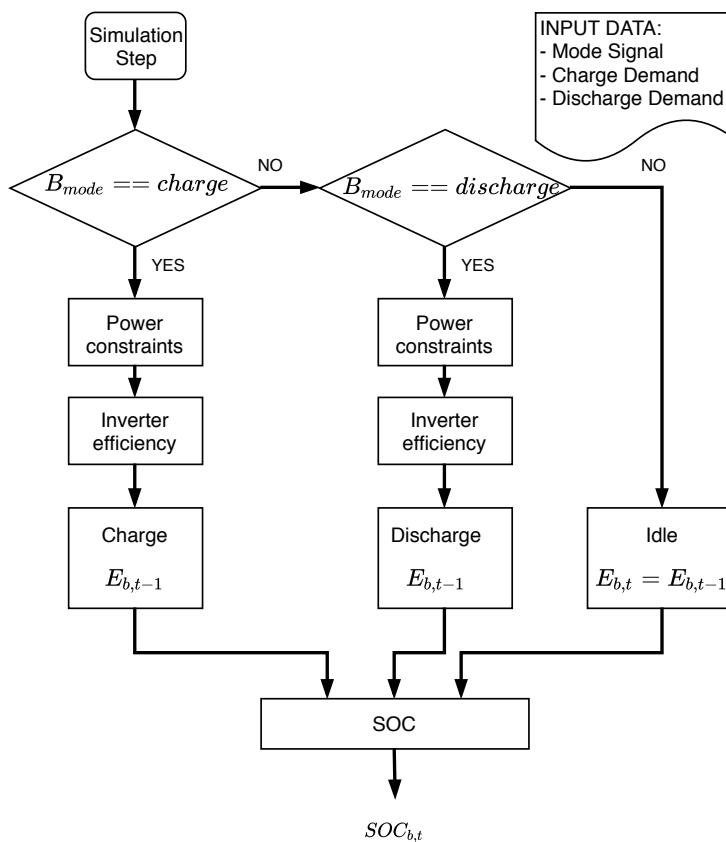


Figure 3.5: Control flowchart for the BESS model

$$E_{b,t} = \begin{cases} E_{b,t-1} + \frac{P_{b,ch,t}}{60} \cdot \eta(P_{b,ch,t}), & B_{mode} = \text{Charge} \\ E_{b,t-1} - \frac{P_{b,dis,t}}{60} \cdot \frac{1}{\eta(P_{b,dis,t})}, & B_{mode} = \text{Discharge} \\ E_{b,t-1}, & B_{mode} = \text{Idle} \end{cases} \quad (3.5)$$

$$0 \leq E_{b,t} \leq E_b^{cap} \quad (3.6)$$

$$SoC_{b,t} = \frac{E_{b,t}}{E_b^{cap}} \cdot 100\% \quad (3.7)$$

3.5.2. Power capability

To ensure the BESS model (dis)charges within its power capabilities, power constraints are applied according to the BESS's rating and physical limitations. The following constraints, (3.8) and (3.9) limits the charging and discharging power of the battery to its maximum power rating found in the battery's data sheet. For simplicity this model assumes that both the charging and discharging ratings are equal, meanwhile in real life depending on the technology this can differ.

$$0 \leq P_{b,ch,t} \leq P_b^{max} \quad (3.8)$$

$$0 \leq P_{b,dis,t} \leq P_b^{max} \quad (3.9)$$

As previously explained in section 2.1.3, the charge/discharge power of a battery is not fully constant over the full range of SOCs, at low (around 15%) levels and high (around 80%) levels the power linearly decreases [73]. This linear decrease during discharging and charging can be described by the following constraints (3.10) and (3.11). Here $S_{b,ch}$ and $S_{b,dis}$ are defined as the upper and lower SOC limits for maximum power delivery, these equals 80% and 15%, respectively. Figure (3.6) gives a plot of the four different constraints applied to the BESS model.

$$P_{b,ch,t} \leq \frac{P_b^{max}}{1 - S_{b,ch}} \left(\frac{E_{b,t}}{E_b^{max}} - 1 \right) \quad (3.10)$$

$$P_{b,dis,t} \leq \frac{P_b^{max}}{S_{b,dis}} \left(\frac{E_{b,t}}{E_b^{max}} \right) \quad (3.11)$$

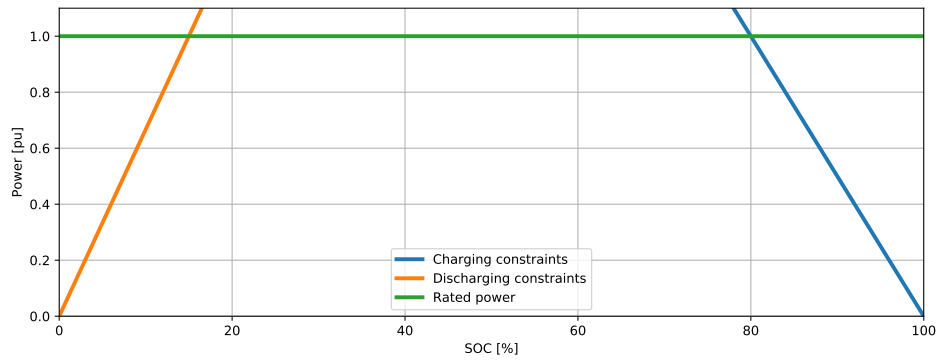


Figure 3.6: Power capability curve obtained with the BESS power constraints

3.5.3. Inverter efficiency

The efficiency of a BESS is a combination of the battery efficiency and invert efficiency. Inverter efficiencies are normally very high ($\geq 98\%$), however at low power this weakens allot. These losses are caused by converter losses. The battery efficiencies on the other hand are caused by ohmic losses and are very high at low power (almost 100% efficiency) and linearly weakens up to around 96% as the power increases to full power [85].

The charging and discharging power flows between the battery and inverter are depicted in Figure 3.7a. In this figure, the AC side power flows (P^{ac}) are assumed to represent the BESS power ($P_{b,ch,t}$ or $P_{b,dis,t}$) including their constraints. Furthermore, the DC side power flows (P^{dc}) represents the actual energy being charged or discharged from the battery after the efficiencies are applied. From (3.5), it is clear that the inverter efficiency $\eta_{inv}(P)$ is a function of these AC side power flows.

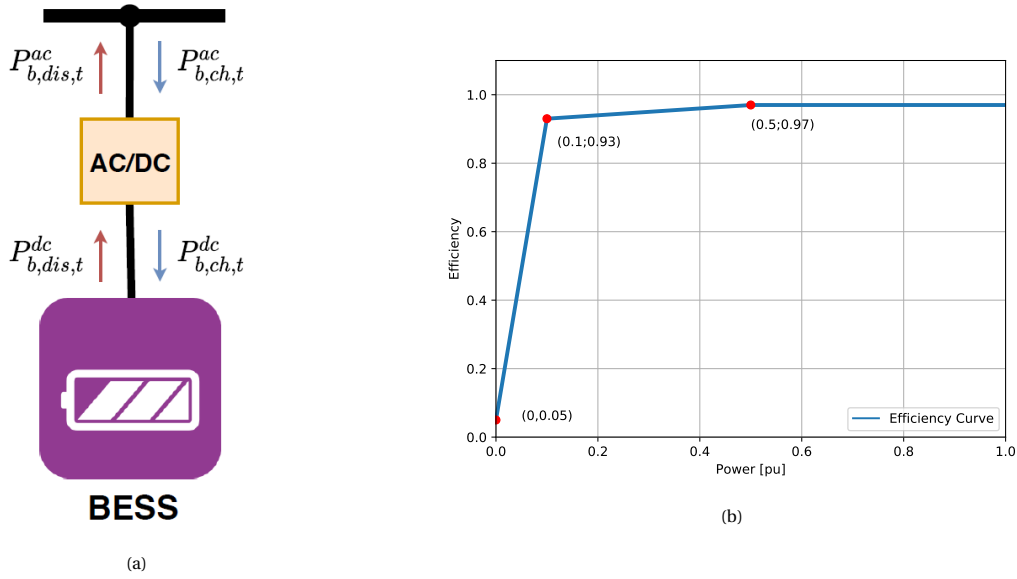


Figure 3.7: (a) Power flows between the BESS and inverter, (b) Piece-wise inverter efficiency curve model

The easiest approach to model an inverter efficiency function $\eta_{inv}(P)$ is as constant of 96% which can be seen as an average. However, this will result in large errors at low power ranges in applications where full range of power is required such as in peak-shaving. Another approach is to model the complete non-linear efficiency curve using piece-wise linear segments. This approach increases model accuracy while still retaining computational simplicity [85].

In this BESS module a 3 segment piece-wise linear approximation of an inverter curve model found in [86] is implemented. This efficiency curve η_{inv} start from 5%, linearly increases to 93% at 0.1 pu (P^{ac}) and further increases to 97% after 0.5 pu (P^{ac}). This piece-wise linear segments are plotted in Figure 3.7b and depicts the efficiency function (3.12) for the complete BESS power range.

$$\eta = \begin{cases} 8.8 \cdot P^{ac} + 0.05, & P^{ac} \leq 0.1 \text{ pu} \\ 0.93 + (0.1 \cdot (P^{ac} - 0.1)), & P^{ac} \leq 0.5 \text{ pu} \\ 0.97, & P^{ac} \leq 1 \text{ pu} \end{cases} \quad (3.12)$$

3.5.4. Model Verification

The BESS module is verified using a procedure proposed in [87]. The models SOC estimations are compared to physical test values performed using the IEC 62660-1 dynamic stress test (DST) [88]. The IEC standard applies to the performance testing of Li-ion batteries in EVs rather than stationary applications. Nevertheless, the DST power profile resembles the BESS power profiles that would be expected for peak-shaving in the FCS domain. This test will allow the BESS model to perform a DOD of almost 100% with a power profile ranging

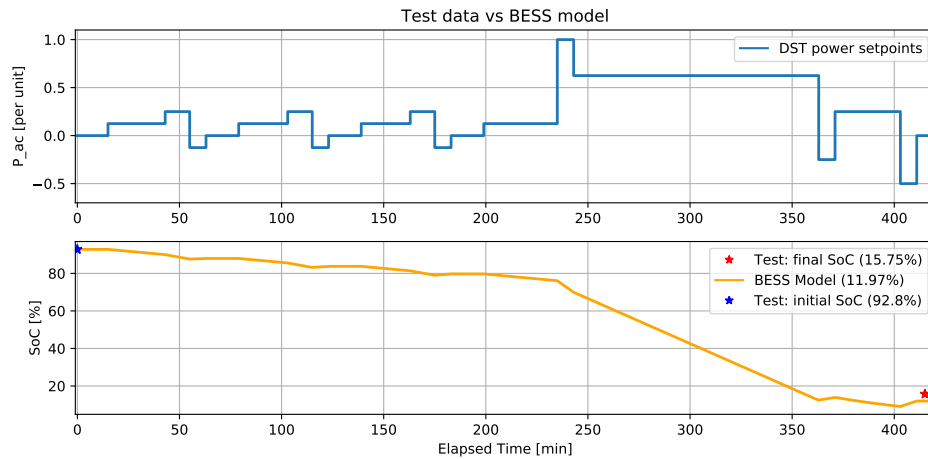


Figure 3.8: Top: IEC 62660-1 DST power set-points. Bottom: BESS model simulation results in SOC

from -125 to 250 kW.

Using the IEC 62660-1 DST power set-points the model was simulated against the test data and results are compared in Figure 3.8 and Table 3.2. In both the test data and simulation a BESS capacity and power rating of 570 kWh and 250 kW, respectively were employed. It should be also mentioned, that for this verification a simple EMS was used to convert the minus power values to the corresponding discharge power for our BESS model. Additionally, the upper SOC constraint was extended to 95% during the verification test.

From these results it can be concluded that our model underestimates the SOC by 3.78% and lies within the accepted error range. The complete verification process of the BESS model is continued in appendix D.

Table 3.2: Verification IEC 62660-1 performance test summary

| Test data | |
|-------------------------------|-------|
| Initial SOC [%] | 92.80 |
| Final SOC [%] | 15.75 |
| BESS model performance | |
| Initial SOC [%] | 92.80 |
| Estimated final SOC [%] | 11.97 |
| e_{SOC} [%] | -3.78 |

3.6. Lifetime Model

The goal of the lifetime module is to estimate the expected lifetime of the BESS using its SOC profile. As explained in section 2.3.5, battery ageing is due to a combination of two components, the cycle-life degradation and calendar-life degradation. This module uses the post-processing lifetime model (3.13) proposed in [52] to determine the capacity fade being induced by these two degradation factors on LFP/C batteries. By knowing the degradation for a certain SOC profile, one can estimate the time it takes for the battery to reach its EOL criterion of 80% [50]. This is taking the assumption that the battery will repeat this SOC profile during the entirety of its lifetime. Here the SOC profile is defined as the complete SOC history the BESS experienced during a simulated time. Due to this post-processing nature, this module performs its simulation step at the end of the simulation time. The diagram of the complete lifetime module presented in Figure 3.10 is implemented in Mosaik.

$$\begin{aligned} C_{cycle} &= 0.021 \cdot e^{-0.01943 \cdot SOC_{avg}} \cdot DOD^{0.7162} \cdot nc^{0.5} \\ C_{cal} &= 0.1723 \cdot e^{0.007388 \cdot SOC_{lvl}} \cdot t^{0.8} \end{aligned} \quad (3.13)$$

Cycle-life degradation

Using (3.13) the cycle-life degradation (D_{cycle}) can be determined by the number of cycles being performed nc , the DOD, and the average SOC during each cycle [76]. Due to the irregular demand profile for FCS applications, these 3 parameters can vary significantly on a daily basis and can be different depending on the station's usage. For this reason, this module uses a slightly modified version of the rain-flow cycle counting algorithm found in [50], this algorithm is further explained in detail in section 2.3.5 and appendix A. In addition to the frequency and range of cycles this modified version also extracts the average SOC from each cycle. Once these values are obtained, the cycles are counted based on a discrete n segments of DOD ranges and average SOC. These discrete segments are used in order to obtain computational simplicity, however, to preserve model accuracy a minimum of 20 discrete segments are selected [89]. An example of the results that can be obtained from this cycle count method is shown in Figure 3.9.

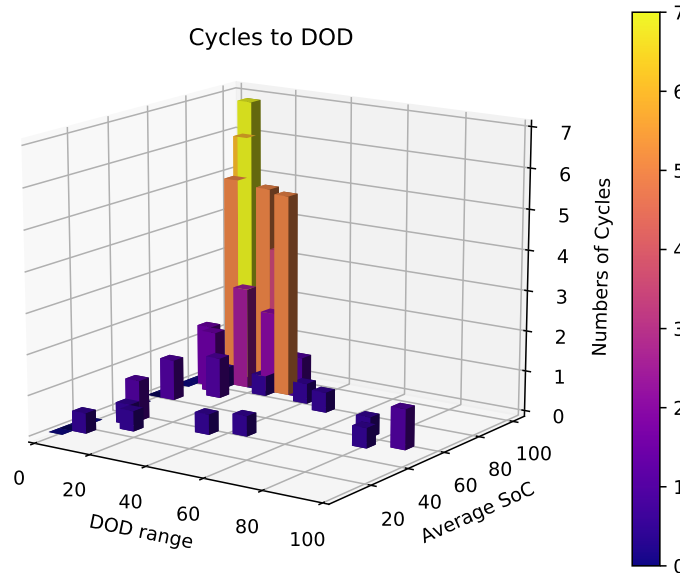


Figure 3.9: Example of a cycle count obtained from the modified rain-flow cycle counting algorithm

Lastly, the cycle lifetime consumed is calculated with (3.14) by comparing the obtained count for each n segments against the maximum cycles defined from the cycle lifetime model (3.13) at 80% EoL. Here n equals the number of segments, N_c the consumed cycles by the BESS at a given DOD and average SOC range, N_{max} and maximum number of cycles at a given DOD and SOC range obtained by the cycle-life model.

$$D_{cycle} = \sum_{DOD=1/n}^{DOD=100\%} \frac{N_c(dod, soc)}{N_{max}(dod, soc)} \quad (3.14)$$

Calendar-Life degradation

Calendar degradation (D_{cal}) occurs when the battery is idle. From the same SOC profile a total idle time to SOC level range data can be extracted. Using the calendar-life model (3.13), one can obtain the calendar lifetime consumed in the same procedure using (3.15). Where n equals the number of SOC segments, $T_c(SoC)$ the time consumed at a given SOC range and $T_{max}(SoC)$ the maximum calendar lifetime at a given SOC level obtained from the lifetime model.

$$D_{cal} = \sum_{SoC=1/n}^{SoC=100\%} \frac{T_c(SoC)}{T_{max}(SoC)} \quad (3.15)$$

Both degradation's are then summed together to find the total lifetime consumed LC . Assuming the BESS continues the same operation, the expected lifetime (L_{exp}) can be estimated with (3.17). Where Tp represents the length of the degradation period, which in this case is equal to the FCS simulation length.

$$LC = D_{cycle} + D_{cal} \quad (3.16)$$

$$L_{exp} = \frac{1}{LC} \cdot Tp \quad (3.17)$$

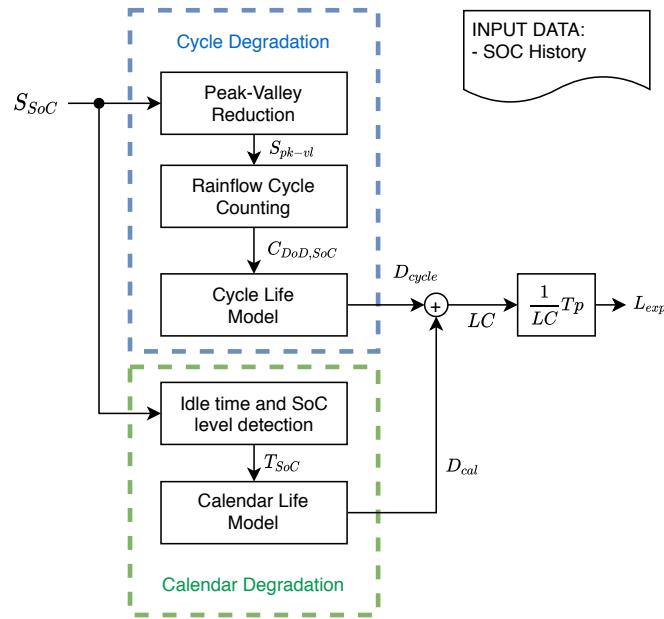


Figure 3.10: Diagram of the BESS lifetime model

3.7. Quality of Service

The QoS module determines the performance of a BESS assisted FCS design in terms of charging delays. Charging delays would be experienced at times when the power delivered from both the grid-tie and BESS cannot meet the EV demand, and thus resulting in a longer charging session due to the reduced charging speeds. These periods with power differences between the EV demand $P_{EV,t}$ and the FCS power capability $P_{fcs,t}$ are called power mismatch periods, where $P_{fcs,t}$ is defined by (3.18)

$$P_{fcs,t} = P_{G,t} + P_{b,dis,t} \quad (3.18)$$

At each simulation step the following flow-chart shown in Figure 3.13 is performed to give an estimate of the charging delays caused during power mismatch periods. The module starts by identifying power mismatch moments, if a power mismatch moment is identified ($\Delta P_t > 0$), then the extra time (Δt_d) it takes to charge the missed energy (3.19) at the available FCS power is given by (3.20). This is then summed up until a mismatch period ends.

When a mismatch period ends ($\Delta P_t \leq 0$), an estimate of the total charging delay ($T_{delay,t}$) for the ending power mismatch period is obtained by equally dividing the summed Δt_d over the number of charging EVs ($N_{EV,t}$) as shown in (3.21). This delay then represents the total extra time a connected EV would have experienced after the power mismatch period if it had continued to charge at the available power. Figure 3.11 depicts an example of such power mismatch periods and its resulting charging delays. The red shading represents the missed energy during these mismatch periods.

$$\Delta E_t = (P_{EV,t} - P_{fcs,t}) \cdot t_{step} \quad (3.19)$$

$$\Delta t_d = \frac{\Delta E_t}{P_{fcs,t}} \quad (3.20)$$

$$T_{delay,t} = \sum \frac{\Delta t_d}{N_{EV,t}} \quad (3.21)$$

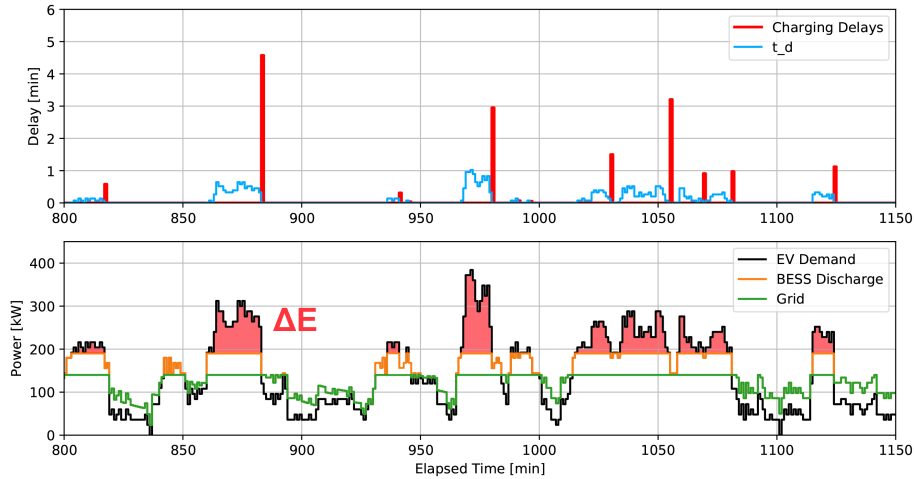


Figure 3.11: Charging delay concept

The number of EV's that experienced a power mismatch can be either obtained from data (if available) or be estimated using additional station information such as number of charging stalls N_{stalls} and total rated power $P_{stations}^{rated}$. Due to the absence of EV data for this project, the module estimates the number of EVs connected during a power mismatch period using (3.22).

$$N_{EV,t} = \frac{\max(P_{vect})}{P_{station}^{rated}} \cdot N_{stalls} \quad (3.22)$$

Here P_{vect} contains the history of the EV demand during a power mismatch period. This vector is used to output the maximum EV demand at the end of the mismatch period. The procedure is performed in parallel to the summation of Δt_d as shown in figure 3.13. By finding the ratio between this $\max(P_{vect})$ and the installed rated power of the station the percentage of stalls in use during the mismatch period can be calculated. This would give an indication of how many stalls were actively charging, and thus how many EV's were connected. It should be noted, that this estimation assumes that every charging stalls at the station posses equal power ratings. Figure 3.12 shows an EV profile generated for the above example using this estimation. Furthermore, at the end of each power mismatch period the values are reset before continuing to the next mismatch. Lastly, for all situations outside a power mismatch period the delay is equal to zero.

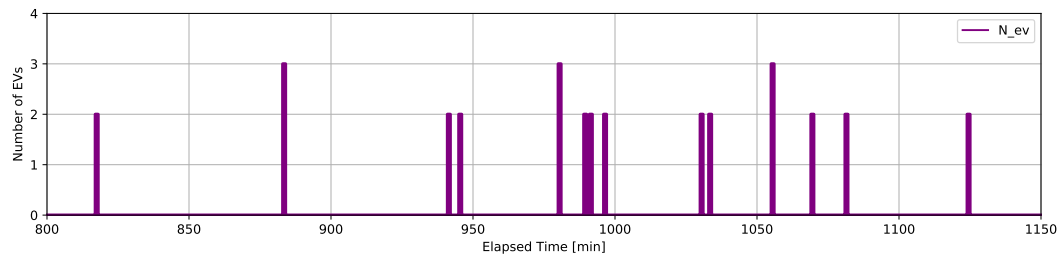


Figure 3.12: The number of charging EVs during mismatch periods for a station with 450kW installed capacity and - stalls

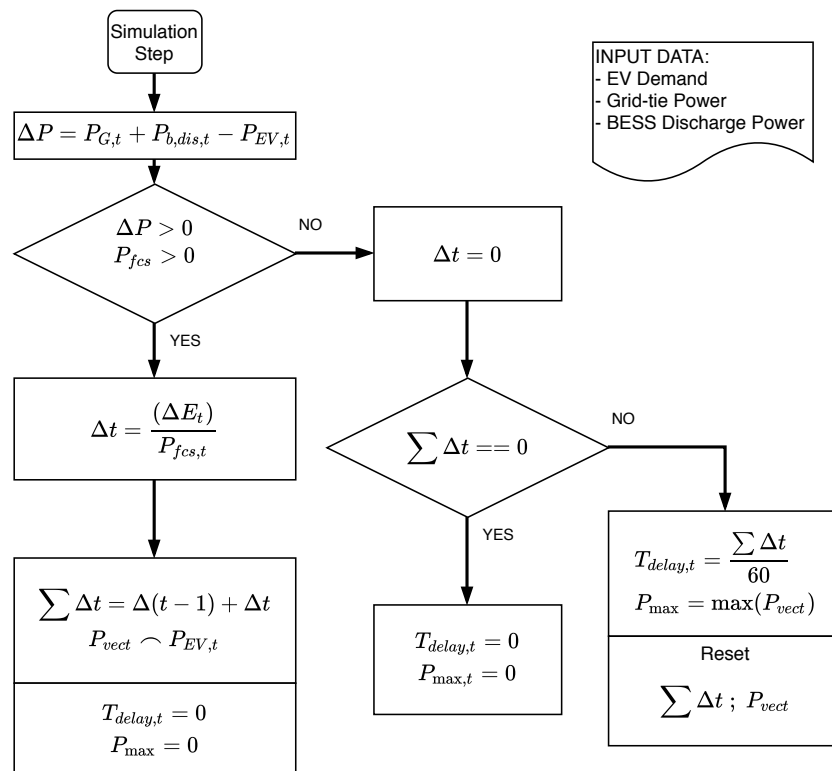


Figure 3.13: Quality of Service implementation flowchart

4

Multi-Objective Design Problem Formulation

This chapter introduces the challenges faced when designing a BESS integrated FCS for DCM purposes. The main challenge for the design is to determine the optimal grid-tie and BESS sizing. The ratio between these two components introduces a trade-off between the DCM costs and the performance of a FCS station. This trade-off is then formulated into a multi-objective design problem and a framework using genetic algorithms is proposed to find the Pareto front for a specific station. The Pareto front can then be used by a FCS owners as a sizing guide to optimally apply DCM to an existing station.

4.1. FCS Design Problem

The main objective for this thesis is to study the optimal BESS sizing for DCM in FCS applications. In general this translates to a trade off between the grid-tie power reduction and BESS sizing. As stated in section 2.3.4, sizing of a battery for grid-connected applications can be a complicated process. This complexity is found in the irregular demand profiles of FCSs, which lead to complex cycling of the BESS in peak-shaving applications. The framework being proposed in this thesis considers 2 contradicting design objectives, the associated DCM costs and the station performance. The DCM cost component consists of the annual (reduced) demand charges and the annual BESS investments required to perform the peak-shaving. The performance is measured in the charging delays customers experience when there is not sufficient power capacity available from both the grid-tie and BESS to meet the EV demand. Moreover, both objectives are evaluated using the FCS model proposed in chapter 3.1. This model requires as input the station's demand profile and 3 design parameters, maximum grid-tie power P_G^{max} , BESS capacity E_b^{max} and BESS power rating P_b^{max} .

To determine the demand charges, this framework will assume P_G^{max} to be equal the the maximum peak demand during a billing cycle. Moreover, another assumption made is that the BESS will be in service for the duration of its expected lifetime. This way the initial BESS investments are spread over its lifetime to be included in the annual DCM cost.

To properly asses a stations performance, two KPIs are derived from the charging delays, the maximum charging delay and the increase in station utilization. The maximum charging delay is the maximum extra time an EV might experience to complete it's charging session. This primarily affects the EV customers and should not surpass 6 minutes in order to avoid poor customer satisfaction [6]. The utilization time T_{util} of a station is the total amount of time the station is being occupied for charging. Increase in utilization is here defined as the percentage increase in station utilization caused by the total amount of extra charging time. This KPI gives an indication on how frequent delays occur, and thus affecting the owner's sales potential due to increased station occupation. Using $T_{delay,t}$ from the FCS model, the two KPIs can be obtained using (4.1) and (4.2).

$$T_{max} = \max(T_{delay,t}) \quad (4.1)$$

$$T_{freq.} = \frac{\sum T_{delay,t}}{T_{util}} \cdot 100\% \quad (4.2)$$

4.2. Objective Functions

This multi-objective design problem can be considered a two contradicting objective problem. However, due to the subtle differences in dependencies between (4.1) and (4.2) the performance objective is separated into a two separate objective functions (4.4) and (4.5). This ensures separate minimization of the maximum charging delays and frequency of charging delays, hence avoid resulting with solutions with low maximum delays but frequent delays.

Objective function (4.3) represents the DCM cost function, this function describes the BESS related investments associated to the DCM design and the reduced demand charges. This is calculated on an annual basis. The annual BESS costs comprises of energy capacity investments in [€/kWh] and the power converter investment in [€/kW] divided by the expected BESS lifetime in years. An additional over-sizing factor β_{cap} and β_{pow} are included to take into consideration the capacity and power fade due to degradation. Factor β_{cap} takes into account the EoL criterion of 20% capacity fade and therefore equals 1.2. Factor β_{pow} takes into account the power fade, which according to literature can result in the worst-case for LFP batteries in 7% power capability fade when the capacity reaches it's EoL criterion and therefore β_{pow} equals 1.07 [76]. Furthermore, The demand charges comprises of monthly demand tariffs C^{dem} in [€/kW] times the maximum grid-tie power and are annualized using the factor α which is 1/12. Additionally, the costs related to perform power balance are not considered in this framework. It is assumed here that the initial software investments for this technology will be divided among a complete network of stations, hence making the costs irrelevant when compared to the large BESS investments and demand charges.

The second objective is the maximum charging delay, this objective is obtained by simply extracting the maximum delay peak from the series $T_{delay,t}$ using 4.1. Whereas, the third objective is the delay frequency, this is defined as the worst total charging delay as a percentage of the total charging time at the station.

$$\min_x f_1(x) = C^{DCM} = \frac{C^{bess} E_b^{max} \beta_{cap} + C^{conv} P_b^{max} \beta_{pow}}{L_{exp}} + \frac{C^{dem} P_G^{max}}{\alpha} \quad (4.3)$$

$$\min_x f_2(x) = T_{max} = \max(T_{delay,t}) \quad (4.4)$$

$$\min_x f_3(x) = T_{freq} = \frac{\sum T_{delay,t}}{T_{util}} \cdot 100\% \quad (4.5)$$

$$s.t. X^{\min} P_b^{max} \leq E_b^{cap} \leq X^{\max} P_b^{max} \quad (4.6)$$

$$P_{fcs-avg} \leq P_G^{max} + P_b^{max} \leq P_{fcs-max} \quad (4.7)$$

$$T_{max} \leq 10 \quad (4.8)$$

4.3. Design Constraints

Apart from the constraints included inside the FCS model, a set of design constraints are applied to restrict our search during the optimization using previous knowledge and technological constraints obtained from literature.

Equation (4.6) represents the P/E ratio constraint related to the BESS chemistry being considered in the design. In this thesis the Lithium LFP/C chemistry is considered, which has a P/E ratio at 1C of $X^{\min} = 1$ and $X^{\max} = 8$ [37]. Depending on the charge/discharge times of an application, a BESS can charge/discharge at higher C-rates. The constraint can be extended for situations where 2C is possible. However, discharging at 2C can only be done continuously for 20min which falls exactly on the boundaries of our systems requirements. Nevertheless, at 2C the P/E constraints are $X^{\min} = 1.3$ and $X^{\max} = 8$ [90].

Equations (4.7) and (4.8) are constraints that restricts the optimization search with knowledge from literature. Where (4.7) constraints the optimization from selecting solutions with a combined grid-tie and BESS power below the average power of a station's demand and above the maximum stations peak power. Furthermore, constraint (4.8) restricts the optimization from selecting solutions with maximum delays longer than 10 minutes. This constraint is applied due to the fact that FCS customers are highly likely to leave for delays longer than 6 minutes [6, 15].

4.4. Optimal Sizing Framework

Using the FCS model proposed in section 3.1, a framework shown in Figure 4.1 is set up to solve the design optimization problem. The framework comprises of the FCS model using a worst case demand profile, and an optimization model using the NSGA-II algorithm.

In general FCSs and BESSs are designed to endure usage during worst case scenarios [68], hence the selection of a worst case demand profile as input for the FCS model. The notion is that if the design performs to specifications in the worst case scenarios, it will also perform correctly in all other scenarios. Furthermore, as explained in section 2.1.3, a FCS demand has a repeating daily pattern (24-hours) and the worst case usage period is around the Christmas holidays. For this reason the demand profile comprises of two worst 24-hour periods extracted from this worst case scenario. A 24-hour period with the worst peak demand and a 24-hour period with the worst energy density. Consequently, following the sizing principles of the duty cycle analysis explained in section 2.3.4. The worst peak demand day ensures the proper power requirements, and the worst energy density day ensures the BESS energy requirements.

Note that because two worst 24 hours periods are used, the increase in utilization and expected BESS lifetime is assessed separately for each 24 hour period, where then the worst from these two 24 hour periods are selected. The total charging delay is analysed for both 24 hour worst case load and the day with the worst total charging delay is inserted into the objective.

4.4.1. Optimization Model

Due to the modeling complexities and some non-linearity within the FCS model, the optimization model uses a meta-heuristic optimization approach based on the genetic algorithm NSGA-II. Using the formulated objective functions and design constraints this is implemented in the Pymoo environment. Pymoo is a Python based environment that offers the modular implementation of genetic algorithms, a detailed introduction of this is included in appendix C. The modular aspects of Pymoo grants the possibility to tailor the genetic operators of the NSGA-II algorithm to a specific problem. In the proposed framework the population size and termination criterion is modified. For reasonable computational time the population size is set to a fixed size of $n_{pop} = 50$ and the termination criterion is defined by a design space tolerance of 1%. The design space tolerance tracks the change in design space per generation and terminate the optimization when the tolerance is reached. Since for FCS applications the design space will be in the range of 10 to 1000 kWh/kW a Pareto front in the precision of 1% is sufficient to give an accurate indication of the sizing.

4.4.2. Sizing Procedure

The following steps describes the procedure that is executed with this optimization framework.

- Step 1: An initial population consisting of the 3 design parameters (P_G^{max} , P_b^{max} and E_b^{max}) are generated using the NSGA-II operators.
- Step 2: The population is then simulated by the FCS model, to extract the performance parameters, L_{exp} , T_{max} and T_{freq} .
- Step 3: The design parameters together with the simulation results are evaluated using the objective functions subject to the design constraints.
- Step 4: Using the NSGA-II operators, a new parent population is selected for the next generation.
- Step 5: Step 2-4 are then repeated until the termination criterion is met and the Pareto front is found.

- Step 6: Lastly, once the optimization terminates, the design space and objective space of the final generation is stored and visualized.

Using this objective space and design space data, the FCS host can use higher level information to select the optimal station design. Such higher level information can be for example investment budgets or location specific QoS requirements.

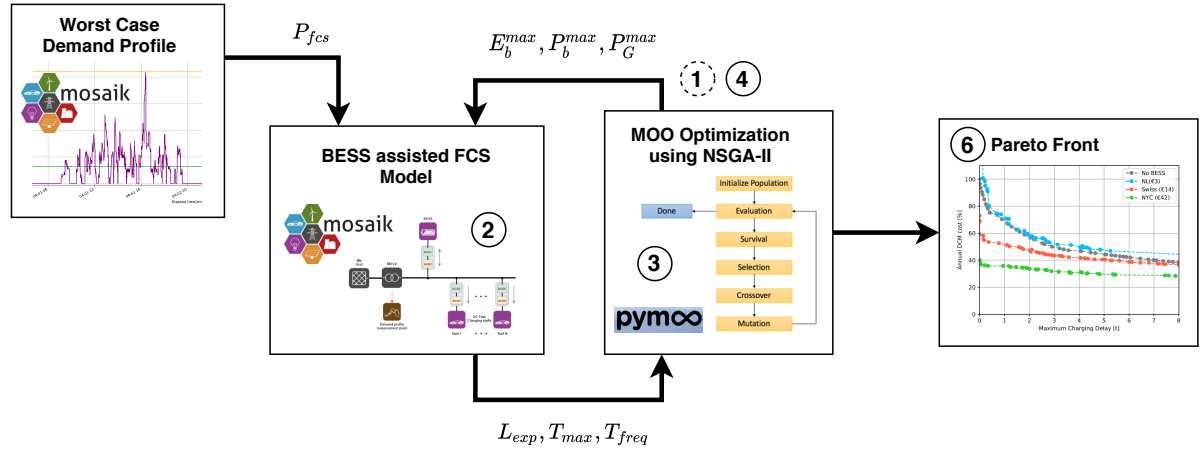


Figure 4.1: A schematic overview of the proposed design optimization framework

5

Optimization and Simulation Results

This chapter is dedicated to present the results obtained from the optimizations and simulations. Several numerical case studies are conducted on four FCS station worst case demand profiles to analyse how the Pareto front and optimal designs are impacted. These 4 stations differ in station's utilization and installed charging capacity. First, the four stations are analysed performing DCM with only power balance. Second, the difference in station types are analysed in the scenario where BESS assisted DCM is being performed in a country with mid range demand tariffs. Third, the impact of different demand tariffs, reduced BESS costs and increased C-rate on the optimal design are all individually investigated. Fourth, the impact of DCM on the optimal BESS lifetime is analysed. Lastly, several solutions are selected and simulated on a weekly load to assess the performance of the proposed optimization. The tabulation of all results presented are included in appendix E.

5.1. Stations and Case Studies description

To assess the proposed optimization framework and give answers to the research questions, the optimization is performed for five case studies on four different station demands.

As previously mentioned, for this thesis the optimizations are performed using demand profiles extracted from energy measurements taken at four FCS stations in the Netherlands. These measurements were performed for a month during the worst case use period at a sampling frequency of 1 minute. Table 5.1 shows the additional station information and performance metrics extracted from the measurement data for stations A to D.

Using these station information, the stations are categorized based on their utilization and installed capacity. Here the utilization is considered the total average daily minutes the station is occupied charging and the installed capacity is total charging stall capacity installed at the station. Station A, is considered an under utilized station with a large installed capacity (U+L), station B a highly utilized station with a large installed capacity (H+L), station C an under utilized station with a small installed capacity (U+S) and station D a highly

Table 5.1: FCS station details in worst-case usage period (some data are excluded in this version)

| Station Name | A | B | C | D |
|----------------------------------|----------------|----------------|----------------|----------------|
| Installed Capacity | 625 kW | 600 kW | 450 kW | 450 kW |
| Peak Demand | 288 kW | 421 kW | 325 kW | 384 kW |
| Average Demand | 29 kW | 63 kW | 40 kW | 60 kW |
| Total Energy Charged | - MWh | - MWh | - MWh | - MWh |
| Stalls | - | - | - | - |
| Average Daily Utilization | 533 min (37 %) | 821 min (57 %) | 533 min (37 %) | 734 min (51 %) |
| Category | U+L | H+L | U+S | H+S |

utilized station with a small installed capacity (H+S). Furthermore, the peak demand is the actual power demand reached within the measured period. This together with the average demand are used for the design constraints (4.7). The installed capacity and the number of stalls (excluded from the public thesis due to data sharing compliance) are used to estimate the number of charging EVs with (3.22). In this estimate the assumption is made that all charging stalls possess equal power rating.

For each station its worst case demand profile described in section 4.4 is extracted from the measurement data. The worst case demand profile for station A to D is shown in Figure 5.1. These worst case demand profiles consist of a 24 hour with the worst peak demand followed by a 24 hour with the worst energy density. From analyzing these profiles it is directly evident that stations with larger installed capacity carry larger and more isolated demand peaks than the stations with smaller installed capacity. Furthermore, underutilized stations tend to possess lower average demand than highly utilized stations, and the difference between the average demand and peak demand seems to be larger for highly utilized stations. On the basis of these differences in station characteristics, conclusions can be drawn based on the optimization results.

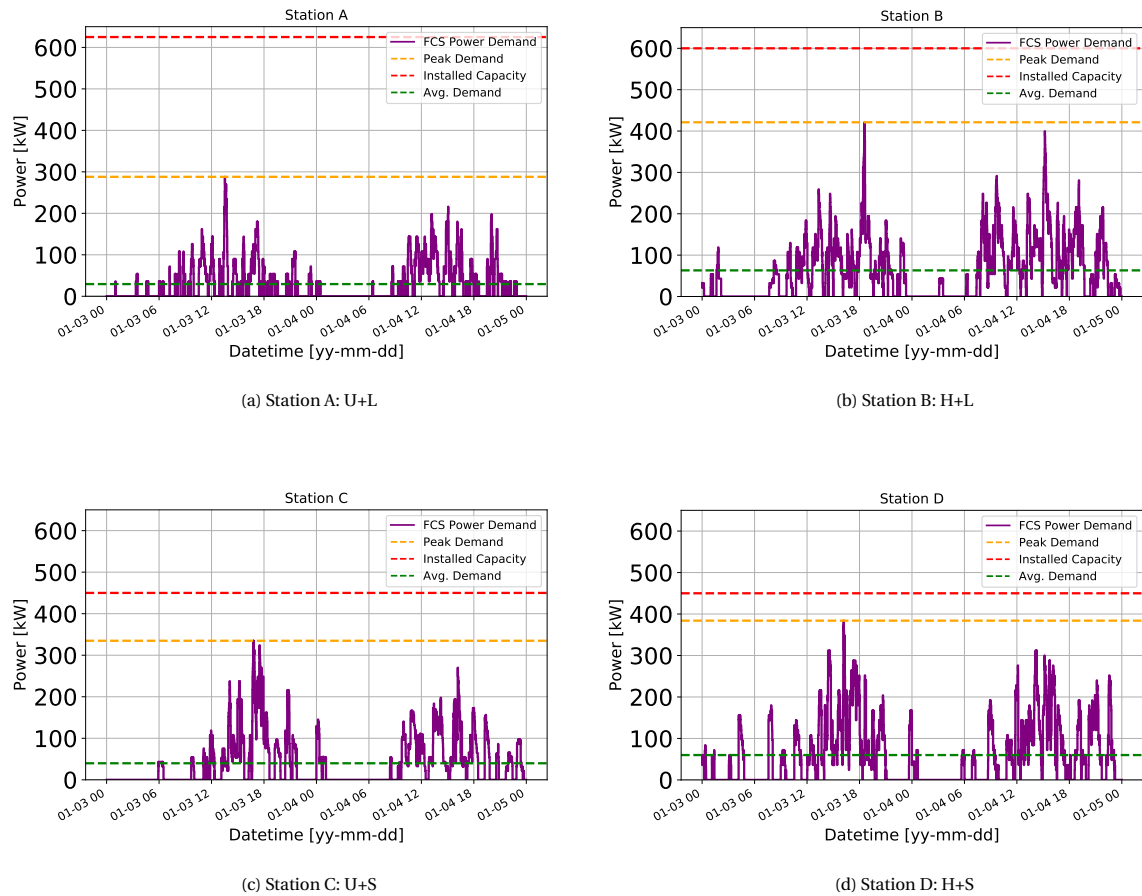


Figure 5.1: Worst case demand profile for all stations

In order to assess the DCM costs, the BESS project costs and monthly demand tariffs are required. As explained in section 4, the BESS project cost comprises of the energy capacity cost C^{bess} and the power capability costs C^{conv} . The energy capacity cost is dependent on the energy storage chemistry and the power capability cost are associated with the cost of the power electronic converter. The project costs found in literature for the LFP battery chemistry is shown in table 5.2. Included in this Table is also the expected price drop for LFP batteries in 2030.

To calculate the total demand charges, the demand tariff per kW from the station's region is required. To properly assess the effects of different demand tariffs on our optimization 3 regions are selected, the Netherlands which possesses a low demand tariff, Switzerland which has an upper mid range tariff and NYC which is an extreme case with high demand tariff. Table 5.3 includes the monthly demand tariffs for these regions.

Table 5.2: BESS project costs for LFP chemistry and associated power converter.

| Energy Capacity cost (C^{bess}) | | Power capability cost (C^{conv}) |
|-------------------------------------|---------------|--------------------------------------|
| 2020 | 2030 | |
| €490/kWh [20] | €190/kWh [20] | €110/kW [91] |

To answer the research questions of this thesis and analyse how the optimum sizing is influenced by different factors such as station type, demand tariffs, BESS cost and maximum power capability. The following 5 study cases described in Table 5.4 will be used to run the optimizations.

Table 5.3: DSO monthly demand tariffs per region

| Region | Demand Tariff | |
|---------------|---------------|------|
| Netherlands | €2.7/kW [92] | Low |
| Switzerland | €14.4/kW [15] | Mid |
| New York City | €42.3/kW [14] | High |

Table 5.4: List of the study cases for the optimization

| Study Case | Description | Demand Profile | BESS | Demand Tariffs |
|------------|--|-------------------------------|---------------------------------------|----------------|
| Case 0: | DCM without BESS | (U+L), (H+L), (U+S), (H+S) | Not incl. | NL, Swiss, NYC |
| Case 1: | BESS assisted DCM for different station types in Switzerland | (U+L), (H+L), (U+S), (H+S) | Incl. €490 / kWh P/E ratio <1 | Swiss |
| Case 2: | BESS assisted DCM in different demand tariff regions | (U+L), (H+L), (U+S), (H+S) | Incl. €490 / kWh P/E ratio <1 | NL, Swiss, NYC |
| Case 3: | BESS assisted DCM in 2030 | (U+L), (H+L), (U+S), (H+S) | Incl. €190 / kWh P/E ratio <1 | NL, Swiss |
| Case 4: | BESS assisted at 2C power capability | (H+L) | Incl. €490 / kWh P/E ratio <1.3 | NL |

The results obtained from these optimizations are presented in the following way. Because the maximum charging delays has more significance for the quality of service of a station, the objective space will be analysed in terms of annual DCM costs against maximum charging delays in minutes. The movement of the design space will be analysed based on the grid-tie capacity, BESS energy capacity, and BESS power rating against the maximum charging delays. Lastly, the power to energy (P/E) of the BESS is analysed for the optimum solutions.

When assessing the objective space it should be noted that the annual DCM cost is given as a percentage of the stations annual demand charges without DCM presented in Table 5.5. The demand charges are here based on the station's peak demand value presented in Table 5.1. Similarly, the grid-tie size and BESS power capability is given in per units, with the base value being the peak demand of the station also given in Table 5.1.

Table 5.5: The annual demand charges without DCM per station in considered regions

| Station: | A | B | C | D |
|---------------|----------|----------|----------|----------|
| Netherlands | €9,331 | €13,640 | €10,530 | €12,441 |
| Switzerland | €49,766 | €72,749 | €56,160 | €66,355 |
| New York City | €146,188 | €213,700 | €164,970 | €194,918 |

5.2. Case 0: DCM without BESS

Case 0 assumes that DCM is being performed on a FCS without the inclusion of a BESS. This implies that only power balance is being employed for peak-shaving, and thus accepting delays. This reduces the design parameters to only the grid-tie size reduction, which will correspond one to one with DCM costs. Figure 5.2a displays the objective space results in terms of annual DCM cost and maximum charging delay and Figure 5.2b in terms of the annual DCM cost and utilization time increase in percentages.

When comparing the 3 objective functions in these results, the trend reveals that reducing the DCM costs exponentially increases both charging delay components. However, the maximum charging delays increases harder initially than the utilization time. Furthermore, when analyzing the different station categories, it can be observed that regarding the maximum charging delays, both highly utilized station B and D was able to obtain more DCM cost reduction than the underutilized stations A and C. Whereas, when considering the utilization time increase, the stations with larger capacities A and B obtained more DCM cost reduction than stations with smaller installed capacities C and D.

These results concludes that maximum charging delays correlates with the peak-demand to average demand differences found in the station's characteristics. This difference is larger in highly utilized stations than in under utilized stations. While increase in utilization time is caused more by energy dense peaks, which are more commonly found in stations with smaller capacities. The isolated peaks found in highly utilized stations allow for more grid-tie reduction. Furthermore, it can also be concluded that power balance alone performs surprisingly well considering no large investments are required. However, also evident from the results, this technique should not be considered for stations where delays cannot be permitted.

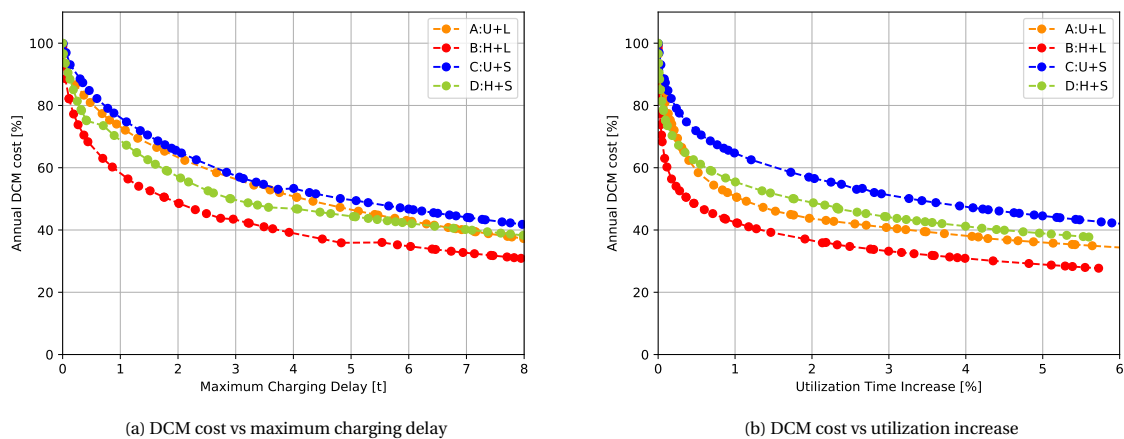


Figure 5.2: Results for Case 0: DCM without BESS

5.3. Case 1: BESS assisted DCM for different station types in Switzerland

This case demonstrates the effect different station categories can have on the optimal sizing for BESS assisted DCM. Since prior studies suggested \$9/kW to be the break-even point for most DCM applications in North America, the demand tariffs of Switzerland is selected to ensure that a feasible BESS included solution can be analysed [4]. Furthermore, the following optimization results will be viewed in terms of maximum charging delay. This is done because this delay component has direct impact to charging customers, and thus more impact on the quality of service of the FCS.

Figure 5.3a displays the movement of the objective space in terms of annual DCM cost and maximum delay. Figures 5.3b, 5.4a and 5.4b displays the movement of the design space in terms of the maximum delay. Analysing the results for the different station categories, it becomes clear that for BESS assisted stations with larger capacities can achieve more DCM cost reduction. Almost 10% to 15% more depending on the delay permitted. Nevertheless, with all station categories around 40% of DCM cost reductions can be obtained without any delays. With designs permitting 6 minutes delays providing a 50% to 60% in cost savings. Moreover, relative to the peak demand the grid-tie lies between 0.2 to 0.4 p.u for every station category and remains relatively constant as the delay time increases.

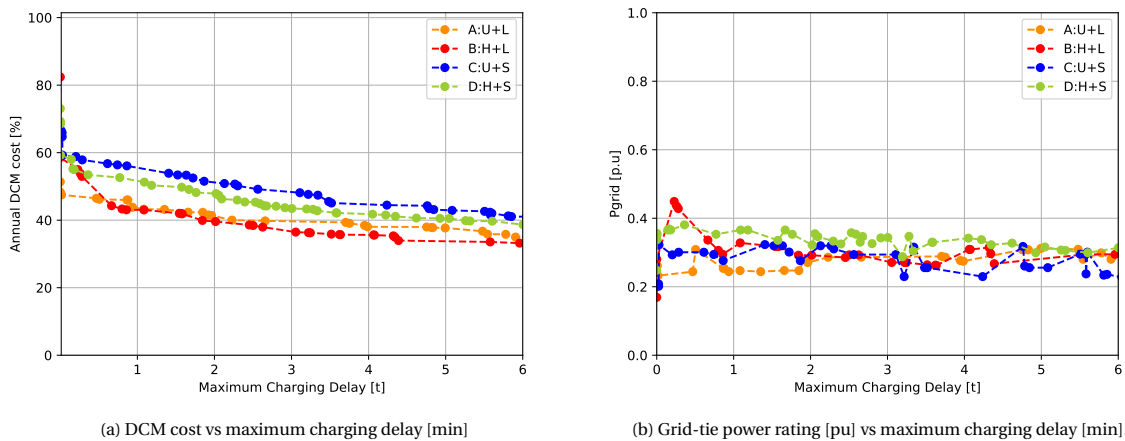


Figure 5.3: Results for Case 1: BESS assisted DCM in Switzerland - A

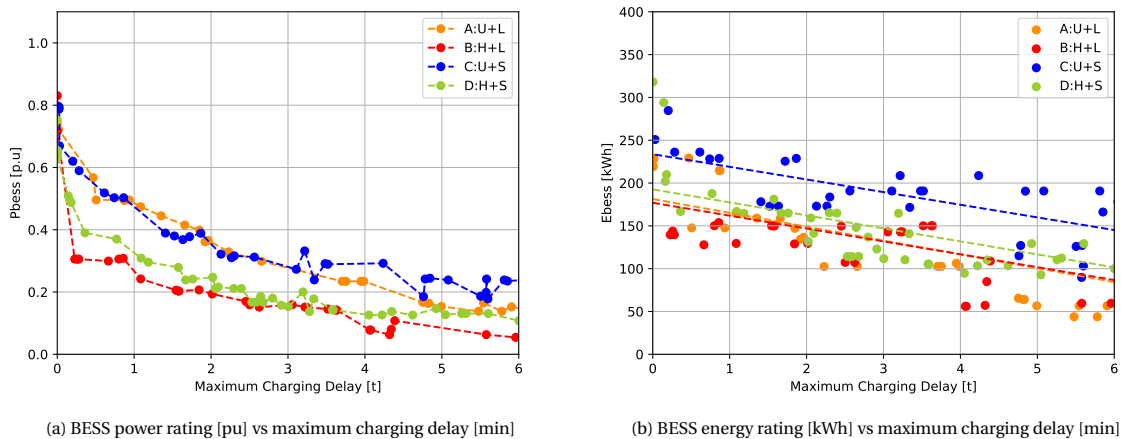


Figure 5.4: Results for Case 1: BESS assisted DCM in Switzerland - B

As for the BESS sizing rating, this is split on the basis of station utilization, stations with high utilization requires smaller power ratings (relative to their peak demand), than for stations with low utilization rates. Furthermore, as the delay increases, the required BESS power capabilities exponentially decreases and BESS capacities decreases in an almost linear trend. This off course due to the fact that maximum charging delays are determined from the integral during power miss-match periods. Additionally, it can be concluded that the proposed framework reduces the grid-tie to an optimal point and sizes the BESS accordingly to adhere to the objectives.

When observing the P/E ratio of the design space given in Figure 5.5, all station categories except for station A sits around a PE ratio of 1/2. Station A instead follows a P/E ratio much more closer to 1. This

difference might be due to the fact that underutilized stations with large capacities tend to have large isolated demand spikes relative to their average power as can be seen in Figure 5.1a. These demand spikes are most likely caused at underutilized stations by chance when a large number EVs charge simultaneously. However, since these spikes are isolated it is not as energy demanding. Thus, requiring designs with higher P/E ratios.

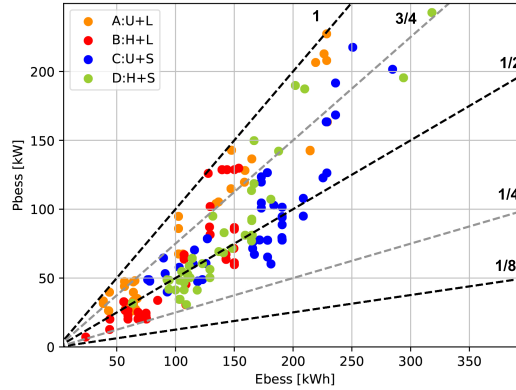


Figure 5.5: BESS power rating [kW] vs BESS energy rating [kWh] (P/E ratio) in Switzerland

5.4. Case 2: BESS assisted DCM in different demand tariff regions (low, mid, high)

These results are intended to show how the optimum sizing is influenced by different demand tariffs. In this case we optimize for the 3 study case locations presented in Table 5.3. This illustrates how the objective and design space moves for a certain station demand employed in different demand charge regions. Based on previous results, station D is selected to observe since this represents a station with balanced characteristics. Once more, Figure 5.6a displays how the objective space move in terms of DCM cost and maximum charging delays and Figures 5.6b, 5.7a, 5.7b, and 5.8 shows how the design parameters move with respect to maximum charging delays for the different regions. Additionally, to serve as a benchmark, the DCM solutions without BESS are included to assess the effectiveness of the optimum solutions with BESS included.

The results in Figure 5.6a show that a significant DCM cost reduction can be obtained in high demand tariff regions relative to applying only power balance. However, this is not the case for regions with low demand tariffs. In the Netherlands case, BESS assisted DCM performs worse than power balancing in terms of costs. Making power balancing the preferred option for DCM in the Netherlands assuming cost is the driving factor. In contrast to the Netherlands, in Switzerland and NYC, DCM reductions between 41-61% and 60-71%, respectively can be obtained depending on the delays. Furthermore, observing how the grid-tie moves in Figure 5.6b with respect to the different regions, a dramatic 80% of grid-tie reduction can be achieved in NYC.

Nevertheless, when the movement is analysed in terms of delays, as longer delays are permitted, the differences in performance between power balance only and the other two regions diminishes. Where for 6 minute delays, in Switzerland the station performs almost equally and in NYC with a difference of only 10% in terms of cost. In terms of grid-tie, a difference of 11% and 26% can be obtained with 6 minute delays, respectively. When comparing these BESS included solutions to case 0, the following can be concluded. First, in the Netherlands BESS assisted DCM is not feasible in terms of costs. Second, in Switzerland BESS assisted DCM can always be beneficial for grid-tie reduction at FCSs. However, in terms of cost, a BESS should only be considered for FCSs where the charging delays need to remain low. Third, in NYC BESS assisted DCM can always be always beneficial for FCS applications.

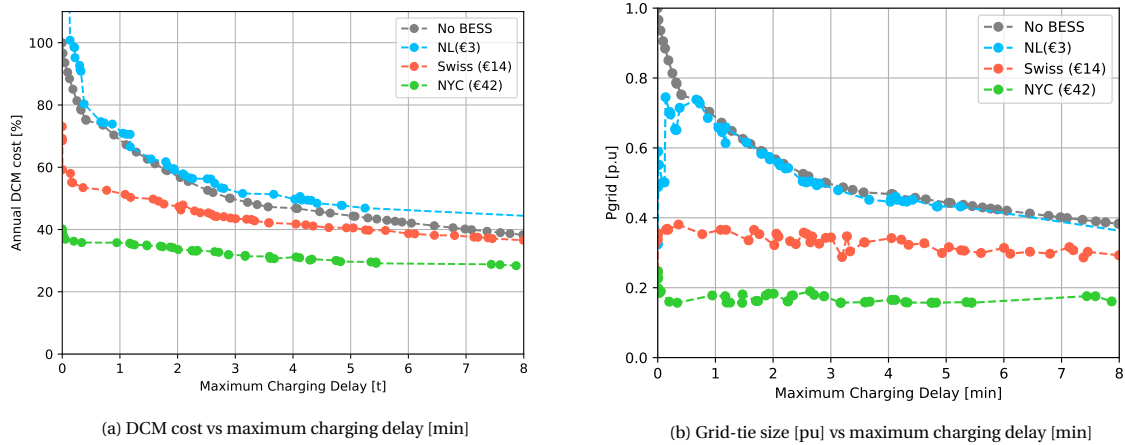


Figure 5.6: Results for Case 2: BESS assisted DCM in different regions - A

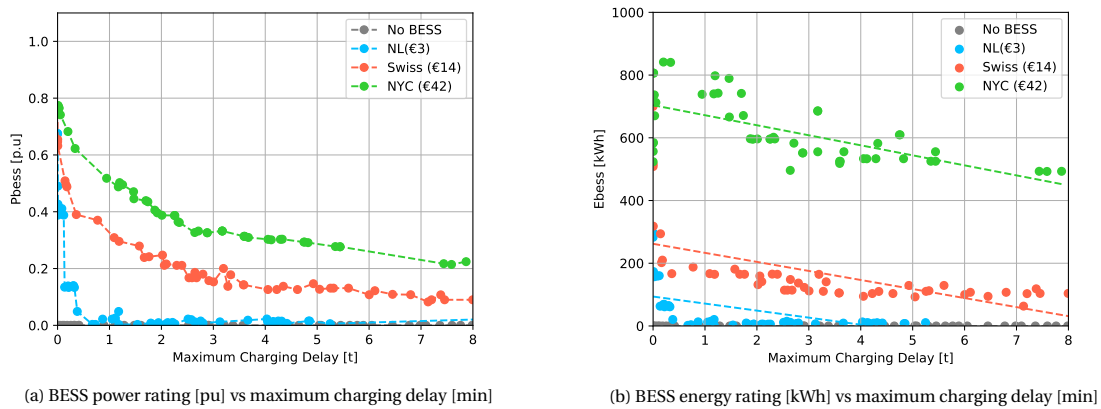


Figure 5.7: Results for Case 2: BESS assisted DCM in different regions - B

Regarding the BESS sizing shown in Figure 5.7a and 5.7b, except for some expensive solutions around zero delays, in the Netherlands the BESS is excluded for most of the solutions and the power balance curve is given as the optimal solution. For the NYC case, the BESS sizing behaves similarly to the Swiss case in terms of delays. However, it also evident that high demand tariffs directly impact the feasible BESS capacities, a 3x difference in demand tariff between Switzerland and NYC is reflected in the BESS capacity increase. Furthermore, the same is observed between the two power parameters, the additional 20% decrease in the grid-tie can be found in the increase of the BESS power capabilities.

Figure 5.8 illustrates how the different demand tariffs influence the optimal BESS P/E ratios for each station. For the dutch case, except for some expensive outliers, the optimal solutions concentrate around the origin, due to either a really small BESS is suggested or none at all. As previously shown, for the Swiss case, the PE ratio of the optimal solutions for this region (highlighted in orange) concentrates between 1 and 1/2. As for the NYC case, larger BESS capacities are introduced, making the optimal solutions (highlighted in green) concentrate between 1/2 and 1/8. To conclude, due to the almost direct correlation between the demand tariffs and BESS capacities, FCSs located in regions with high demand tariffs optimally should possess larger capacities, and thus lower PE ratios than for stations in regions with mid demand tariffs.

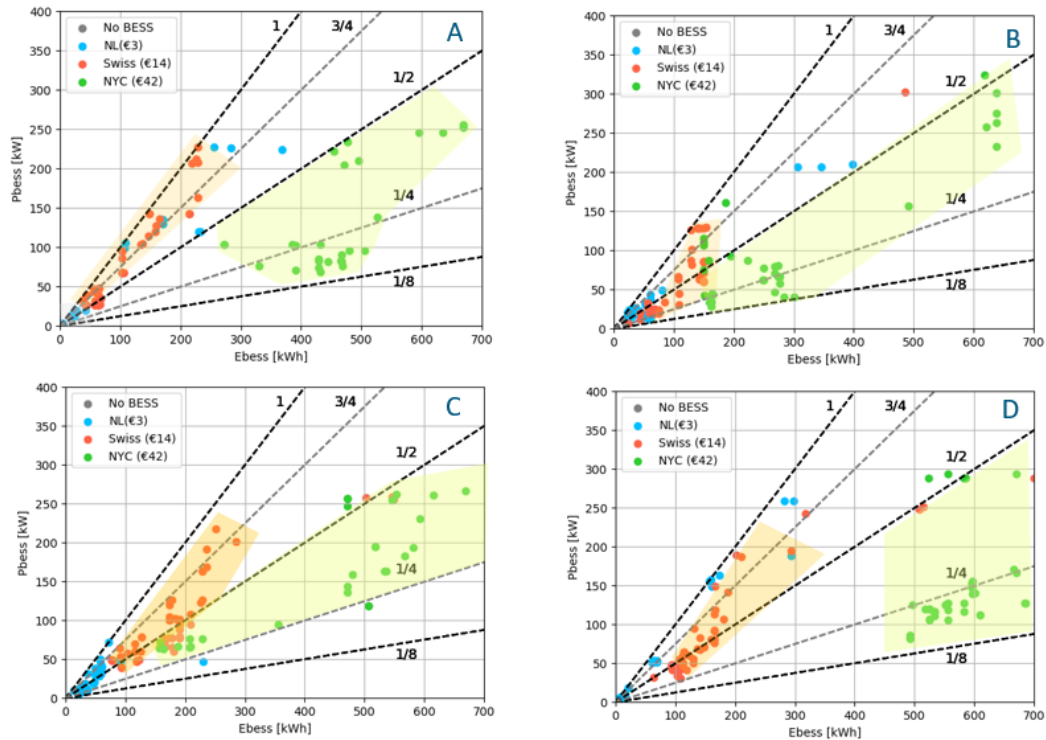


Figure 5.8: BESS P/E ratio in regions with different demand tariffs for all stations.

5.5. Case 3: BESS assisted DCM with expected BESS price drop in 2030

In this case study, the impact of the expected BESS cost reduction for 2030 will be taken into consideration. Estimates obtained from literature projects a capacity price drop from €490/kWh to €190/kWh for LFP type batteries by 2030 [20]. This price is inserted into the optimization and the results are presented in this section.

Figure 5.9a compares the objective space from the 2020 situation against the expected 2030 situation. From this graph it can be seen that an extra 14% reduction in DCM costs can be obtained in 2030 for stations with small delays. However, as the delays increase this 14% diminishes. As for the grid-tie shown in Figure 5.9b, almost the same reduction is obtained for 2030 between 15-17%.

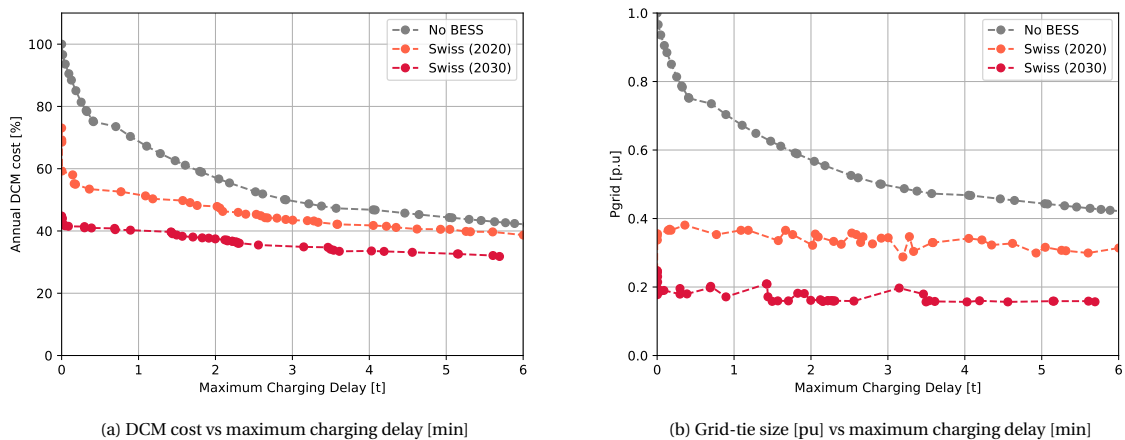


Figure 5.9: Results for Case 3: BESS assisted DCM for Switzerland in 2030

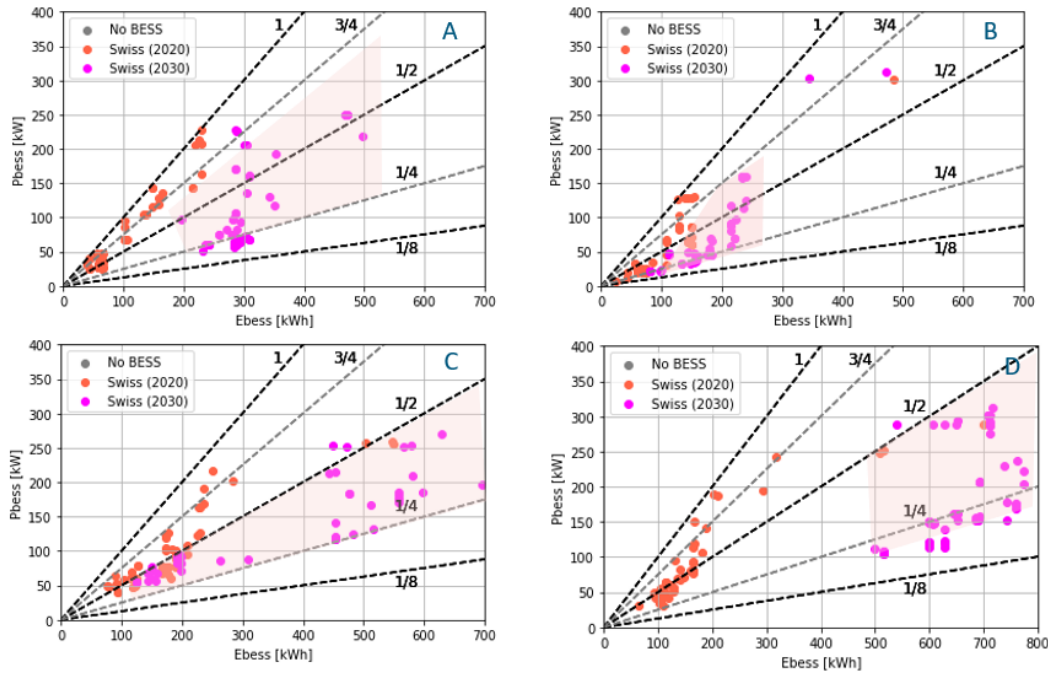


Figure 5.10: PE ratio in countries for Switzerland in 2030 for all stations

Regarding the P/E ratio differences shown in Figure 5.10, similarly is observed for BESS price reduction. Due to cheaper prices in 2030, the PE ratio for the optimal solutions (highlighted in pink) include larger BESS capacities and lower PE ratios than the current case. For most solution these concentrate between 1/2 and 1/4.

Furthermore, the results for the dutch case is plotted in Figures 5.11b and 5.11b. From these results it can be seen that by 2030 in the Netherlands the BESS assisted DCM, begins to perform equally well as power balance. Another interesting finding is a grid-tie reduction of almost 60% can be obtained for designs below 2 minutes. Increasing the potential for other objectives.

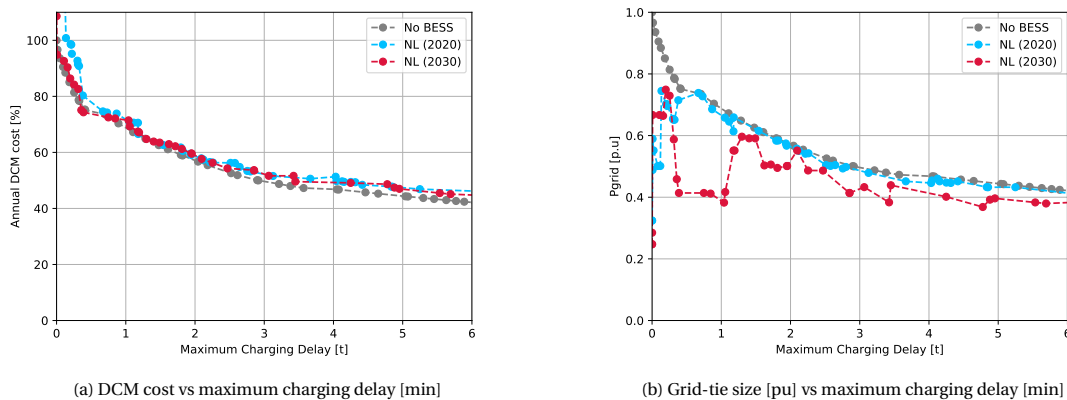


Figure 5.11: Results for Case 3: BESS assisted DCM for the Netherlands in 2030

5.6. Case 4: BESS assisted DCM with BESS power capability of 2C

Lastly, case 4 analyses the influence of increased discharging capabilities on the optimal sizing. A BESS can discharge at 2C for about 20minutes, this case takes the assumption that 2C C-rates can be implemented at FCSs via a smart charging algorithms. To make our optimization include designs with 2C discharge rates,

the P/E ratio constraints are extended from 1 to 1.3 [90]. Since this extension in our constraints only impact situations that requires higher P/E ratios such as stations with large capacities, station B is analysed in the Netherlands. From the results shown in Figure 5.12 we can see that due to the introduction of solutions with higher P/E ratio, the DCM cost is further reduced where the case in the Netherlands performs equally as well as case 0. Leaving us to the conclusion that higher P/E ratios can be beneficial for stations with large capacities.

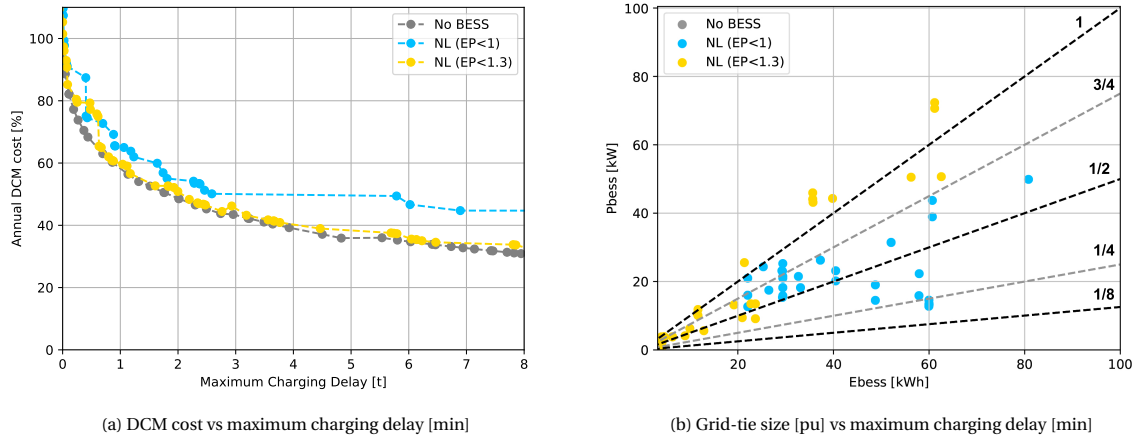


Figure 5.12: Results for Case 4: BESS assisted DCM for the Netherlands with 2C power capability

5.7. Impact of DCM on BESS Lifetime

in this section we want to assess the impact our optimization has on the BESS lifetime. The results in figure 5.13 show the expected lifetime of each optimal solution for every stations in a Swiss demand charge region. It can be seen that there is no direct correlation between the expected lifetime and any other objective functions. However, it is noticeable that the lifetime concentrates between 10 to 14 years, with station C having some solutions around 8 years. Since most battery integrator assumes a 10 year lifetime for most lithium ion chemistries. It can be concluded that the proposed sizing optimization in this thesis does not pose detrimental concerns related to BESS lifetime.

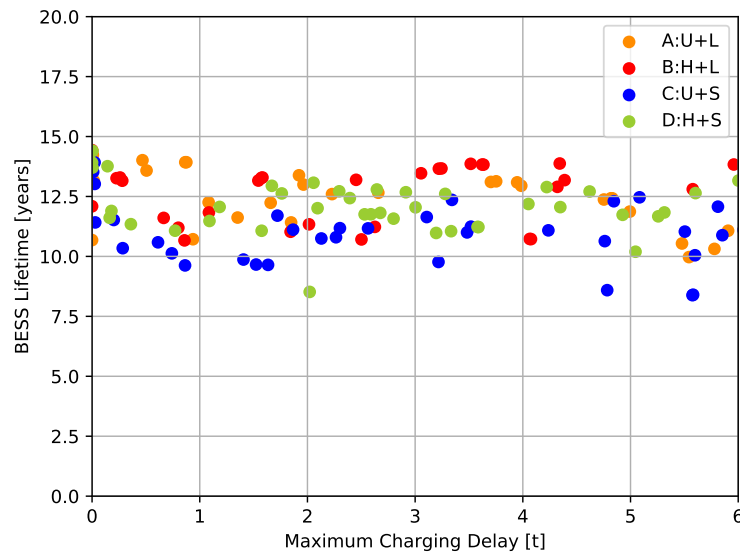


Figure 5.13: Expected BESS lifetime in Switzerland for all stations

5.8. Impact on performance

In this section the performance of the FCS is assessed by selecting a number of optimally sized solutions and simulate this on an entire week demand. The week demand selected is the week wherein the peak demand occurs. The results include the charging delays, the SOC profile of the BESS and the power flows. The power flows displayed is the grid-tie power, the BESS discharge power and the EV demand. Furthermore, it should be noted, that the optimal solutions are rounded up to the nearest 5 kWh/kW. In real-life this rounding is dependent on the options available to the designer on the battery market.

The simulation results of an optimal 2 minute delay design without BESS is shown in Figure 5.14 and in Figure 5.15 an optimal 2 minute BESS included solution. Both are simulated using demand D and with solutions for the Switzerland demand tariff case. When these results are compared, it becomes clear that in the BESS included design the BESS power and grid-tie combined are slightly larger than the grid-tie size in the non-BESS solution. This small difference in rating and maximum delay are due to the fact that the BESS reaches below it's 15% SOC threshold, causing the power capabilities of the to BESS decreases, and thus causing additional power mismatch. This is also visible in the way the delay peaks differ during this period. Nevertheless, the BESS included solution will result in a 12.3% lower DCM cost compared to the DCM solution without BESS and a total of 53.7% reduction in demand charges.

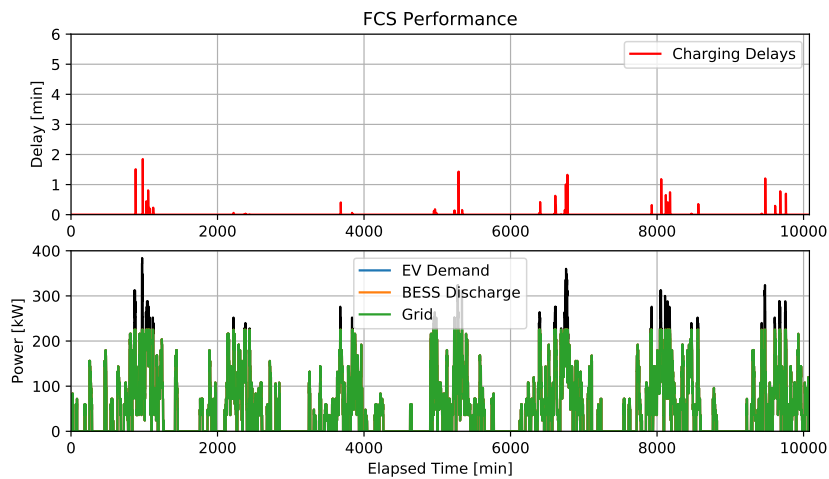


Figure 5.14: Station: D - $E_b=0$, $P_b=0$, $P_G=225$ - - Annual DCM Cost = €38,880 (-41.4%)

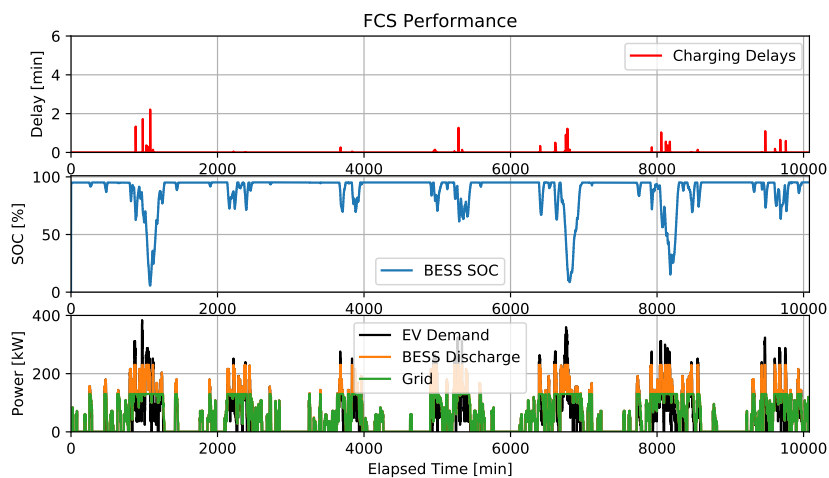


Figure 5.15: Performance of a 2 minute delay optimal FCS design with demand D in Switzerland using $E_b^{max} = 135$, $P_b^{max} = 100$, $P_G^{max} = 130$, $C_{kW} = €14.4/kW$, and $L_{exp} = 11$ Years - Annual DCM Cost = €30,750 (-53.7%)

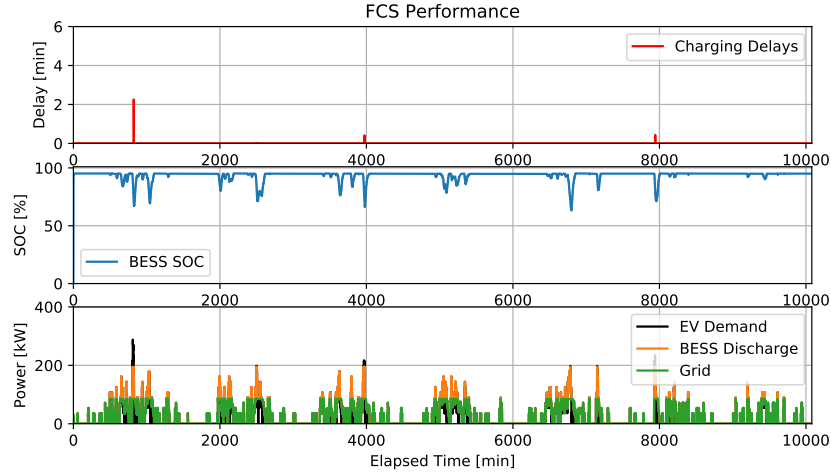


Figure 5.16: Performance of a 2 minute delay optimal FCS design with demand A in Switzerland using $E_b^{\max}=140$, $P_b^{\max}=110$, $P_G^{\max}=85$, $C_{kW}=14/\text{kW}$, $L_{\text{exp}}=14$ Years - Annual DCM Cost = €21,492 (-56.8%)

To assess the performance with different characteristics, a station demand with the opposite characteristics (Station A) is simulated. The results from this simulation is displayed in figure 5.16. From this solution there is a significant difference in the frequency of charging delays. This again infers our previous conclusion that that charging stations with larger installed capacities can obtain better performances in terms of how frequent delays occur. However, it is also evident that there are significant differences in the use of the BESS. For the underutilized station the cycle depths are low and as expected the battery is not being used as frequent. This can give under utilized stations more opportunity to employ their BESS for other ancillary services, such as frequency containment reserve even during peak-shaving operation. Further improving their business case. The lifetime for the BESS at these under utilized station is slightly better due to less cycling, however, these gains are overshadowed by the increased calendar degradation due to high SOC idling.

Figure 5.17 shows the results of a 2-minute optimal solution for D demand FCS located in NYC. These results show that even with different design ratios, the optimal charging delay performances do not differ much per region. However, as observed from the optimizations, the P/E ratios are reduced, and thus larger BESS capacities are introduced to the optimal design space. Additionally, because of these larger BESS capacities, the discharging and charging periods are longer, causing longer cycles.

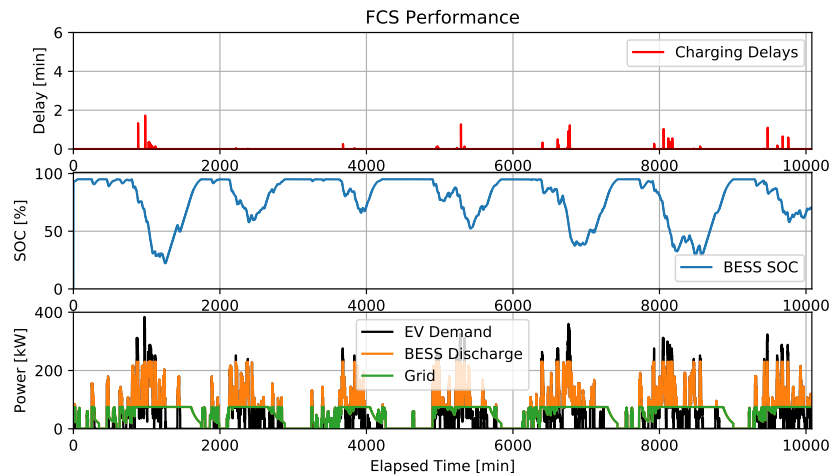


Figure 5.17: Performance of a 2 minute delay optimal FCS design with demand D in NYC using $E_b^{\max}=600$, $P_b^{\max}=155$, $P_G^{\max}=75$, $C_{kW}=14/\text{kW}$ - $L_{\text{exp}}=14$ years - Annual DCM Cost = €64,573 (-66.9%)

This reduces the opportunity to dispatch the BESS for other ancillary services. However, these longer cycle periods are more shallow and the high SOC idling periods are shorter, resulting in improved BESS lifetimes. The cycle counting comparison between the two designs are shown in 5.18. In the NYC case it is evident that less micro-cycles are occurring at high average soc levels and that the large cycles has lower DOD ranges.

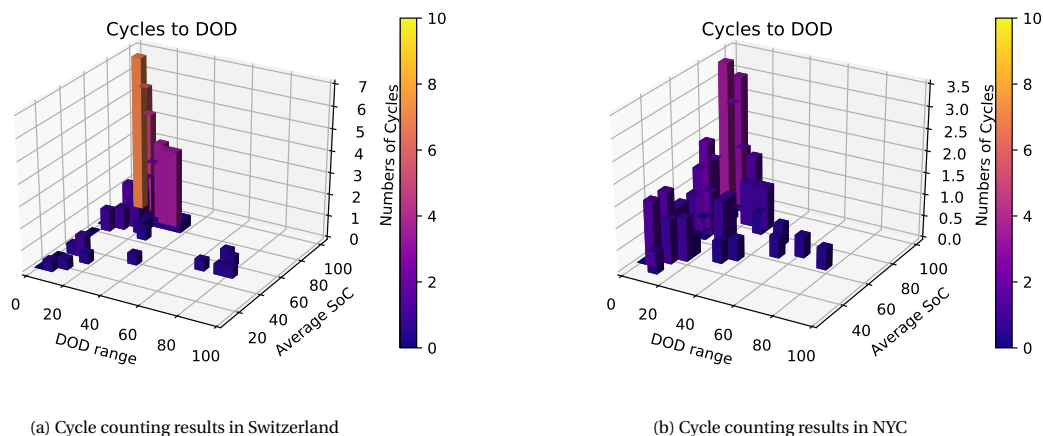


Figure 5.18: Comparison of the performed BESS cycles at a 2 minute delay FCS located in Switzerland and one in NYC

5.9. Key Results

- The maximum charging delays correlates with the utilization of a station and the increase in utilization time with the installed capacities of a station.
- Power balance alone performs surprisingly well for stations where delays can be accepted.
- In the Swiss demand tariff case, all station categories 40% of demand charge reduction can be obtained without any delays. Designs permitting 6 minutes delays a 50 - 60% in demand charge reduction can be obtained.
- In the Swiss case, the grid-tie reduction ranges from 0.4 to 0.2 pu for every station category and the sizing trend remain constant as the delay length increases. It can also be concluded that stations with larger installed capacities can profit more from demand charge reduction than stations with smaller installed capacities.
- BESS assisted DCM in the Netherlands performs worse than power balancing alone in terms of cost. Meanwhile, in Switzerland and NYC, demand charge reductions can be between 41-61% and 60-71%, respectively depending on the delays.
- Due to the almost direct correlation between the demand tariffs and BESS capacities, FCSs located in regions with high demand tariffs optimally should possess larger energy capacities. Hence lower P/E ratios than for stations in regions with lower demand tariffs.
- For the Swiss case, an extra 17% reduction in DCM costs can be obtained in 2030 for stations with short delays.
- Extending the BESS discharging constraints to higher C-rates can be beneficial for stations with large installed capacities in regions with low demand tariffs.
- There does not seem to be any correlation between the objectives and lifetime, however this ranges between 10-14 years. Hence, the optimal results do not pose detrimental concerns related to BESS lifetime.
- For the underutilized stations the BESS cycle depths are shallow and consequently, the BESS is not utilized as frequent. This can give underutilized stations more opportunity to employ their BESS for other ancillary services that further improve their business case.

- Lastly, because the optimal P/E ratio is lower for regions with high demand tariffs, the discharging and charging periods also becomes longer and causes longer cycles. This reduces the opportunity to dispatch the BESS for secondary ancillary services. However these longer cycle depths are more shallow and introduces less micro-cycles at high average SOC. Hence, improving BESS lifetime.

6

Conclusion

This chapter concludes this thesis by firstly, giving answers to the research questions. Secondly, give a review of the main contributions of this thesis and lastly, recommendations are provided on the suggested further research in the studied domain.

6.1. Answers to research questions

In section 1.5.3 the four main research questions are defined. These questions are intended to help fill the literature gap identified in the previous work survey. Using the results obtained in this thesis, these questions are answered below.

6.1.1. How to formulate a multi-objective optimization framework for optimal BESS and grid-tie sizing in order to minimize demand charges and charging delays at FCS?

Using the following 3 sub-questions an answer is given to this main question.

- **How is the BESS modeled in the system?**

From the literature it is clear that an analytical BESS model suffices. However, these studies lack the usage of power capability curves. Which in the results of this thesis has shown to cause additional delays when the BESS is below its maximum power capability threshold. Leading us to the conclusion that including these power capabilities in the model is essential when analysing delays caused by power differences.

- **How are the charging delays modeled in the system?**

Most literature used stochastic simulations to generate a demand profile, where the SOC, number of connected EVs ect. are known and estimated the waiting times based on queuing. The challenge in this thesis was to estimate these delays from energy measurements. By identifying power miss-matches between the demand and the modeled FCS's capabilities included with knowing the number of EVs charging. The delays can be determined under the assumption that power balance is applied and the EVs continued to charge at the available speed.

- **What objective functions are required for the proposed optimization strategy?**

In literature only single objective optimizations were found on FCSs and this mostly cost related. This thesis incorporates charging delays as a contradicting objective to cost. The cost is analysed based on the annual demand charges and BESS investment. The charging delay objective gives an assessment of the performance of the station. Furthermore, it was also concluded that this delay objective, includes two deviating aspects. The frequency of delays and maximum length of delays that can be experienced. The first affects the charging host and the second gives an indication of the quality of service provided to the FCS customers. In the proposed framework these are separated and minimized individually. The results show that station with different characteristics perform better in terms of cost depending on which objective is being observed.

6.1.2. How do FCS demand influences the optimal design?

In this thesis the optimization was performed on demand data from stations that differ in utilization and installed capacity. This combination introduces noticeable differences in the power demand profiles. When considering DCM without BESS we can conclude that highly utilized stations retrieves more cost reductions than under-utilized stations in terms of maximum charging delays. Moreover, when observing the increase in utilization (frequency of delays), stations with larger capacities will retrieve more cost reduction than stations with smaller capacities. When considering BESS assisted DCM, the stations with larger capacities obtain more cost reduction than stations with smaller capacities. Furthermore, when the design space is observed, stations with high utilization requires less BESS power (relative to the station's peak demand) than stations with lower utilization. Therefore, this leads to larger BESS capacities being suggested due to the P/E ratio constraints.

6.1.3. How do demand tariffs and BESS costs influence the optimal design parameters?

The demand tariffs can vary significantly per region. In this research we investigated tariffs in the Netherlands (€2.7), Switzerland (€14.4) and NYC (€42.3). From the optimizations we can conclude that for the Netherlands nowadays the BESS costs are too high for profitability. This causes the optimization to roughly follow the power balance without BESS solutions. For Switzerland the optimization results in feasible solutions with BESS. Where a 41% DCM reductions can be obtained without delays and a maximum of 61% reduction permitting 6 minutes delay. However, this is close to the power balance curve, leading us to the conclusion that this should only be considered for low delay solutions. For NYC a reduction between 60-71% is obtained, for this region the grid-tie is 10% smaller and P/E ratio of the BESS design smaller than Switzerland. Leaving us to the conclusion that in high demand tariff regions, lower PE ratio designs are optimal. Furthermore, in this also the impact on reduced BESS prices were investigated, taking the expected prices for 2030. This resulted in the same effect as higher demand tariffs, as the BESS prices decreases larger BESS capacities are selected and lowers the P/E ratio of the solution.

6.1.4. What impact do the sizing framework have on the BESS lifetime?

Using a post-processing BESS lifetime model this thesis included the lifetime in the objective functions. From the results it is shown that LFP BESS lifetime would optimally be between 10-14 years. From this we can conclude that for peak-shaving no significant degradation occurs. However, it is noticeable that for under utilized stations, the BESS tend to be oversized, where the BESS would introduce large calendar degradation due to a high resting SOC. For these stations a combination between peak-shaving and ancillary service should be further investigated. Furthermore, for stations located in high demand tariff regions, longer BESS cycling periods are introduced due to the low P/E ratio. This reduces the possibility of dispatching the BESS for secondary ancillary services.

6.2. Main Contributions

- The main contribution of this thesis is the proposed multi-objective BESS sizing framework. This framework uses the genetic algorithm NSGA-II to find the Pareto front that includes a set of solutions with the optimal trade-offs between DCM cost and charging delays for BESS assisted FCSs. This framework can be employed by FCS hosts as a sizing guide to determine the BESS and grid-tie sizing that offers an optimal trade-off between demand charges and charging delays at an existing FCS.
- Furthermore, by using station demand measurements, the numerical results from this thesis has shown how the FCS utilization rate and installed capacity can affect the optimal BESS sizing. Additionally, the results also present how different demand tariffs and BESS cost can result in different optimal design P/E ratios, and thus affecting the performance of a BESS.

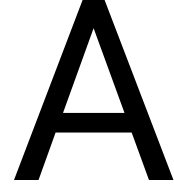
From the results of the thesis, a conference paper titled "Optimal Battery Energy Storage System Sizing for Demand Charge Management in EV Fast Charging Stations" has been drafted. This can be found in appendix F.

6.3. Further research

- **Include RES sizing into the framework (PV):** Because it is likely that FCSs have solar panels on the rooftop. The sizing of RES can be investigated. A PV model can be incorporated to the FCS to determine

the optimal trade-off. This also introduces the possibilities to investigate an emission related objective [48].

- **Asses the effectiveness on other fast charging applications (electric busses):** This framework can be implemented for other EV modalities where fast charging is a key objective. Electric busses are a great example of this, where the charging speeds have consequences on the bus schedule.
- **Perform an optimization based on DSO related objectives:** Using the advantages of Mosaik, this FCS model can be easily connected to a grid model to assess the performance based on grid-impact. With this an optimization regarding objectives related to DSOs can be investigated.
- **Investigate additional ancillary services such as FCR using the sizing framework:** The EMS algorithm can be broaden to include FCR capabilities to a BESS assisted FCS. This can then be included in the framework to determine the optimal BESS sizing.
- **Study the sizing using second life batteries:** This thesis investigated new LFP BESS solutions. As the EV market matures, so does the second life battery market. Second life batteries are considered batteries that surpassed their EoL criterion of 80% capacity. To integrate these batteries into the framework, a lifetime model should be developed for second life batteries, associated costs should be analysed, and technology constraints should be modified.



Rain flow Cycle-counting Algorithm

S_{dod} is a time series that contains a SOC profile resulting from a BESS in operation for a certain period. To determine the partial cycles the algorithm follows the following steps:

- Step 1: S_{dod} is reduced to a peak-valley time series denoted by S_{pk-vl} .
- Step 2: Two ranges R_x and R_y are constructed from the first 3 points in S_{pk-vl} using (A.1).

$$\begin{aligned} R_x &= |S_{pk-vl}(i) - S_{pk-vl}(i+1)| \\ R_y &= |S_{pk-vl}(i+1) - S_{pk-vl}(i+2)| \end{aligned} \tag{A.1}$$

- Step 3: A half (0.5) or full (1) cycle is identified using (A.2)

$$\text{Cycle} = \begin{cases} 0.5, & R_x \leq R_y \text{ and } i = 1 \\ 1.0, & R_x \leq R_y \end{cases} \tag{A.2}$$

- Step 4: If a cycle is identified and RX is the first range in the time series SPkVl, only the first point of the range RX is removed and the second point is considered as the beginning of SPkVl. If RX is not the first range of SPkVl, then both points of RX are removed. Steps 2 to 4 are continued until all the data points are considered.
- "Step 5: Once all data points in SPkVl are considered, each of the ranges discarded before due to not qualifying as a cycle or half-cycle, is considered as a half cycle.

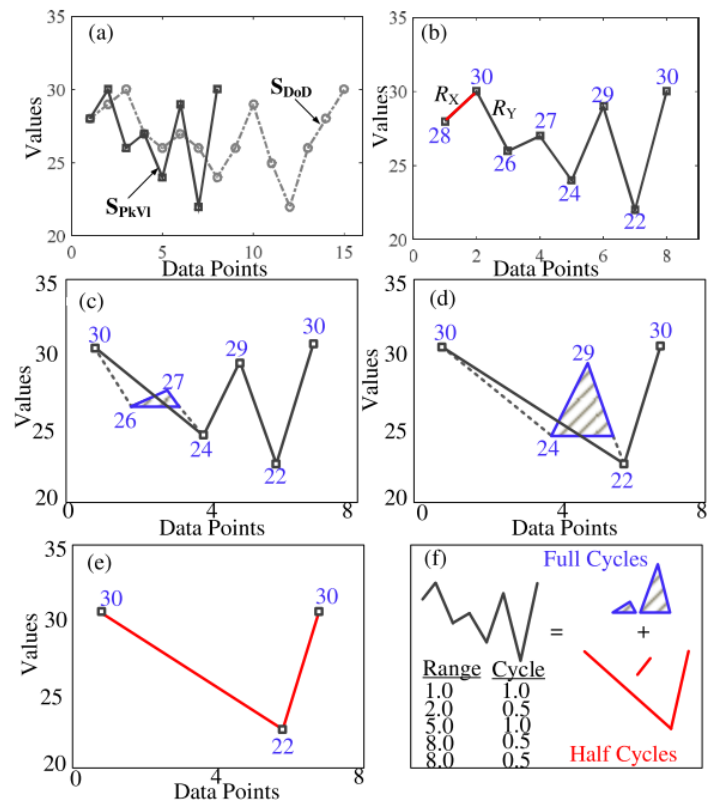


Figure A.1: An overview on how the the rain-flow algorithm works [50]

B

Mosaik

Mosaik is a flexible smart grid co-simulation framework. This framework allows the reuse and combination of existing simulation models and simulators to create large-scale smart grid scenarios. This serves as a test bed for various control strategies such as multi-agent systems (MAS) or centralized control [93]. In addition Mosaik also contains a powerful ecosystem of libraries such as:

- Mosaik Web: a web visualization for mosaik simulations
- Mosaik Pypower: is an adapter for the PYPOWER load flow analysis library.
- Mosaik CSV: A simulator wrapper for CSV files that enables the simulation of collection of discrete values (loads).

The Mosaik's core architecture consists of a simulator manager (sim-manager) and scheduler. The Sim-Manager establishes TCP connections with the simulators to enable the exchange of data between them. The scheduler employs a common simulation clock to exchange data between all connected simulators in a discretely-timed manner. The overall Mosaik eco-system also includes a component-API and a scenario-api. The component-API can be seen as a Mosaik wrapper for each simulator. It sets up a TCP socket and organizes data exchange with Mosaik in the JSON format. This API is available in different programming languages such as Python, MATLAB or Java. The scenario-API contains commands that allows the user to employ scenario scripts where model entities from integrated simulators can be instantiated and connections established between them. This API also contains powerful tools that utilizes the capabilities of Python to enable the creating of large-scale scenarios with a large set of entities [94]. An overview of this architecture is given in figure B.1.

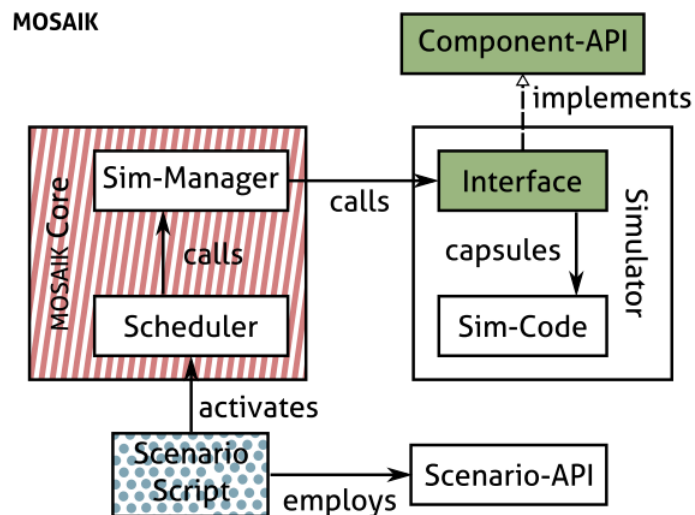


Figure B.1: An overview of Mosaik's architecture [94]

It should be noted missing in this architecture overview is a proper database or data analysis system. For this research project the Mosaik API along with pandas library was used to integrate this inside a monitor block. Apart from the standard in simulation data viewing included from Mosaik, this block also outputs the bulk data to a xlsx data-base and further plots selected data for visualisation.

In a study done at the TU Delft [94], the framework was compared against High Level Architecture (HLA) with co-simulation experiments to assess its performance. The results reveal that Mosaik produces more accurate results than older versions HLA. However this accuracy difference disappears when using current versions of HLA that provides zero look-ahead services. While HLA was more versatile and powerful, the paper found Mosaik to be an easier entry into co-simulation and recommended its use when large number of simulators and typologies needed to be tested.

C

Pymoo

Pymoo is a Python based framework that offers state of the art single and multi-objective optimization algorithms and is designed to be extendable through its modular implementation. Furthermore, it includes visualization and decision making tools related to multi-objective optimizations. The framework was developed under the supervision of Kalyanmoy Deb, one of the co-authors of NSGA-II. For this reason this framework is primarily focused on the genetic algorithms NSGA-II and NSGA-III. However, these algorithms are highly customizable and can easily be tailored to user needs. For instance the genetic algorithms are assembled in a plug-and-play fashion and utilize specific sub-modules like, initial sampling, mating selection, crossover, mutation and survival selection [95].

The architecture of Pymoo consists of 3 abstractions, Problems, Optimization and Analytics. The problems abstraction includes single, multi and many objective test problems, in this part the objective functions and constraints are defined. Furthermore, this section also includes gradients through automatic differentiation and parallelization can be achieved by a variety of techniques. The optimization abstraction includes the genetic algorithm based sub-modules mentioned above, along with decomposition and termination criterion tools. Lastly, the analytic abstraction supports the understanding of the data during and after an optimization with tools that visualize the design space, objective space, Pareto-front and more. In addition performance indicators can also be visualized to assess the performance of the algorithm [96]. Figure C.1 gives an overview of these Pymoo architecture abstractions.

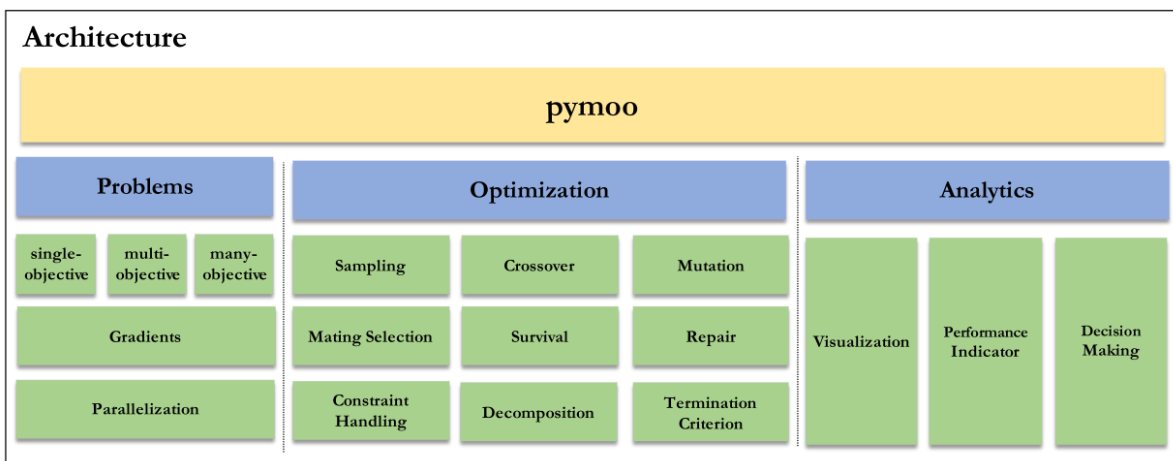


Figure C.1: An overview of Pymoo's architecture [96]

In [96] a short review was performed on some existing Python compatible MOO frameworks. From this it can be concluded that based on the following criteria shown in figure C.2, Pymoo provides a rather

complete package when solving multi-objective problems.

| Name | License | Focus on multi-objective | Pure Python | Visualization | Decision Making |
|----------|------------|--------------------------|-------------|---------------|-----------------|
| jMetalPy | MIT | ✓ | ✓ | ✓ | ✗ |
| PyGMO | GPL-3.0 | ✓ | ✗ | ✗ | ✗ |
| Platypus | GPL-3.0 | ✓ | ✓ | ✗ | ✗ |
| DEAP | LGPL-3.0 | ✗ | ✓ | ✗ | ✗ |
| Inspyred | MIT | ✗ | ✓ | ✗ | ✗ |
| pymoo | Apache 2.0 | ✓ | ✓ | ✓ | ✓ |

Figure C.2: An overview of some existing multi-objective frameworks in Python [96]

D

BESS Model Verification

This procedure prevents the possibility of error during coding and verify that the model is simulating the system with proper accuracy on the coverage of the proposed operating conditions. This include different power demands to the BESS (in the kW range) and all SOC conditions (0% - 100%).

D.1. BESS constraints

This test validates the operating coverage of the power constraints. This will cover the min/max SOC range of the battery and display the min/max discharge/charging power coverage. Also, the power constraint curves should be visible for discharging at low SOC and charging at high SOC. To achieve this test a full BESS is discharged from 100% SOC to 0% and charged again from 0% to 100%. This is achieved by applying a constant power set point to the battery long enough for the battery to fully discharge and charge as shown in Figure D.1. Furthermore, the charge and discharge power is set to 0.2 p.u above the rated power in order to validate the BESS power rating constraints.

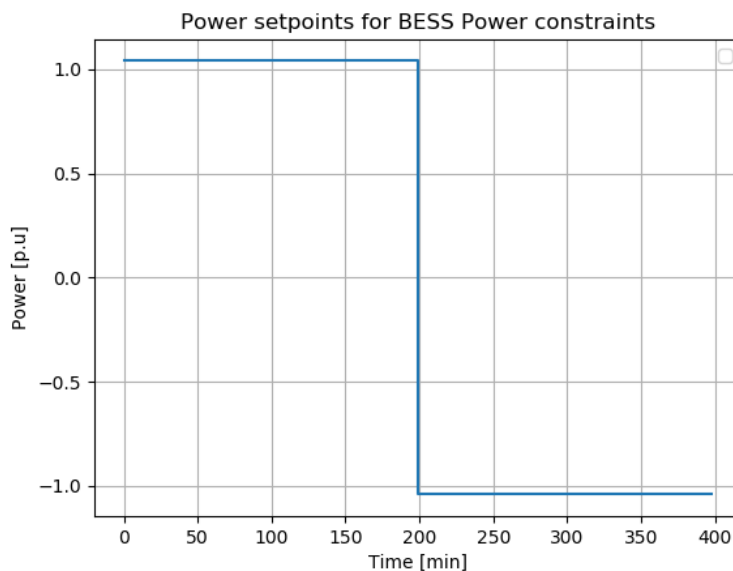


Figure D.1: Power set-points for the BESS power constraints

From the results shown in Figure D.2, it can be seen that the power constraints are according to the

desired design. The maximum rated power of 1.0 pu is met within the SOC limits and outside these a linear decrease in power is observed at the correct SoC points.

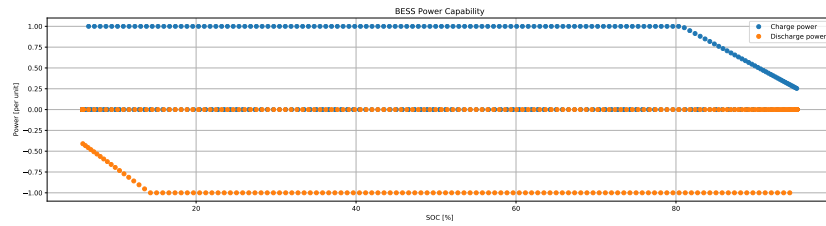


Figure D.2: Power constraints verification results

D.2. BESS efficiencies

This test is to validate the BESS efficiency curve. By injecting the full range of power, the efficiency curve can be plotted. The efficiency curve is achieved by applying a load profile where both the charge and discharge power climbs/decent from 0 [pu] up to 1 [pu] with steps of 0.05 [pu]. These set-points observes the full range of the inverter power characteristics. The power set points related to this test is shown in Figure D.3.

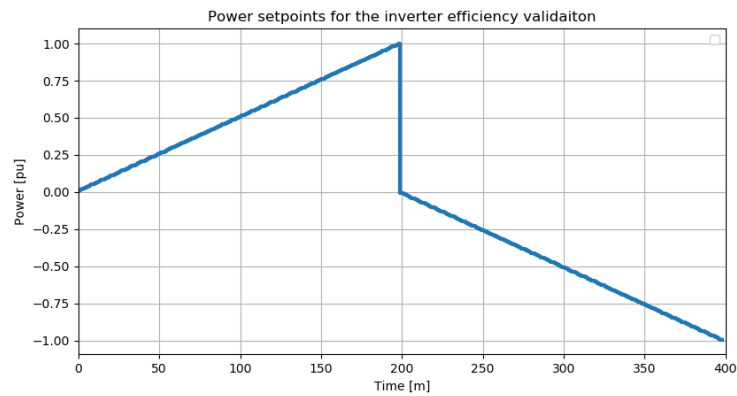


Figure D.3: power set-points for the BESS efficiency verification

After performing a simulation with this profile the following results shown in Figure D.3 were obtained. From this curve it is evident that the inverter characteristics of our model correspond with the piecewise curves defined in the design.

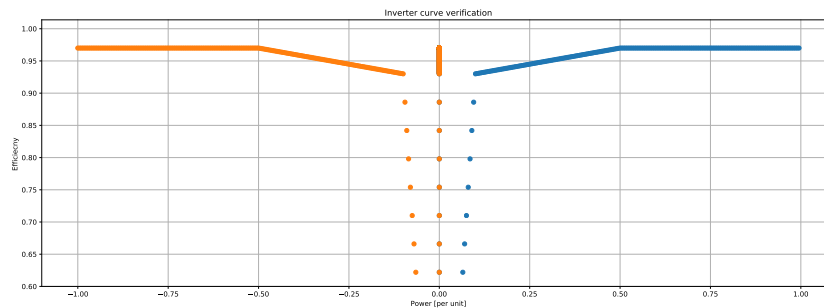


Figure D.4: Initial efficiency verification results

E

Result Tables

Table E.1: Case 0 results DCM without BESS - DCM Cost [%]

| Case 0 - Results DCM without BESS - DCM Cost [%] | | | | | | | | |
|--|-----------|-------------|-----------|-------------|-----------|-------------|-----------|-------------|
| Delay [min] | Station A | | Station B | | Station C | | Station D | |
| | Max Delay | Utilization |
| 0 | 100.0 | 100.0 | 100.0 | 100.0 | 100.0 | 100.0 | 100.0 | 100.0 |
| 1 | 74.0 | 50.5 | 56.4 | 42.3 | 74.7 | 64.7 | 67.2 | 55.4 |
| 2 | 62.4 | 43.8 | 48.6 | 37.1 | 65.6 | 56.5 | 56.7 | 48.7 |
| 3 | 54.4 | 40.8 | 43.5 | 33.2 | 57.0 | 51.6 | 50.0 | 44.2 |
| 4 | 50.5 | 38.0 | 39.2 | 30.9 | 53.1 | 47.7 | 46.8 | 41.2 |
| 5 | 46.0 | 36.2 | 36.0 | 28.7 | 49.4 | 44.5 | 44.3 | 39.0 |
| 6 | 43.1 | 34.2 | 34.7 | 27.7 | 46.7 | 41.8 | 42.0 | 37.7 |

Table E.2: Case 1 results - BESS assisted DCM in Swiss - Station A

| Case 1 - Results BESS Assisted DCM in Swiss - Station A | | | | |
|---|---------------------|-------------------|------------------|------------------|
| Delay [min] | Annual DCM cost [%] | E_b^{max} [kWh] | P_b^{max} [kW] | P_G^{max} [kW] |
| 0 | 48.2 | 219.0 | 210.2 | 60.7 |
| 1 | 43.8 | 147.6 | 142.8 | 70.3 |
| 2 | 41.4 | 136.6 | 105.3 | 77.9 |
| 3 | 39.8 | 102.6 | 86.0 | 82.4 |
| 4 | 38.0 | 102.6 | 67.5 | 79.0 |
| 5 | 37.7 | 56.6 | 44.3 | 89.8 |
| 6 | 35.0 | 56.6 | 43.9 | 80.7 |

Table E.3: Case 1 results - BESS assisted DCM in Swiss - Station B

| Case 1 - Results BESS Assisted DCM in Swiss - Station B | | | | |
|---|---------------------|-------------------|------------------|------------------|
| Delay [min] | Annual DCM cost [%] | E_b^{max} [kWh] | P_b^{max} [kW] | P_G^{max} [kW] |
| 0 | 58.4 | 177.0 | 130.0 | 117.0 |
| 1 | 43.0 | 129.4 | 101.9 | 138.1 |
| 2 | 39.6 | 129.5 | 81.5 | 122.9 |
| 3 | 36.5 | 143.0 | 67.1 | 114.0 |
| 4 | 35.6 | 56.0 | 32.8 | 130.1 |
| 5 | 33.6 | 59.6 | 26.6 | 124.0 |
| 6 | 33.2 | 59.6 | 22.8 | 124.0 |

Table E.4: Case 1 results - BESS assisted DCM in Swiss - Station C

| Case 1 - Results BESS Assisted DCM in Swiss - Station C | | | | |
|--|----------------------------|-------------------|------------------|------------------|
| Delay [min] | Annual DCM cost [%] | E_b^{max} [kWh] | P_b^{max} [kW] | P_G^{max} [kW] |
| 0 | 66.6 | 250.1 | 217.7 | 65.9 |
| 1 | 56.1 | 228.8 | 163.4 | 89.8 |
| 2 | 50.9 | 173.0 | 104.5 | 103.9 |
| 3 | 48.1 | 190.7 | 88.7 | 95.5 |
| 4 | 44.5 | 208.7 | 95.0 | 74.6 |
| 5 | 42.9 | 190.7 | 77.6 | 83.1 |
| 6 | 41.0 | 178.3 | 77.5 | 73.9 |

Table E.5: Case 1 results - BESS assisted DCM in Swiss - Station D

| Case 1 - Results BESS Assisted DCM in Swiss - Station D | | | | |
|--|----------------------------|-------------------|------------------|------------------|
| Delay [min] | Annual DCM cost [%] | E_b^{max} [kWh] | P_b^{max} [kW] | P_G^{max} [kW] |
| 0 | 59.3 | 318.0 | 238.0 | 138.2 |
| 1 | 51.3 | 166.8 | 118.6 | 140.4 |
| 2 | 47.9 | 131.7 | 95.0 | 123.6 |
| 3 | 43.5 | 111.7 | 58.8 | 132.0 |
| 4 | 41.8 | 94.6 | 48.4 | 131.3 |
| 5 | 40.5 | 92.8 | 48.8 | 121.4 |
| 6 | 38.7 | 100.0 | 41.3 | 120.5 |

Table E.6: Case 2 results - DCM without BESS

| Case 2 - Results DCM without BESS - Station D | | | | |
|--|------------------------|-------------|-------------|-------------|
| Delay [min] | Annual DCM cost | E_b^{max} | P_b^{max} | P_G^{max} |
| 0 | 100.0 | 0.0 | 0.0 | 384.0 |
| 1 | 67.2 | 0.0 | 0.0 | 258.2 |
| 2 | 56.7 | 0.0 | 0.0 | 217.7 |
| 3 | 50.0 | 0.0 | 0.0 | 192.0 |
| 4 | 46.8 | 0.0 | 0.0 | 179.7 |
| 5 | 44.3 | 0.0 | 0.0 | 170.2 |
| 6 | 42.0 | 0.0 | 0.0 | 161.5 |

Table E.7: Case 2 results - BESS assisted DCM in NL

| Case 2 - Results BESS Assisted DCM in NL - Station D | | | | |
|---|----------------------------|-------------------|------------------|------------------|
| Delay [min] | Annual DCM cost [%] | E_b^{max} [kWh] | P_b^{max} [kW] | P_G^{max} [kW] |
| 0 | 100.8 | 63 | 49.9 | 284 |
| 1 | 70.9 | 12.4 | 8.4 | 252.7 |
| 2 | 59.1 | 5.7 | 3.6 | 217.8 |
| 3 | 51.6 | 6.7 | 4.7 | 183.9 |
| 4 | 51.3 | 13.0 | 8.6 | 171.3 |
| 5 | 47.7 | 7.7 | 5.9 | 166.1 |
| 6 | 46.9 | 10.7 | 2.3 | 166.1 |

Table E.8: Case 2 results - BESS assisted DCM in NYC

| Case 2 - Results BESS Assisted DCM in NYC | | | | |
|--|----------------------------|-------------------|------------------|------------------|
| Delay [min] | Annual DCM cost [%] | E_b^{max} [kWh] | P_b^{max} [kW] | P_G^{max} [kW] |
| 0 | 40.2 | 804.1 | 288.9 | 76.8 |
| 1 | 35.8 | 738.7 | 198.8 | 68.3 |
| 2 | 33.6 | 596.4 | 148.8 | 70.2 |
| 3 | 31.9 | 551.7 | 125.2 | 67.5 |
| 4 | 31.4 | 533.4 | 116.3 | 63.4 |
| 5 | 29.7 | 533.3 | 111.8 | 60.4 |
| 6 | 29.1 | 525.2 | 106.3 | 60.3 |

Table E.9: Case 3 results - BESS assisted DCM in Swiss - Station D - 2030

| Case 3 - Results BESS Assisted DCM in Swiss - Station D - 2030 | | | | |
|---|----------------------------|-------------------|------------------|------------------|
| Delay [min] | Annual DCM cost [%] | E_b^{max} [kWh] | P_b^{max} [kW] | P_G^{max} [kW] |
| 0 | 44.8 | 717.0 | 288.9 | 72.9 |
| 1 | 40.3 | 772.9 | 204.3 | 65.8 |
| 2 | 37.5 | 693.2 | 157.6 | 61.9 |
| 3 | 34.9 | 498.5 | 112.6 | 75.7 |
| 4 | 33.6 | 628.5 | 119.8 | 60.1 |
| 5 | 32.6 | 514.9 | 108.3 | 61.0 |
| 6 | 31.8 | 514.9 | 104.2 | 60.2 |

Table E.10: Case 3 results - BESS assisted DCM in NL - Station F - 2030

| Case 3 - Results BESS Assisted DCM in NL - Station F - 2030 | | | | |
|--|----------------------------|-------------------|------------------|------------------|
| Delay [min] | Annual DCM cost [%] | E_b^{max} [kWh] | P_b^{max} [kW] | P_G^{max} [kW] |
| 0 | 94.8 | 142.6 | 119.4 | 253.4 |
| 1 | 71.4 | 134.1 | 114.9 | 146.9 |
| 2 | 59.6 | 50.6 | 28.7 | 192.5 |
| 3 | 51.6 | 33.3 | 23.5 | 166.2 |
| 4 | 49.1 | 33.3 | 23.5 | 154.2 |
| 5 | 47.0 | 41.7 | 18.8 | 152.2 |
| 6 | 44.7 | 41.7 | 14.3 | 147.1 |

Table E.11: Case 4 results - BESS assisted DCM in NL - Station F - 2C

| Case 4 - Results BESS Assisted DCM in NL - Station F - 2C | | | | |
|--|----------------------------|-------------------|------------------|------------------|
| Delay [min] | Annual DCM cost [%] | E_b^{max} [kWh] | P_b^{max} [kW] | P_G^{max} [kW] |
| 0 | 100.0 | 21.3 | 25.3 | 374.6 |
| 1 | 59.6 | 35.7 | 43.2 | 199.4 |
| 2 | 50.9 | 9.0 | 4.1 | 200.9 |
| 3 | 44.4 | 3.3 | 1.1 | 182.5 |
| 4 | 40.9 | 3.8 | 2.5 | 165.4 |
| 5 | 39.0 | 6.3 | 3.8 | 152.9 |
| 6 | 35.6 | 3.5 | 1.0 | 145.0 |

F

Conference Paper Draft

Included in this appendix is a paper that is written in the IEEE conference format on the main contributions of this thesis with the focus laid on the results obtained for the different demand tariff regions. The goal of this paper is to submit this work to the IEEE Transportation Electrification Conference and Expo (ITEC) 2021.

Optimal Battery Energy Storage System Sizing for Demand Charge Management in EV Fast Charging Stations

1st George Koolman

Dept. of Electrical Sustainable Energy
Delft University of Technology
Delft, Netherlands
georgekoolman@gmail.com

2nd Pavol Bauer

Dept. of Electrical Sustainable Energy
Delft University of Technology
Delft, Netherlands
p.bauer@tudelft.nl

Abstract—The need for proper fast charging infrastructures is one of the key challenges for the wide adoption of electrical vehicles (EV). The high pulsating demand of fast charging stations (FCS) together with high demand tariffs can cause monthly DSO demand charges to account for a significant fraction of a station's electric bill. Therefore, weakening the business case for stations located in these high tariff regions. To tackle this issue, demand charge management (DCM) can be applied to suppress peak power demands at FCSs using battery energy storage systems (BESS). This enables the reduction of cost while retaining the station's fast charging capabilities. However, the implementation of such systems remains a large investment and the proper BESS sizing in fast charging applications is not well studied. This paper proposes a multi-objective approach for optimal BESS sizing at FCSs considering demand charges and station performance. A BESS assisted FCS model is formulated to analyse the performance of a station's design based on power flow, charging delays and the expected BESS lifetime. Furthermore, based on a worst-case demand scenario, a multi-objective optimization framework is formulated using the genetic algorithm NSGA-II to obtain the optimal BESS and grid-tie sizing for an existing FCS. Lastly, with demand data measured at four FCSs in the Netherlands, a set of numerical case studies has been conducted in the Mosaik and Pymoo environments to assess the feasibility and the effectiveness of the proposed formulation.

Index Terms—battery energy storage systems, demand charge management, electrical vehicles, fast charging stations, genetic algorithms, multi-objective optimizations, NSGA-II

I. INTRODUCTION

The transportation sector accounts for approximately 25% of these global energy-related emissions. Of these emissions, around 70% is due to the use of combustion vehicles [1]. These appalling figures have promoted people to become more aware of protecting the environment and enabled governments around the globe to set emission goals and introduce regulatory changes that encourage the reduction of CO₂ emissions. One of the major disruptions to the transportation sector, set to tackle our carbon emission problem, is the wide adoption of electrical vehicles (EV). However, concerns related to charging

speeds and driving range continue to be wide spread among consumers. This fear is known as 'range anxiety' or 'charging anxiety' [2]. 83% of consumers who would not consider an EV, cites this fear as the reason [3].

Therefore, worldwide, ambitious plans are in place for expanding the current fast charging infrastructures. In Europe, five of the largest car manufacturers are collaborating under the name Ionity to build a fast-charger network of 400 stations by 2020 [4]. In the US, one manufacturer is investing USD 2 billion in fast-charging stations along freeways in 39 US states and public chargers in 17 metropolitan areas [5].

Currently, fast charging is mostly only seen as a facilitator of long-distance driving for electric vehicles. For this reason, the deployment of FCS generally occurs next to freeways. However, as EV ownership increases in urban areas, city planners and officials are contemplating whether inner-city FCS can be the alternative for the growing congestion of slow public chargers [6].

ElaadNL list location issues and demand charges as the two major concerns related to installing FCSs [7]. Demand charges is a fee based on the highest measured peak power (in kW) during a monthly billing period. The demand tariff is the price per kW the DSO uses to determine these monthly fees. These tariffs can vary significantly between regions, where e.g. the Netherlands this can be around 3 €/kW and in places such as NYC, around 50 \$/kW [8]. These demand charges can therefore account for a significant portion (up to 90%) of a FCSs electric bill, consequently weakening the business case for a FCS [9]. Under such circumstances there is a clear incentive for FCS owners to limit their peak power usage by implementing BESS assisted DCM at their stations [8].

The papers [2], [10]–[14] study the integration of energy storage in EV fast charging applications. Papers [10], [12], [14] all present a mixed-integer linear programming (MILP) formulation of these systems and performs a single objective optimization based on operational costs. In [10] and [11] the feasibility of adding frequency containment reserve (FCR) as second function for the BESS is investigated. Both papers concluded that FCR does not impact performance on the

FCS. However, it should be mentioned that the cost analysis is performed on one case that is sized specifically for FCR inclusion. Furthermore, this study also contained an analysis of the BESS degradation using a thermal model and concluded that a FCS does not have significant impact on the degradation. It should be noted, that the amount of cycles and cycle depth were not taken into consideration in the degradation model and the EoL criterion was set to 30%. In [13] and [2] a FCS sizing methods based on waiting times at the station is proposed. Remarkable is that both study suggests these waiting times to not exceed 5 to 6 minutes. In both study the waiting times are dependent on the stochastic EV arrival times, number of charging points available and size of the BESS implemented. Both papers performed a simple cost analysis on the sizing calculated and confirmed it's economical feasibility.

Currently to the author's knowledge the literature does not include studies performing a multi-objective optimization for BESS assisted FCSs. However, there is extensive literature on MOOs being applied to sizing for micro-grid and distribution grid applications. In the studies performed in [15]–[21] all authors employed genetic algorithms (GA) to solve multi-objective energy storage related challenges for the distribution grid or micro-grid applications. Where operational costs, RES production, BESS lifetime and location were taken into consideration.

From the literature it is clear that BESS is a feasible solution for reducing the peak power demands and demand charges at FCS. Currently, the literature contains mostly research on sizing optimizations based on one objective, either costs or waiting times. Whereas research into multi-objective optimizations investigating how both objectives impact the BESS sizing and limited grid-tie ratings is lacking. These aspects are important to FCS owners due to the large investments of BESS projects and the limited trade-off on waiting times (quality of service) at FCSs. Furthermore, all literature implemented a stochastic method based on petrol station data for estimating the FCS load profile. This gives a good example for a scenario where the activities at FCSs resembles petrol station activities. However, as suggested in [6] and [22], even in a fully adopted EV scenario this would never be the case since EV possesses multiple charging (tanking) options compared to conventional combustion vehicles (which only possesses one).

With this paper energy measurement data are acquired from a normally utilized FCS located in the Netherlands, from this data, demand profiles are generated to perform the design optimizations. This truly assesses the feasibility and effectiveness of BESS assisted FCSs for the current situation. In short this paper proposes a multi-objective optimization (MOO) framework using GAs for the optimal BESS and grid-tie sizing at FCSs in order to reduce demand charges and charging delays.

The remainder of this paper is structured as follows. In Section II the BESS assisted FCS modeling approach is presented. The multi-objective problem is formulated and the proposed sizing framework is presented in Section III. Section V describes the case studies and the optimization, and the numerical simulation

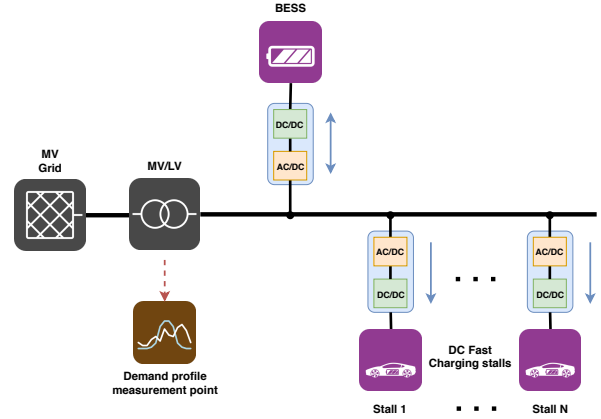


Fig. 1: A system diagram of a BESS integrated AC connected FCS

results are presented. Lastly, the paper is concluded in Section VI.

II. FCS MODELING

In general this model simulates the power flows inside a BESS assisted AC configuration FCS. This FCS configuration is shown in Fig. 1. It includes a N number of DC fast charging stalls, a BESS and a MV/LV transformer that couples the station to the MV grid. An AC configuration is selected due to it's maturity and standard of application at most FCS [23]. Furthermore, the task intended for the BESS is to perform peak-shaving on the demand in order to restrict the grid-tie power to a set limit, and thus reducing the stations demand charges.

Based on 3 design parameters and a FCS demand profile, this system models the following electrical components, the grid-tie demand, the FCS demand profile, the energy management system (EMS) and stationary LFP/C BESS. The lithium LFP/C chemistry is selected due to its high suitability for grid-connected applications [24]. Moreover, the model includes the performance parameters BESS lifetime and charging delays. The BESS lifetime helps to asses the costs associated to the BESS and the charging delays give an assessment of the quality of service being provided by the FCS design. An important assumption made regarding the charging delays, is that when both the restricted grid-tie and BESS reaches their designed power limits, it is assumed that a simple power balancing technique is being employed by the charging stalls. This results in equally divided charging delays among active stalls. The input and output parameters associated with the model are given in Table I.

Charging sessions at FCSs can range from 10-30 minutes. During these sessions the charging power varies per EV model and is not constant for the entire charging duration [25]. Furthermore, the maximum permissible charging delays can be between 0-6 minutes [2]. Hence, a model resolution (simulation step t) of 1 minute is selected to ensure capture of the session scale charging characteristics in the FCS demand

TABLE I: Input and output parameters for the FCS models.

| Input | Unit |
|-------------------------|---------|
| BESS Capacity | kWh |
| BESS Power Rating | kW |
| Maximum Grid-tie Power | kW |
| FCS Demand (1 min res.) | kW |
| Output | Unit |
| BESS SoC | % |
| Power Flow | kW |
| Charging Delays | minutes |
| BESS Lifetime | years |

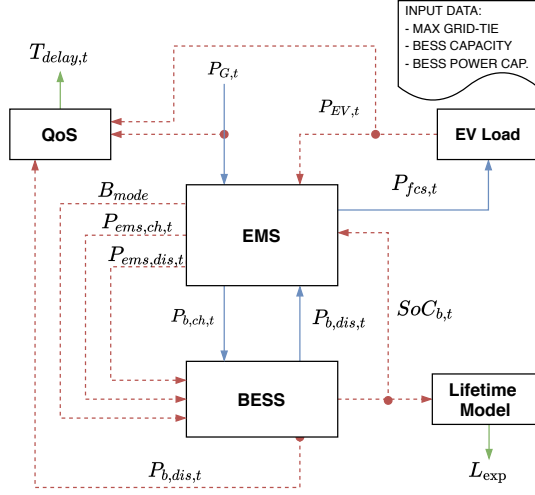


Fig. 2: System diagram of the complete simulation model.

profile and help give a close approximation of the charging delays. It should be noted however, that due to the post-processing nature of the BESS lifetime model, only this parameter is calculated at the end of the simulation.

Fig. 2 depicts the corresponding inter-connection and data exchange between the 5 modules included in this model, the EV demand, EMS, BESS, lifetime and QoS. The blue lines represents the physical power flows, the red dotted lines the signal exchange between each modules and the green lines the performance related results. During the simulation only the red signals are exchanged between modules and the blue and green lines are represented as output results from these modules. This complete model is implemented using the python based Mosaik smart-grid simulation environment [26].

A. Station Demand

The module "EV demand" models the total power demand of all EVs charging at the FCS. For each simulation interval t , this module generates the EV power demand $P_{EV,t}$ in kW for a defined station. For this a pre-defined minute scale power demand profile of a FCS is required for the initialization. These profiles can either be estimated from stochastic models or obtained from measurement data. This paper uses energy measurements in kWh (1 minute samples) from January obtained at a FCS in the Netherlands. Using these measurements a demand profile can be generated. Using actual demand

data has it's advantages of giving a more realistic view of the current power demands at FCSs. Furthermore, it will make session level power variations and differences in station utilization rates visible in the simulation.

B. Energy Management System

In this model the EMS is regarded as the central unit of the system. This model performs the correct power flow controls for the FCS in order to dispatch the BESS correctly for peak-shaving purposes, and thus avoid exceeding the designed grid-tie values.

The objectives of the EMS module are the following:

- Limit the grid-tie power to an assigned value.
- Determine the required charge and discharge power from the BESS.
- Apply typical SOC constraints to the BESS in order to avoid accelerated degradation.
- Determine the system's power capability to supply the stalls.

The control can be described by (1) and (2). Charging of the BESS occurs when the demand of the station $P_{EV,t}$ is smaller than the maximum grid-tie capacity P_G^{max} . On the contrary, discharging occurs when the FCS demand is larger than the grid-tie capacity. Both are only valid when the BESS is within its SOC constraints given by (3). If this is not the case the BESS will go into idle mode. For each condition a BESS mode signal B_{mode} is generated. Furthermore, the EMS determines the grid-tie demand during both periods using (4).

$$P_{ems,ch,t} = \begin{cases} P_G^{max} - P_{EV,t}, & P_{EV,t} < P_G^{max} \\ 0, & SoC_{b,t} > 90\% \end{cases} \quad (1)$$

$$P_{ems,dis,t} = \begin{cases} P_{EV,t} - P_G^{max}, & P_{EV,t} \geq P_G^{max} \\ 0, & SoC_{b,t} < 5\% \end{cases} \quad (2)$$

$$5\% \leq SoC_{b,t} \leq 90\% \quad (3)$$

$$P_{G,t} = \begin{cases} P_{EV,t} + P_{b,ch,t}, & P_{EV,t} < P_G^{max} \\ P_G^{max}, & P_{EV,t} \geq P_G^{max} \end{cases} \quad (4)$$

C. Battery Energy Storage System

Because only energy content and power flows are being analysed by our model, the analytical BESS modeling approach suffices. This modeling approach describes the BESS at a higher level of abstraction and requires only the SOC, charging/discharging power, efficiency and energy capacity to model it's performance [27].

The objectives of the BESS module are the following:

- Dispatch the BESS in the correct mode according to the EMS signals.
- Model the inverter efficiency curve.
- Model the physical power and energy constraints.
- Model the charge and discharge of energy.

According to the battery mode signal received from the EMS, the battery either goes into charge, discharge or idle mode. In both charge and discharge mode, the power constraints are applied to the power signal, the inverter efficiency determined and energy added or removed from the previous BESS energy content ($E_{b,t-1}$). In idle mode the BESS does not charge nor discharge any energy. (5) describes this charging, discharging and idling procedure, and (6) the energy constraint applied to the BESS. This constraint ensures that the BESS cannot be charged or discharged outside of the physical boundaries. Lastly, at the end of each step the SOC is determined by (7).

$$E_{b,t} = \begin{cases} E_{b,t-1} + \frac{P_{b,ch,t}}{60} \cdot \eta(P_{b,ch,t}), & B_{mode} = \text{Charge} \\ E_{b,t-1} - \frac{P_{b,dis,t}}{60} \cdot \frac{1}{\eta(P_{b,dis,t})}, & B_{mode} = \text{Discharge} \\ E_{b,t-1}, & B_{mode} = \text{Idle} \end{cases} \quad (5)$$

$$0 \leq E_{b,t} \leq E_b^{cap} \quad (6)$$

$$SoC_{b,t} = \frac{E_{b,t}}{E_b^{cap}} \cdot 100\% \quad (7)$$

To ensure the BESS model (dis)charges within its power capabilities, power constraints are applied according the BESS's rating and physical limitations. The following constraints, (8) and (9) limits the charging and discharging power of the battery to its maximum power rating found in the battery's data sheet. For simplicity, this model assumes that both the charging and discharging ratings are equal. Furthermore, the charge/discharge power of a battery is not fully constant over the full range of SOCs, at low (around 15%) levels and high (around 80%) levels the power linearly decreases [28]. This linear decrease during discharging and charging can be described by the following constraints (10) and (11).

$$0 \leq P_{b,ch,t} \leq P_b^{max} \quad (8)$$

$$0 \leq P_{b,dis,t} \leq P_b^{max} \quad (9)$$

$$P_{b,ch,t} \leq \frac{P_b^{max}}{1 - S_{b,ch}} \left(\frac{E_{b,t}}{E_b^{max}} - 1 \right) \quad (10)$$

$$P_{b,dis,t} \leq \frac{P_b^{max}}{S_{b,dis}} \left(\frac{E_{b,t}}{E_b^{max}} \right) \quad (11)$$

To model the BESS inverter, a 3 segment piece-wise linear approximation of an inverter curve model found in [29] is implemented. This efficiency curve η_{inv} start from 5%, linearly increases to 93% at 0.1 pu (P^{ac}) and further increases to 97% after 0.5 pu (P^{ac}). This piece-wise linear segments represents the efficiency function for the complete BESS power range and is described by (12).

$$\eta = \begin{cases} 8.8 \cdot P_{b,t} + 0.05, & P_{b,t} \leq 0.1\text{pu} \\ 0.93 + (0.1 \cdot (P_{b,t} - 0.1)), & P_{b,t} \leq 0.5\text{pu} \\ 0.97, & P_{b,t} \leq 1\text{pu} \end{cases} \quad (12)$$

D. BESS Lifetime

The lifetime module estimates the expected lifetime of the BESS using its SOC profile. Battery ageing is due to a combination of two components, the cycle-life degradation and calendar-life degradation. This module uses the post-processing lifetime model proposed in [24] to determine the capacity fade being induced by these two degradation factors on LFP/C batteries. By knowing the degradation for a certain SOC profile, one can estimate the time it takes for the battery to reach its EOL criterion of 80% [30]. This is taking the assumption that the battery will repeat this SOC profile during the entirety of its lifetime. Here the SOC profile is defined as the complete SOC history the BESS experienced during a simulation.

Due to the irregular demand profile for FCS applications, these 3 parameters can vary significantly on a daily basis and can be different depending on the station's usage. For this reason, this module uses a slightly modified version of the rain-flow cycle counting algorithm found in [30]. In addition to the frequency and range of cycles, this modified version also extracts the average SOC from each cycle. Once these values are obtained, the cycles are counted based on a discrete n segments of DOD ranges and average SOCs. These discrete segments are used in order to obtain computational simplicity. However, to preserve model accuracy a minimum of 20 discrete segments are selected [31]. Lastly, the cycle lifetime consumed is calculated using (13) by comparing the obtained count for each n segments against the maximum cycles defined from the cycle lifetime model at 80% EoL.

$$D_{cycle} = \sum_{DOD=1/n}^{DOD=100\%} \frac{N_c(dod, soc)}{N_{max}(dod, soc)} \quad (13)$$

Calendar degradation occurs when the battery is idle. From the same SOC profile a total idle time to SOC level range data can be extracted. Using the calendar-life model found in [24], one can obtain the calendar lifetime consumed in the same procedure. Both degradation's are then summed together to find the total lifetime consumed LC . Assuming the BESS continues the same operation, the expected lifetime L_{exp} can be estimated with (16). Where T_p represents the length of the degradation period.

$$D_{cal} = \sum_{SoC=1/n}^{SoC=100\%} \frac{T_c(SoC)}{T_{max}(SoC)} \quad (14)$$

$$LC = D_{cycle} + D_{cal} \quad (15)$$

$$L_{exp} = \frac{1}{LC} \cdot T_p \quad (16)$$

E. Charging Delay

The QoS module determines the performance of a BESS assisted FCS design in terms of charging delays. Charging delays would be experienced at times when the power delivered from both the grid-tie and BESS cannot meet the EV demand, and thus resulting in a longer charging session due to the reduced charging speeds. These periods with power differences between the EV demand $P_{EV,t}$ and the FCS power capability $P_{fcs,t}$ are called power mismatch periods, where $P_{fcs,t}$ is defined by (17)

$$P_{fcs,t} = P_{G,t} + P_{b,dis,t} \quad (17)$$

At each simulation step the following flow-chart shown in Fig. 3 is performed to give an estimate of the charging delays caused during power mismatch periods. The module starts by identifying power mismatch moments, if a power mismatch moment is identified ($\Delta P_t > 0$), then the extra time (Δt_d) it takes to charge the missed energy (18) at the available FCS power is given by (19). This is then summed up until a mismatch period ends.

When a mismatch period ends ($\Delta P_t \leq 0$), an estimate of the total charging delay ($T_{delay,t}$) for the ending power mismatch period is obtained by equally dividing the summed Δt_d over the number of charging EVs ($N_{EV,t}$) as shown in (20). This delay then represents the total extra time a connected EV would have experienced after the power mismatch period if it had continued to charge at the available power.

$$\Delta E_t = (P_{EV,t} - P_{fcs,t}) \cdot t_{step} \quad (18)$$

$$\Delta t_d = \frac{\Delta E_t}{P_{fcs,t}} \quad (19)$$

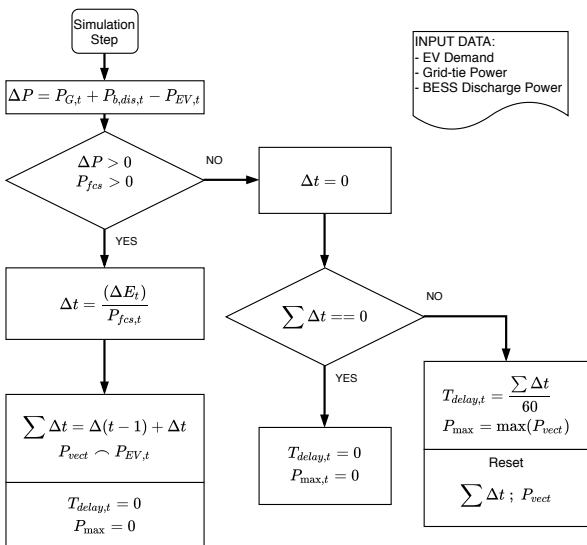


Fig. 3: Quality of Service implementation flowchart

$$T_{delay,t} = \sum \frac{\Delta t_d}{N_{EV,t}} \quad (20)$$

The number of EV's that experienced a power mismatch can be either obtained from data (if available) or be estimated using additional station information such as number of charging stalls (N_{stalls}) and total rated power ($P_{stations}^{rated}$) using (21).

$$N_{EV,t} = \frac{\max(P_{vect})}{P_{station}^{rated}} \cdot N_{stalls} \quad (21)$$

III. MULTI-OBJECTIVE PROBLEM FORMULATION

A. FCS Design Problem

Sizing of a battery for grid-connected applications can be a complicated process. This complexity is found in the irregular demand profile of FCSs, which can lead to complex cycling of the BESS in peak-shaving applications. The framework proposed in this paper considers 2 contradicting design objectives, the associated DCM costs and the station performance. The DCM cost component consists of the annual (reduced) demand charges and the annual BESS investments required to perform the peak-shaving. The performance is measured in the charging delays customers experience when there is not sufficient power capacity available from both the grid-tie and BESS to meet the EV demand. Using a station's demand profile and the 3 design parameters, maximum grid-tie power P_G^{max} , BESS capacity E_b^{max} and BESS power rating P_b^{max} both objectives can be evaluated with the FCS model proposed in Section II.

To determine the demand charges, this framework will assume P_G^{max} to be equal the the maximum peak demand during a billing cycle. Moreover, another assumption made is that the BESS will be in service for the duration of its expected lifetime. This way the initial BESS investments are annualized to be included in the annual DCM cost.

To properly asses a stations performance, two KPIs are derived from the charging delays $T_{delay,t}$, the maximum charging delay and the increase in station utilization. The maximum charging delay is the maximum extra time an EV might experience to complete it's charging session.

The utilization of a station is the total amount of time the station is being occupied for charging. Hence, increase in utilization is here defined as the percentage increase in station utilization caused by the total amount of extra charging time. This KPI gives an indication on how frequent delays occur, and thus affecting the owner's sales potential due to increased station occupation.

B. Objective functions & Design Constraints

This multi-objective design problem can be considered a two contradicting objective problem. However, due to the subtle differences in dependencies between the maximum charging delays and the utilization time increase, the performance objective is separated into a two separate objective functions (23) and (24). This avoid resulting with solutions with low maximum delays but frequent delays.

Objective function (22) represents the DCM cost function, this function describes the BESS related investments associated to the DCM design and the reduced demand charges. This is calculated on an annual basis. The annual BESS costs comprises of BESS project costs annualized by the expected BESS lifetime in years. An additional over-sizing factor $\beta_{cap}=1.2$ and $\beta_{pow}=1.07$ are included to take into consideration the capacity and power fade due to degradation [32]. Furthermore, The demand charges comprises of monthly demand tariffs C^{dem} times the maximum grid-tie power and are annualized using the factor $\alpha = 1/12$. Additionally, the costs related to perform power balance are not considered in this framework. It is assumed here that the initial software investments for this technology will be divided among a complete network of stations, hence making the costs irrelevant when compared to the large BESS investments and demand charges.

Apart from the constraints included inside the FCS model, a set of design constraints are applied to restrict our search during the optimization using previous knowledge and technological constraints obtained from literature.

Constraint (25) represents the P/E ratio constraint related to the LFP/C chemistry considered, which has a P/E ratio at 1C of $X^{\min} = 1$ and $X^{\max} = 8$ [14].

Constraint (26) restricts the optimization from selecting solutions with a combined grid-tie and BESS power below the average power of a station's demand or above the maximum stations peak power [13]. Furthermore, constraint (27) restricts the optimization from selecting solutions with maximum delays longer than 10 minutes. This constraints is applied due to the fact that FCS customers are highly likely to leave for delays longer than 6 minutes [2].

$$\min_x f_1(x) = C^{DCM} = \frac{C^{bess} E_b^{\max} \beta_{cap} + C^{conv} P_b^{\max} \beta_{pow}}{L_{exp}} + \frac{C^{dem} P_G^{\max}}{\alpha} \quad (22)$$

$$\min_x f_2(x) = T_{max} = \max(T_{delay,t}) \quad (23)$$

$$\min_x f_3(x) = T_{freq} = \frac{\sum T_{delay,i}}{T_{charging}} \cdot 100\% \quad (24)$$

$$s.t. X^{\min} P_b^{max} \leq E_b^{cap} \leq X^{\max} P_b^{max} \quad (25)$$

$$P_{fcs-avg} \leq P_G^{max} + P_b^{max} \leq P_{fcs-max} \quad (26)$$

$$T_{max} \leq 10 \quad (27)$$

C. Sizing Framework

Using the FCS model proposed in Section II, a framework shown in Figure 4 is set up to solve the design optimization problem. The framework comprises of the FCS model using a worst case demand profile, and a optimization model using the NSGA-II algorithm.

In general FCSs and BESSs are designed to endure usage during worst case scenarios [33], hence the selection of

a worst case demand profile as input for the FCS model. Furthermore, FCS demands have a repeating daily pattern (24-hours) and the worst case usage period is around the Christmas holidays [33]. For this reason the demand profile comprises of two worst 24-hour periods extracted from this worst case scenario. A 24-hour period with the worst peak demand and a 24-hour period with the worst energy density. The worst peak demand day ensures the proper power requirements, and the worst energy density day ensures the BESS energy requirements.

Because two worst 24 hours periods are used, the increase in utilization and expected BESS lifetime is assessed separately for each 24 hour period, where then the worst from these two 24 hour periods are selected. The total charging delay is analysed for both 24 hour worst case load and the day with the worst total charging delay is inserted into the objective.

Due to the modeling complexities and some non-linearity within the FCS model, the optimization model uses a meta-heuristic optimization approach based on the genetic algorithm NSGA-II. Using the formulated objective functions and design constraints this is implemented in the Pymoo environment [34]. The modular aspects of Pymoo grants the possibility to tailor the genetic operators of the NSGA-II algorithm to a specific problem. For reasonable computational time the population size is set to a fixed size of $n_{pop}=50$ and the termination criterion is defined by a design space tolerance of 1%. Since for FCS applications the design space will be in the range of 10 to 1000 kWh/kW a Pareto front in the precision of 1% should be sufficient to give an accurate indication of the sizing.

The following steps describes the procedure that is executed with this optimization framework.

- Step 1: An initial population consisting of the 3 design parameters (P_G^{max} , P_b^{max} and E_b^{max}) are generated using the NSGA-II operators.
- Step 2: The population is then simulated by the FCS model, to extract the performance parameters, L_{exp} , T_{max} and T_{freq} .
- Step 3: The design parameters together with the simulation results are evaluated using the objective functions subject to the design constraints.
- Step 4: Using the NSGA-II operators, a new parent

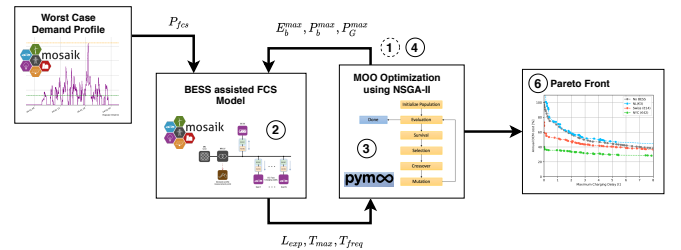


Fig. 4: A schematic overview of the proposed design optimization framework

TABLE II

| Station Name | D |
|---------------------------|----------------|
| Installed Capacity | 450 kW |
| Peak Demand | 384 kW |
| Average Demand | 60 kW |
| Total Energy Charged | 35.9 MWh |
| Stalls | 4 |
| Average Daily Utilization | 734 min (51 %) |
| Category | H+S |

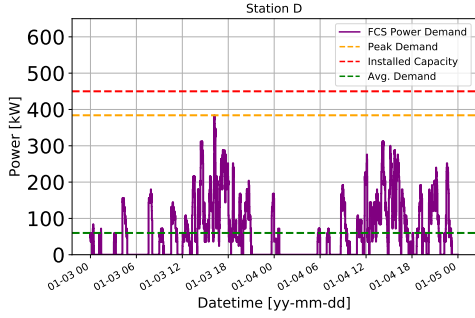


Fig. 5: Station D: H+S

population is selected for the next generation.

- Step 5: Step 2-4 are then repeated until the termination criterion is met and the Pareto front is found.
- Step 6: Lastly, once the optimization terminates, the design space and objective space of the final generation is stored and visualized.

Using this objective space and design space data, an FCS host can use higher level information to select the optimal station design. Such higher level information can be for example investment budgets or location specific QoS requirements.

IV. CASE DESCRIPTION

Table II shows the additional station information and performance metrics extracted from the measurement data. The worst case demand profile for station D is shown in Fig. 5. These worst case demand profiles consists of a 24 hour with the worst peak demand followed by a 24 hour with the worst energy density.

To asses the effects of different demand tariffs on our optimization framework, the optimization is performed for several demand tariff cases described in Table III.

When assessing the objective space the annual DCM cost is given as a percentage of the stations annual demand charges without DCM. Similarly, the grid-tie size and BESS power capability is given in per units. Both are based on the station's peak power demand as the base value.

V. NUMERICAL RESULTS

A. Optimal design in different demand tariffs

These results are intended to show how the optimum sizing is influenced by different demand tariffs. This illustrates how the objective and design space moves for a certain

TABLE III: List of the study cases for the optimization

| Study Case | Description | Demand Profile | BESS | Demand Tariffs |
|------------|--------------------|----------------|---|--|
| Case 1: | DCM without BESS | Station D | Excl. | |
| Case 2: | BESS assisted BESS | Station D | Incl. $C^{bess} = \text{€}490/\text{kWh}$ $C^{conv} = \text{€}110/\text{kW}$ P/E ratio < 1 | NL = €2.7/kW Swiss = €14.4/kW NYC = €42.3/kW |

station demand employed in different demand charge regions. Fig. 6 displays how the objective space move in terms of DCM cost and maximum charging delays and Figures 7, 8, 9, and 10 shows how the design parameters move with respect to maximum charging delays for the different regions. Additionally, to serve as a benchmark, the DCM solutions without BESS are included to asses the effectiveness of the optimum solutions with BESS included.

The results in Fig. 6 show that a significant DCM cost reduction can be obtained in high demand tariff regions relative to applying only power balance. However, this is not the case for regions with low demand tariffs. In the Netherlands case, BESS assisted DCM performs worse than power balancing in terms of costs. Making power balancing the preferred option for DCM in the Netherlands assuming cost is the driving factor. In contrast, for Switzerland and NYC, DCM reductions between 40-60% and 60-70%, respectively can be obtained depending on the delays. Furthermore, observing how the grid-tie moves in Fig. 7 with respect to the different regions, a dramatic 80% of grid-tie reduction can be achieved in NYC.

Nevertheless, as longer delays are permitted, the differences in performance between power balance only and the other two regions diminishes. Where for 8 minute delays, in Switzerland the station performs equally and in NYC with a difference of only 10% in terms of cost. In terms of grid-tie, a difference of 10% and 20% can be obtained with 8 minute delays, respectively. When comparing these BESS included solutions to case 1, the following can be concluded. First, in the Netherlands BESS assisted DCM is not feasible in terms of costs. Second, in Switzerland BESS assisted DCM can

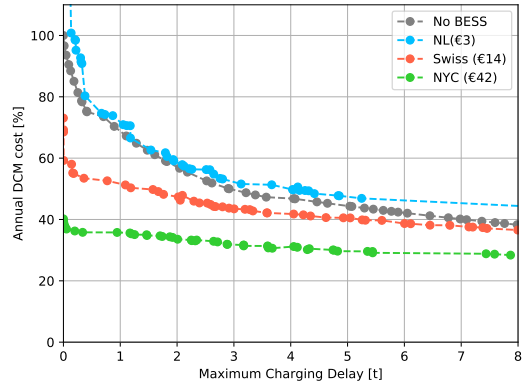


Fig. 6: DCM cost vs maximum charging delay [min]

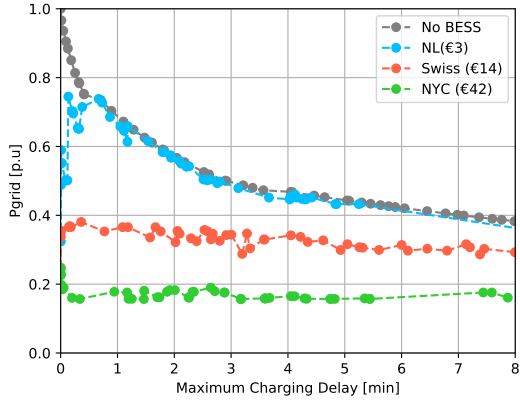


Fig. 7: Grid-tie size [pu] vs maximum charging delay [min]

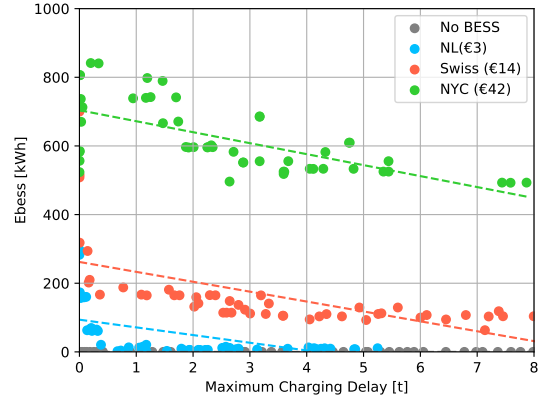


Fig. 9: BESS energy rating [kWh] vs maximum charging delay [min]

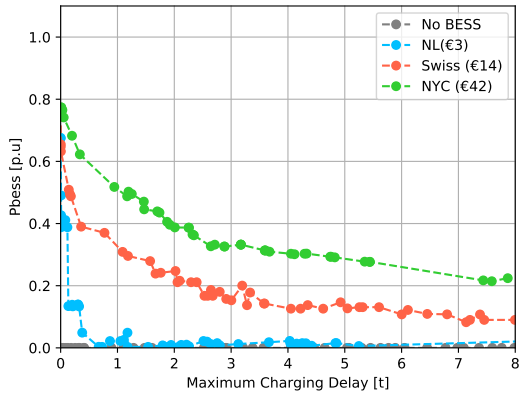


Fig. 8: BESS power rating [pu] vs maximum charging delay [min]

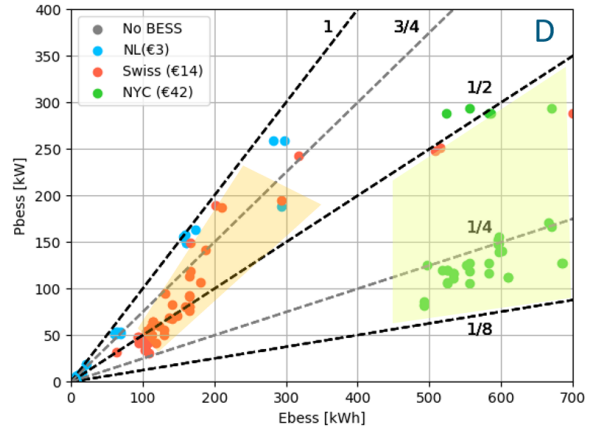


Fig. 10: BESS power [kW] vs energy rating [kWh]

always be beneficial for grid-tie reduction at FCSs. However, in terms of cost, a BESS should only be considered for FCSs where the charging delays need to remain low. Third, in NYC BESS assisted DCM can always be always beneficial for FCS applications.

Regarding the BESS sizing shown in Figure 8 and 9, except for some expensive solutions around zero delays, in the Netherlands the BESS is excluded for most of the solutions and the power balance curve is given as the optimal solution. For the NYC case, the BESS sizing behaves similarly to the Swiss case in terms of delays. However, it also evident that high demand tariffs directly impact the feasible BESS capacities, a 3x difference in demand tariff between Switzerland and NYC is reflected in the BESS capacity increase. Furthermore, the same is observed between the two power parameters, the additional 20% decrease in the grid-tie can be found in the increase of the BESS power capabilities.

Fig. 10 illustrates how the different demand tariffs influence

the optimal BESS PE ratios. For the dutch case, except for some expensive outliers, the optimal solutions concentrate around the origin, due to either a really small BESS is suggested or none at all. For the Swiss case, the PE ratio (highlighted in orange) concentrates between 1 and 1/2. The NYC case, larger BESS capacities are introduced, making the optimal solutions (highlighted in green) concentrate between 1/2 and 1/8. Due to the almost direct correlation between the demand tariffs and BESS capacities, FCSs located in regions with high demand tariffs optimally should possess larger capacities, and thus lower PE ratios than for stations in regions with mid range demand tariffs.

B. Performance simulations

In this section the performance of the FCS is assessed by selecting a number of optimally sized 2 minute delay solutions (rounded to the nearest 5 kW/kWh) and simulate this on an entire week demand. The week demand selected is the week wherein the peak demand occurs. The results include the charging delays, the SOC profile of the BESS and the

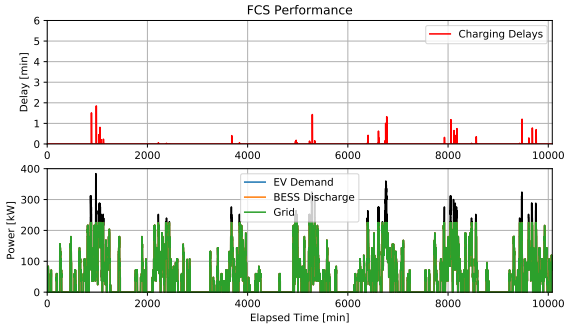


Fig. 11: Station: D - $E_b=0$, $P_b=0$, $P_G=225$ - - Annual DCM Cost = €38,880 (-41.4%)

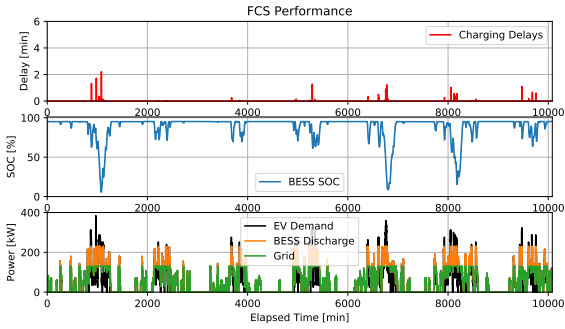


Fig. 12: Performance of a 2 minute delay optimal FCS design with demand D in Switzerland using $E_b^{\max}=135$, $P_b^{\max}=100$, $P_G^{\max}=130$, $C_{kW}=\text{€}14.4/\text{kW}$, and $L_{\text{exp}}: 11$ Years - Annual DCM Cost = €30,750 (-53.7%)

power flows.

The simulation results of an optimal design without BESS is shown in Fig. 11 and in Fig. 12 a BESS included solution. Both are simulated for station D and with solutions for the Swiss demand tariff case. When these results are compared, it becomes clear that in the BESS included design the BESS power and grid-tie combined are slightly larger than the grid-tie size in the non-BESS solution. This small difference in rating and maximum delay are due to the fact that the BESS reaches below its 15% SOC threshold, causing the power capabilities of the BESS to decrease, and thus causing additional power mismatch. This is also visible in the way the delay peaks differ during this period. Nevertheless, the BESS included solution will result in a 10% lower DCM cost compared to the DCM solution without BESS and a total of 53% reduction in demand charges.

Fig. 13 shows the results of a 2-minute optimal solution for D demand FCS located in NYC. These results show that even with different design ratios, the optimal charging delay performances do not differ much per region. However, as observed from the optimizations, the P/E ratios are reduced, and thus larger BESS capacities are introduced to the optimal design space. Because of these larger BESS capacities, the

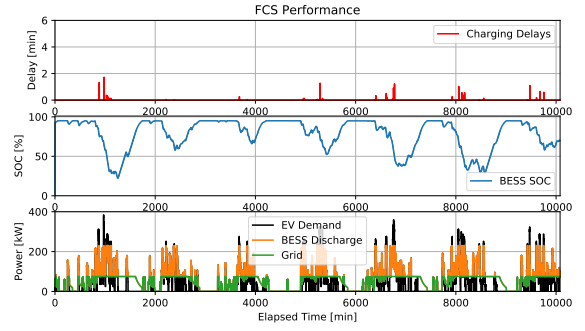


Fig. 13: Performance of a 2 minute delay optimal FCS design with demand D in NYC using $E_b^{\max}=600$, $P_b^{\max}=155$, $P_G^{\max}=75$, $C_{kW}=14/\text{kW}$ - $L_{\text{exp}}: 14$ years - Annual DCM Cost = €64,573 (-66.9%)

discharging and charging periods are longer, causing longer cycles.

This reduces the opportunity to dispatch the BESS for other ancillary services. However, these longer cycle periods are more shallow and the high SOC idling periods are shorter, resulting in improved BESS lifetimes. Furthermore, it is evident that less micro-cycles are occurring at high average soc levels.

VI. CONCLUSION

By identifying power miss-matches between the demand and the modeled FCS's capabilities included with knowing the number of EVs charging. The delays can be determined under the assumption that power balance is applied and the EVs continued to charge at the available speed.

From the literature it is clear that an analytical BESS model suffices. However, most studies neglect the BESS power capability curves. Results presented in this paper has to cause additional delays when the BESS is below its maximum power capability threshold. Leading us to the conclusion that including these power capabilities in the model is essential when analysing delays caused by power differences.

The proposed framework incorporates charging delays as a contradicting objective to cost. The cost is analysed based on the annual demand charges and BESS investment. The charging delay objective gives an assessment of the performance of the station. Furthermore, it was also concluded that this delay objective, includes two deviating aspects. The frequency of delays and maximum length of delays that can be experienced. The first affects the charging host and the second gives an indication of the quality of service provided to the FCS customers. In the proposed framework these are separated and minimized individually.

This paper investigated tariffs in the Netherlands (€2.7), Switzerland (€14.4) and NYC (€42.3). From the optimizations we can conclude that for the Netherlands nowadays the BESS costs are too high for profitability. This causes the op-

timization to roughly follow the power balance without BESS solutions. For Switzerland, between 40-60% DCM reductions can be obtained depending on the accepted delays. However, BESS assisted DCM should only be considered for low delay solutions. For NYC a reduction between 60-70% is obtained, for this region the grid-tie is 10% smaller and PE ratio of the BESS design smaller than Switzerland. Leading to the conclusion that in high demand tariff regions introduces lower PE ratio designs. The optimization was simulated against a weekly demand and the effectiveness confirmed. Remarkable is that optimal designs in different regions obtain the same station performance but with different BESS performance. Introducing limitations for secondary BESS grid-services.

REFERENCES

- [1] M. Neaimeh, S. D. Salisbury, G. A. Hill, P. T. Blythe, D. R. Scoffield, and J. E. Francfort, "Analysing the usage and evidencing the importance of fast chargers for the adoption of battery electric vehicles," *Energy Policy*, vol. 108, no. April, pp. 474–486, 2017.
- [2] T. S. Bryden, G. Hilton, B. Dimitrov, C. Ponce De León, and A. Cruden, "Rating a Stationary Energy Storage System Within a Fast Electric Vehicle Charging Station Considering User Waiting Times," *IEEE Transactions on Transportation Electrification*, vol. 5, no. 4, pp. 879–889, 2019.
- [3] Cox Automotive Inc, "Overcoming Electric Vehicle Misconceptions is Crucial to Converting Consideration to Sales." [Online]. Available: <https://www.coxautoinc.com/news/overcoming-electric-vehicle-misconceptions-is-crucial-to-converting-consideration-to-sales/>
- [4] "IONITY EU." [Online]. Available: <https://ionity.eu/>
- [5] McKinsey & Company, "The Road Ahead for e-mobility," *McKinsey Center for Future mobility*, pp. 179–194, 2020.
- [6] R. Wolbertus and R. Van den Hoed, "Electric vehicle fast charging needs in cities and along corridors," *World Electric Vehicle Journal*, vol. 10, no. 2, 2019.
- [7] Elaadnl, "Snel, sneller, snelst," 2019.
- [8] NREL, "Identifying Potential Markets for Behind-the-Meter Battery Energy Storage: A Survey of U.S. Demand Charges," *NREL*, pp. 1–7, 2017.
- [9] McKinsey & Company, S. Knupfer, and S. Sahdev, "How Battery Storage Can Help Charge the Electric-Vehicle Market," *McKinsey & Company*, no. February, pp. 1–8, 2018.
- [10] L. Richard and M. Petit, "Fast charging station with battery storage system for EV: Grid services and battery degradation," *2018 IEEE International Energy Conference, ENERGYCON 2018*, pp. 1–6, 2018.
- [11] M. Gjelaj, N. B. Arias, C. Traeholt, and S. Hashemi, "Multifunctional applications of batteries within fast-charging stations based on EV demand-prediction of the users' behaviour," *The Journal of Engineering*, vol. 2019, no. 18, pp. 4869–4873, 2019.
- [12] V. Salapic, M. Grzanic, and T. Capuder, "Optimal sizing of battery storage units integrated into fast charging EV stations," *2018 IEEE International Energy Conference, ENERGYCON 2018*, pp. 1–6, 2018.
- [13] Y. Ligen, H. Vrabel, and H. Girault, "Local energy storage and stochastic modeling for ultrafast charging stations," *Energies*, vol. 12, no. 10, 2019.
- [14] M. Moradzadeh and M. M. A. Abdelaziz, "A New MILP Formulation for Renewables and Energy Storage Integration in Fast Charging Stations," *IEEE Transactions on Transportation Electrification*, vol. 6, no. 1, pp. 181–198, 2020.
- [15] M. Sufyan, N. A. Rahim, C. K. Tan, M. A. Muhammad, and S. R. S. Raihan, "Optimal sizing and energy scheduling of isolated microgrid considering the battery lifetime degradation," *PLoS ONE*, vol. 14, no. 2, pp. 1–28, 2019.
- [16] T. Terlouw, T. AlSkaif, C. Bauer, and W. van Sark, "Multi-objective optimization of energy arbitrage in community energy storage systems using different battery technologies," *Applied Energy*, vol. 239, no. February, pp. 356–372, 2019. [Online]. Available: <https://doi.org/10.1016/j.apenergy.2019.01.227>
- [17] Y. Zhang, A. Lundblad, P. E. Campana, F. Benavente, and J. Yan, "Battery sizing and rule-based operation of grid-connected photovoltaic-battery system: A case study in Sweden," *Energy Conversion and Management*, vol. 133, pp. 249–263, 2017. [Online]. Available: <http://dx.doi.org/10.1016/j.enconman.2016.11.060>
- [18] G. Carpinelli, G. Celli, S. Mocci, F. Mottola, F. Pilo, and D. Proto, "Optimal integration of distributed energy storage devices in smart grids," *IEEE Transactions on Smart Grid*, vol. 4, no. 2, pp. 985–995, 2013.
- [19] J. Zhuang, G. Shen, J. Yu, T. Xiang, and X. Wang, "Micro-grid energy storage location and sizing optimization method based on demand response," *Proceedings - 2016 International Conference on Intelligent Transportation, Big Data and Smart City, ICITBS 2016*, no. 4, pp. 517–520, 2017.
- [20] J. Sachs and O. Sawodny, "Multi-objective three stage design optimization for island microgrids," *Applied Energy*, vol. 165, pp. 789–800, 2016. [Online]. Available: <http://dx.doi.org/10.1016/j.apenergy.2015.12.059>
- [21] K. K. Mehmood, S. U. Khan, S. J. Lee, Z. M. Haider, M. K. Rafique, and C. H. Kim, "Optimal sizing and allocation of battery energy storage systems with Wind and solar power DGs in a distribution network for voltage regulation considering the lifespan of batteries," *IET Renewable Power Generation*, vol. 11, no. 10, pp. 1305–1315, 2017.
- [22] T. Gnnann, S. Funke, N. Jakobsson, P. Plötz, F. Sprei, and A. Bennebag, "Fast charging infrastructure for electric vehicles: Today's situation and future needs," *Transportation Research Part D: Transport and Environment*, vol. 62, no. March, pp. 314–329, 2018. [Online]. Available: <https://doi.org/10.1016/j.trd.2018.03.004>
- [23] H. Tu, H. Feng, S. Srdic, and S. Lukic, "Extreme Fast Charging of Electric Vehicles: A Technology Overview," *IEEE Transactions on Transportation Electrification*, vol. 5, no. 4, pp. 861–878, 2019.
- [24] D. I. Stroe, M. Swierczynski, A. I. Stroe, R. Teodorescu, R. Laerke, and P. C. Kjaer, "Degradation behaviour of Lithium-ion batteries based on field measured frequency regulation mission profile," *2015 IEEE Energy Conversion Congress and Exposition, ECCE 2015*, pp. 14–21, 2015.
- [25] Fastned NL, "150+ kW fast chargers – Fastned support." [Online]. Available: <https://support.fastned.nl/hc/en-gb/articles/115015420127-150-kW-fast-chargers>
- [26] S. Schütte, S. Scherfke, and M. Sonnenschein, "mosaik - Smart Grid Simulation API," *Proceedings of SMARTGREENS 2012 - International Conference on Smart Grids and Green IT Systems*, no. 2, pp. 14–24, 2012.
- [27] S. You and C. N. Rasmussen, "Generic modelling framework for economic analysis of battery systems," *IET Conference Publications*, vol. 2011, no. 579 CP, p. 122, 2011.
- [28] DNV GL, "Safety, operation and performance of grid-connected energy storage systems," Tech. Rep. December, 2015.
- [29] Phase to Phase, "Vision Network Analysis." [Online]. Available: <https://phasetophase.nl/vision-network-analysis.html>
- [30] M. J. Alam and T. K. Saha, "Cycle-life degradation assessment of Battery Energy Storage Systems caused by solar PV variability," *IEEE Power and Energy Society General Meeting*, vol. 2016-Novem, pp. 1–5, 2016.
- [31] B. Xu, J. Zhao, T. Zheng, E. Litvinov, and D. S. Kirschen, "Factoring the Cycle Aging Cost of Batteries Participating in Electricity Markets," *IEEE Transactions on Power Systems*, vol. 33, no. 2, pp. 2248–2259, 2018.
- [32] D. Ioan, "Lifetime Models for Lithium Ion Batteries used in Virtual Power Plants Daniel-Ioan Stroe," Ph.D. dissertation, Aalborg University, 2014.
- [33] T. S. Bryden, G. Hilton, A. Cruden, and T. Holton, "Electric vehicle fast charging station usage and power requirements," *Energy*, vol. 152, pp. 322–332, 2018. [Online]. Available: <https://doi.org/10.1016/j.energy.2018.03.149>
- [34] J. Blank and K. Deb, "Pymoo: Multi-Objective Optimization in Python," *IEEE Access*, vol. 8, pp. 89497–89509, 2020.

Bibliography

- [1] M. Neaimeh, S. D. Salisbury, G. A. Hill, P. T. Blythe, D. R. Scoffield, and J. E. Francfort, “Analysing the usage and evidencing the importance of fast chargers for the adoption of battery electric vehicles,” *Energy Policy*, vol. 108, no. April, pp. 474–486, 2017.
- [2] Energy Storage NL, “Nationaal Actieplan Energieopslag en Conversie 2019,” Tech. Rep., 2019. [Online]. Available: <https://www.fme.nl/nl/system/files/publicaties/ESNLNAPEOC2019web.pdf>
- [3] Mckinsey & Company, “The Road Ahead for e-mobility,” *McKinsey Center for Future mobility*, pp. 179–194, 2020.
- [4] McKinsey & Company, S. Knupfer, and S. Sahdev, “How Battery Storage Can Help Charge the Electric-Vehicle Market,” *McKinsey & Company*, no. February, pp. 1–8, 2018.
- [5] Elaadnl, “Truckers komen op stroom - Outlook Q3 2020,” Tech. Rep., 2020.
- [6] T. S. Bryden, G. Hilton, B. Dimitrov, C. Ponce De León, and A. Cruden, “Rating a Stationary Energy Storage System Within a Fast Electric Vehicle Charging Station Considering User Waiting Times,” *IEEE Transactions on Transportation Electrification*, vol. 5, no. 4, pp. 879–889, 2019.
- [7] Cox Automotive Inc, “Overcoming Electric Vehicle Misconceptions is Crucial to Converting Consideration to Sales.” [Online]. Available: <https://www.coxautoinc.com/news/overcoming-electric-vehicle-misconceptions-is-crucial-to-converting-consideration-to-sales/>
- [8] Fastned NL, “Fastned support.” [Online]. Available: <https://support.fastned.nl/hc/en-gb>
- [9] “IONITY EU.” [Online]. Available: <https://ionity.eu/>
- [10] Elaadnl, “Snel, sneller, snelst,” 2019.
- [11] R. Wolbertus and R. Van den Hoed, “Electric vehicle fast charging needs in cities and along corridors,” *World Electric Vehicle Journal*, vol. 10, no. 2, 2019.
- [12] C. Botsford and A. Szczepanek, “Fast charging vs. slow charging: Pros and cons for the new age of electric vehicles,” *24th International Battery, Hybrid and Fuel Cell Electric Vehicle Symposium and Exhibition 2009, EVS 24*, vol. 3, no. February, pp. 1811–1819, 2009.
- [13] GVB, “Testen laadinfra elektrische bussen Garage West in volle gang,” 2019. [Online]. Available: <https://over.gvb.nl/nieuws/testen-laadinfra-elektrische-bussen-garage-west-in-volle-gang/>
- [14] NREL, “Identifying Potential Markets for Behind-the-Meter Battery Energy Storage: A Survey of U.S. Demand Charges,” *NREL*, pp. 1–7, 2017.
- [15] Y. Ligen, H. Vrubel, and H. Girault, “Local energy storage and stochastic modeling for ultrafast charging stations,” *Energies*, vol. 12, no. 10, 2019.
- [16] Alfen N.V., “Shell ultrafast EV charging service to incorporate Alfen energy storage,” 2020. [Online]. Available: <https://alfen.com/en/news/shell-ultrafast-ev-charging-service-incorporate-alfen-energy-storage>
- [17] BloombergNEF, “Energy Storage Investments Boom As Battery Costs Halve in the Next Decade,” 2019. [Online]. Available: <https://about.bnef.com/blog/energy-storage-investments-boom-battery-costs-halve-next-decade/>
- [18] HydroWires US DOE, “Energy storage technology and cost characterization report,” *Pacific Northwest National Laboratory*, no. July, pp. 1–120, 2019. [Online]. Available: https://www.energy.gov/sites/prod/files/2019/07/f65/StorageCostandPerformanceCharacterizationReport_{ }Final.pdf

- [19] H. C. Hesse, M. Schimpe, D. Kucevic, and A. Jossen, *Lithium-ion battery storage for the grid - A review of stationary battery storage system design tailored for applications in modern power grids*, 2017, vol. 10, no. 12.
- [20] International Renewable Energy Agency (IRENA), *Electricity storage and renewables: Costs and markets to 2030*, 2017, no. October.
- [21] W. Kempton and J. Tomić, "Vehicle-to-grid power implementation: From stabilizing the grid to supporting large-scale renewable energy," *Journal of Power Sources*, vol. 144, no. 1, pp. 280–294, 2005.
- [22] G. R. C. Mouli, M. Kefayati, R. Baldick, and P. Bauer, "Integrated PV charging of EV fleet based on energy prices, V2G, and offer of reserves," *IEEE Transactions on Smart Grid*, vol. 10, no. 2, pp. 1313–1325, 2019.
- [23] B. V. Bakolas, P. Bauer, and D. Prins, "Testing of smart charging controller for dynamic charging from solar panels," *2014 IEEE Transportation Electrification Conference and Expo: Components, Systems, and Power Electronics - From Technology to Business and Public Policy, ITEC 2014*, 2014.
- [24] D. Van Der Meer, G. R. C. Mouli, G. M. E. Mouli, L. R. Elizondo, and P. Bauer, "Energy Management System with PV Power Forecast to Optimally Charge EVs at the Workplace," *IEEE Transactions on Industrial Informatics*, vol. 14, no. 1, pp. 311–320, 2018.
- [25] S. Deb, K. Kalita, and P. Mahanta, "Review of impact of electric vehicle charging station on the power grid," *Proceedings of 2017 IEEE International Conference on Technological Advancements in Power and Energy: Exploring Energy Solutions for an Intelligent Power Grid, TAP Energy 2017*, vol. 1, pp. 1–6, 2018.
- [26] K. Yunus, H. Z. De La Parra, and M. Reza, "Distribution grid impact of plug-in electric vehicles charging at fast charging stations using stochastic charging model," *Proceedings of the 2011 14th European Conference on Power Electronics and Applications, EPE 2011*, 2011.
- [27] H. Hõimoja, M. Vasiladiotis, and A. Rufer, "Power interfaces and storage selection for an ultrafast EV charging station," *IET Conference Publications*, vol. 2012, no. 592 CP, 2012.
- [28] S. Bai, Y. Du, and S. Lukic, "Optimum design of an EV/PHEV charging station with DC bus and storage system," *2010 IEEE Energy Conversion Congress and Exposition, ECCE 2010 - Proceedings*, pp. 1178–1184, 2010.
- [29] E. Chiodo, D. Iannuzzi, F. Mottola, M. Pagano, and D. Proto, "A Probabilistic Approach to Assess the Requirements of an Ultra-Fast PEV Charging Station in Extra-Urban Contexts," *2019 AEIT International Annual Conference, AEIT 2019*, pp. 1–6, 2019.
- [30] S. Srdic and S. Lukic, "Toward Extreme Fast Charging: Challenges and Opportunities in Directly Connecting to Medium-Voltage Line," *IEEE Electrification Magazine*, vol. 7, no. 1, pp. 22–31, 2019.
- [31] L. Richard and M. Petit, "Fast charging station with battery storage system for EV: Grid services and battery degradation," *2018 IEEE International Energy Conference, ENERGYCON 2018*, pp. 1–6, 2018.
- [32] M. Gjelij, N. B. Arias, C. Traeholt, and S. Hashemi, "Multifunctional applications of batteries within fast-charging stations based on EV demand-prediction of the users' behaviour," *The Journal of Engineering*, vol. 2019, no. 18, pp. 4869–4873, 2019.
- [33] M. Gjelij, C. Traholt, S. Hashemi, and P. B. Andersen, "Cost-benefit analysis of a novel DC fast-charging station with a local battery storage for EVs," *2017 52nd International Universities Power Engineering Conference, UPEC 2017*, vol. 2017-Janua, pp. 1–6, 2017.
- [34] M. De Freige, M. Ross, G. Joos, and M. Dubois, "Power & energy ratings optimization in a fast-charging station for PHEV batteries," *2011 IEEE International Electric Machines and Drives Conference, IEMDC 2011*, pp. 486–489, 2011.

- [35] V. Salapic, M. Grzanic, and T. Capuder, "Optimal sizing of battery storage units integrated into fast charging EV stations," *2018 IEEE International Energy Conference, ENERGYCON 2018*, pp. 1–6, 2018.
- [36] W. D. Xie and W. Luan, "Modeling and simulation of public EV charging station with power storage system," *2011 International Conference on Electric Information and Control Engineering, ICEICE 2011 - Proceedings*, pp. 2346–2350, 2011.
- [37] M. Moradzadeh and M. M. A. Abdelaziz, "A New MILP Formulation for Renewables and Energy Storage Integration in Fast Charging Stations," *IEEE Transactions on Transportation Electrification*, vol. 6, no. 1, pp. 181–198, 2020.
- [38] T. Oda, M. Aziz, T. Mitani, Y. Watanabe, and T. Kashiwagi, "Mitigation of congestion related to quick charging of electric vehicles based on waiting time and cost–benefit analyses: A Japanese case study," *Sustainable Cities and Society*, vol. 36, no. October 2017, pp. 99–106, 2018. [Online]. Available: <https://doi.org/10.1016/j.scs.2017.10.024>
- [39] Y. Xiang, W. Yang, J. Liu, and F. Li, "Multi-objective distribution network expansion incorporating electric vehicle charging stations," *Energies*, vol. 9, no. 11, pp. 1–17, 2016.
- [40] J. Zhang, H. Zhou, H. Li, H. Liu, B. Li, C. Liu, and J. Yan, "Multi-Objective Planning of Charging Stations Considering Vehicle Arrival Hot Map," pp. 2–7.
- [41] B. Wang, Y. Zhou, and S. Zhang, "Multi-objective Planning Model of Electric Vehicle Charging Station," *Information Systems and Signal Processing Journal*, vol. 2, no. 1, pp. 23–28, 2017.
- [42] S. Kazarlis, A. Bakirtzis, and V. Petridis, "A GENETIC ALGORITHM SOLUTION TO THE UNIT COMMITMENT PROBLEM," vol. 11, no. February, pp. 83–92, 1996.
- [43] M. Sufyan, N. A. Rahim, C. K. Tan, M. A. Muhammad, and S. R. S. Raihan, "Optimal sizing and energy scheduling of isolated microgrid considering the battery lifetime degradation," *PLoS ONE*, vol. 14, no. 2, pp. 1–28, 2019.
- [44] T. Terlouw, T. AlSkaif, C. Bauer, and W. van Sark, "Multi-objective optimization of energy arbitrage in community energy storage systems using different battery technologies," *Applied Energy*, vol. 239, no. February, pp. 356–372, 2019. [Online]. Available: <https://doi.org/10.1016/j.apenergy.2019.01.227>
- [45] Y. Zhang, A. Lundblad, P. E. Campana, F. Benavente, and J. Yan, "Battery sizing and rule-based operation of grid-connected photovoltaic-battery system: A case study in Sweden," *Energy Conversion and Management*, vol. 133, pp. 249–263, 2017. [Online]. Available: <http://dx.doi.org/10.1016/j.enconman.2016.11.060>
- [46] G. Carpinelli, G. Celli, S. Mocci, F. Mottola, F. Pilo, and D. Proto, "Optimal integration of distributed energy storage devices in smart grids," *IEEE Transactions on Smart Grid*, vol. 4, no. 2, pp. 985–995, 2013.
- [47] J. Zhuang, G. Shen, J. Yu, T. Xiang, and X. Wang, "Micro-grid energy storage location and sizing optimization method based on demand response," *Proceedings - 2016 International Conference on Intelligent Transportation, Big Data and Smart City, ICITBS 2016*, no. 4, pp. 517–520, 2017.
- [48] J. Sachs and O. Sawodny, "Multi-objective three stage design optimization for island microgrids," *Applied Energy*, vol. 165, pp. 789–800, 2016. [Online]. Available: <http://dx.doi.org/10.1016/j.apenergy.2015.12.059>
- [49] K. K. Mehmood, S. U. Khan, S. J. Lee, Z. M. Haider, M. K. Rafique, and C. H. Kim, "Optimal sizing and allocation of battery energy storage systems with Wind and solar power DGs in a distribution network for voltage regulation considering the lifespan of batteries," *IET Renewable Power Generation*, vol. 11, no. 10, pp. 1305–1315, 2017.

- [50] M. J. Alam and T. K. Saha, "Cycle-life degradation assessment of Battery Energy Storage Systems caused by solar PV variability," *IEEE Power and Energy Society General Meeting*, vol. 2016-Novem, pp. 1–5, 2016.
- [51] M. Chawla, R. Naik, R. Burra, and H. Wiegman, "Utility energy storage life degradation estimation method," *2010 IEEE Conference on Innovative Technologies for an Efficient and Reliable Electricity Supply, CITRES 2010*, pp. 302–308, 2010.
- [52] D. I. Stroe, M. Swierczynski, A. I. Stroe, R. Teodorescu, R. Laerke, and P. C. Kjaer, "Degradation behaviour of Lithium-ion batteries based on field measured frequency regulation mission profile," *2015 IEEE Energy Conversion Congress and Exposition, ECCE 2015*, pp. 14–21, 2015.
- [53] D. I. Stroe, V. Knap, M. Swierczynski, A. I. Stroe, and R. Teodorescu, "Operation of a grid-connected lithium-ion battery energy storage system for primary frequency regulation: A battery lifetime perspective," *IEEE Transactions on Industry Applications*, vol. 53, no. 1, pp. 430–438, 2017.
- [54] D. I. Stroe, A. I. Stan, R. Diosi, R. Teodorescu, and S. J. Andreasen, "Short term energy storage for grid support in wind power applications," *Proceedings of the International Conference on Optimization of Electrical and Electronic Equipment, OPTIM*, pp. 1012–1021, 2012.
- [55] D. Wang, J. Coignard, T. Zeng, C. Zhang, and S. Saxena, "Quantifying electric vehicle battery degradation from driving vs. vehicle-to-grid services," *Journal of Power Sources*, vol. 332, pp. 193–203, 2016. [Online]. Available: <http://dx.doi.org/10.1016/j.jpowsour.2016.09.116>
- [56] L. Lam and P. Bauer, "Practical capacity fading model for Li-ion battery cells in electric vehicles," *IEEE Transactions on Power Electronics*, vol. 28, no. 12, pp. 5910–5918, 2013.
- [57] T. Gnann, S. Funke, N. Jakobsson, P. Plötz, F. Sprei, and A. Bennehag, "Fast charging infrastructure for electric vehicles: Today's situation and future needs," *Transportation Research Part D: Transport and Environment*, vol. 62, no. March, pp. 314–329, 2018. [Online]. Available: <https://doi.org/10.1016/j.trd.2018.03.004>
- [58] M. C. Falvo, D. Sbordone, I. S. Bayram, and M. Devetsikiotis, "EV charging stations and modes: International standards," *2014 International Symposium on Power Electronics, Electrical Drives, Automation and Motion, SPEEDAM 2014*, pp. 1134–1139, 2014.
- [59] Tesla, "Supercharger | Tesla Nederland." [Online]. Available: https://www.tesla.com/nl_NL/supercharger?redirect=no
- [60] H. Tu, H. Feng, S. Srdic, and S. Lukic, "Extreme Fast Charging of Electric Vehicles: A Technology Overview," *IEEE Transactions on Transportation Electrification*, vol. 5, no. 4, pp. 861–878, 2019.
- [61] IEC, "IEC 62196-3," Tech. Rep. december, 2014.
- [62] Tesla, "Oplaadconnectoren | Tesla Nederland." [Online]. Available: https://www.tesla.com/nl_NL/support/charging-connectors?redirect=no
- [63] G. R. C. Mouli, P. Venugopal, and P. Bauer, "Future of electric vehicle charging," *19th International Symposium on Power Electronics, Ee 2017*, vol. 2017-Decem, pp. 1–7, 2017.
- [64] CharIn, "CharIN is publishing a solution for high power charging of tucks and busses beyond 1 MW: Charging Interface Initiative e. V. (CharIN e. V)." [Online]. Available: <https://www.charinev.org/news/news-detail-2018/news/charin-is-publishing-a-solution-for-high-power-charging-of-tucks-and-busses-beyond-1-mw/>
- [65] Fastned NL, "150+ kW fast chargers – Fastned support." [Online]. Available: <https://support.fastned.nl/hc/en-gb/articles/115015420127-150-kw-fast-chargers>
- [66] FastnedNL, "Why fast charging stations are good for the grid." [Online]. Available: <https://fastnedcharging.com/hq/nl/why-fast-charging-stations-are-good-for-the-gridnl/>
- [67] Q. Deng, S. Tripathy, D. Tylavsky, T. Stowers, and J. Loehr, "Demand Modeling of a dc Fast Charging Station," *2018 North American Power Symposium, NAPS 2018*, 2019.

- [68] T. S. Bryden, G. Hilton, A. Cruden, and T. Holton, "Electric vehicle fast charging station usage and power requirements," *Energy*, vol. 152, pp. 322–332, 2018. [Online]. Available: <https://doi.org/10.1016/j.energy.2018.03.149>
- [69] M. Nicholas and D. Hall, "Lessons Learned on Early Fast Electric Vehicle Charging Systems," *White Paper - The International Council on Clean Transportation*, no. July, 2018. [Online]. Available: www.theicct.org
- [70] P. Bach Andersen, J. Hu, and K. Heussen, "Coordination strategies for distribution grid congestion management in a multi-actor, multi-objective setting," *IEEE PES Innovative Smart Grid Technologies Conference Europe, 2012*.
- [71] R. Moslemi, A. Hooshmand, and R. K. Sharma, "A machine learning based demand charge management solution," *2017 IEEE PES Innovative Smart Grid Technologies Conference Europe, ISGT-Europe 2017 - Proceedings*, vol. 2018-January, pp. 1–6, 2017.
- [72] M. R. Narimani, B. Asghari, and R. Sharma, "Optimal Sizing and Operation of Energy Storage for Demand Charge Management and PV Utilization," *Proceedings of the IEEE Power Engineering Society Transmission and Distribution Conference*, vol. 2018-April, pp. 1–5, 2018.
- [73] DNV GL, "Safety, operation and performance of grid-connected energy storage systems," Tech. Rep. December, 2015.
- [74] Mckinsey & Company, "New economics of energy storage," *IET Power Engineer*, vol. 20, no. 4, pp. 28–31, 2006.
- [75] INVADE European Union's Horizon 2020, "D6.1 Storage system dimensioning and design tool," Tech. Rep. 646476, 2016.
- [76] D. Ioan, "Lifetime Models for Lithium Ion Batteries used in Virtual Power Plants Daniel-Ioan Stroe," Ph.D. dissertation, Aalborg University, 2014.
- [77] S. You and C. N. Rasmussen, "Generic modelling framework for economic analysis of battery systems," *IET Conference Publications*, vol. 2011, no. 579 CP, p. 122, 2011.
- [78] Y. Shi, B. Xu, Y. Tan, and B. Zhang, "A Convex Cycle-based Degradation Model for Battery Energy Storage Planning and Operation," *Proceedings of the American Control Conference*, vol. 2018-June, pp. 4590–4596, 2018.
- [79] S. D. Downing and D. F. Socie, "Simple rainflow counting algorithms," *International Journal of Fatigue*, vol. 4, no. 1, pp. 31–40, 1982.
- [80] E. Mishra and E. Mohapatra, "Multi-Objective Genetic Algorithm: A Comprehensive Survey," *Ijetae.Com*, vol. 3, no. 2, 2013. [Online]. Available: http://www.ijetae.com/files/Volume3Issue2/IJETAE_0213_13.pdf
- [81] N. Gunantara, "A review of multi-objective optimization: Methods and its applications," *Cogent Engineering*, vol. 5, no. 1, pp. 1–16, 2018. [Online]. Available: <https://doi.org/10.1080/23311916.2018.1502242>
- [82] A. M. Mohsen, "Annealing Ant Colony Optimization with Mutation Operator for Solving TSP," *Computational Intelligence and Neuroscience*, vol. 2016, 2016.
- [83] K. Deb, K. Sindhya, and T. Okabe, "Self-adaptive simulated binary crossover for real-parameter optimization," *Proceedings of GECCO 2007: Genetic and Evolutionary Computation Conference*, pp. 1187–1194, 2007.
- [84] K. Deb, A. Pratap, S. Agarwal, and T. Meyarivan, "A fast and elitist multiobjective genetic algorithm: NSGA-II," *IEEE Transactions on Evolutionary Computation*, vol. 6, no. 2, pp. 182–197, 2002.
- [85] INVADE European Union's Horizon 2020, "D5.4 Advanced Optimal Battery operation and control algorithm," Tech. Rep. 731148, 2020.

- [86] Phase to Phase, "Vision Network Analysis." [Online]. Available: <https://phasetophase.nl/vision-network-analysis.html>
- [87] G. Rancilio, A. Lucas, E. Kotsakis, G. Fulli, M. Merlo, M. Delfanti, and M. Masera, "Modeling a large-scale battery energy storage system for power grid application analysis," *Energies*, vol. 12, no. 17, 2019.
- [88] IEC, "IEC 62660-1," Tech. Rep., 2020.
- [89] B. Xu, J. Zhao, T. Zheng, E. Litvinov, and D. S. Kirschen, "Factoring the Cycle Aging Cost of Batteries Participating in Electricity Markets," *IEEE Transactions on Power Systems*, vol. 33, no. 2, pp. 2248–2259, 2018.
- [90] U.S. Department of Energy, "Energy storage for power systems applications: a regional assessment for the northwest power pool (NWPP)," no. April, p. 104, 2010.
- [91] NREL, "2018 U . S . Utility-Scale Photovoltaics- Plus-Energy Storage System Costs Benchmark," *National Renewable Energy Laboratory*, no. November, p. 32, 2018. [Online]. Available: <https://www.nrel.gov/docs/fy19osti/71714.pdf>
- [92] Liander, "Tarieven voor aansluiting en transport gas," pp. 2–3, 2020. [Online]. Available: www.liander.nl/voorwaardenkleinverbruik
- [93] S. Schütte, S. Scherfke, and M. Sonnenschein, "mosaik - Smart Grid Simulation API," *Proceedings of SMARTGREENS 2012 - International Conference on Smart Grids and Green IT Systems*, no. 2, pp. 14–24, 2012. [Online]. Available: http://www-ui.informatik.uni-oldenburg.de/download/Publikationen/Schuette{}_Scherfke{}_Sonnenschein{}_2012{}_mosaik{}_Smart{}_Grid{}_Simulation{}_API.pdf
- [94] C. Steinbrink, A. A. van der Meer, M. Cvetkovic, D. Babazadeh, S. Rohjans, P. Palensky, and S. Lehnhoff, "Smart grid co-simulation with MOSAIK and HLA: a comparison study," *Computer Science - Research and Development*, vol. 33, no. 1-2, pp. 135–143, 2018.
- [95] Pymoo, "Pymoo: Multi-objective Optimization in Python." [Online]. Available: <https://pymoo.org/index.html>
- [96] J. Blank and K. Deb, "Pymoo: Multi-Objective Optimization in Python," *IEEE Access*, vol. 8, pp. 89 497–89 509, 2020.